Depositional slope surface of the western margin of the Nylsvlei, South Africa: Active piedmont aggradation and sedimentation processes

This research has been funded by:
The Jim and Gladys Taylor Trust Fund and the University of the Witwatersrand.

Depositional slope surface of the western margin of the Nylsvlei, South Africa:

Active piedmont aggradation and sedimentation processes

Nicole M. Burri, BSc (Hons.) University of the Witwatersrand

Supervisors: Prof. T.S. McCarthy, Dr G.J. Susino, & D. Hardwick

Thesis submitted to the University of the Witwatersrand in fulfillment of the requirements of candidature for the degree of Master of Science (Research).

Department of Geology, School of Geoscienc, Faculty of Science

August 2013.

Abstract

The Nyl River and its floodplain are situated on the eastern foothills of the Waterberg mountain range in the Limpopo Province of South Africa. Tributaries flowing out of the Waterberg range display unusual downstream changes, as they approach and converge with the Nylsvlei (or Nyl floodplain). Tributary channels decrease in size downstream until, eventually, they disappear altogether forming unchannellized floodouts. On one such floodout, on the farm Driefontein, an actively aggrading piedmont has formed adjacent to the famous Wonderkrater peat mound, known for its pollen record dating back ~45,000 years. Sediments from the aggrading piedmont interlace with Wonderkrater's peat layers, suggesting that as the piedmont aggrades so too does the peat mound. This setting presents a unique opportunity to study active aggradational processes, and their products, on hillslope deposits and floodout environments. This study aims to describe the geomorphology and nature of depositional processes along the length of the piedmont adjacent to the Wonderkrater peat mound. Cross-sections, drainage channels and vegetation indices based on topographic maps, orthophotographs and hyperspectral images, were created using ArcGIS in order to describe and determine the surface morphology and hydrology of the Driefontein piedmont in detail. Surface soil samples were collected in order to determine particle size distribution, which were in turn compared to vegetation indices and changes in slope elevation. Further grain samples were collected from depth for age dating using Optically Stimulated Luminescence (OSL), as well as to determine grain size distribution in relation to surface sediments and other fluvial environments. Hyperspectral indices were found to correlate to surface grain size distribution, demonstrating that the presence of vegetation acts as a retaining mechanism for particles along hillslopes where incline should be too steep to support fine-grained sedimentary material. Surface sediments were found to demonstrate the characteristics of an alluvial floodout system, affected greatly by the presence of vegetation and slope inclination. Sub-surface samples were characteristic of a colluvial setting, suggesting that pediment retreat and basin fill, coupled with evidential climatic changes, were dominant controls on the pediment's morphological and aggradational mechanisms. OSL age results estimated the

sediments to be between 37.33 and 58.66 ka old. As a result of its unique sedimentary characteristics, a new type of ‘slow creep fan’ class was established in order to describe the characteristics of the Driefontein piedmont.

Keywords: aggradation, piedmont, peat mound, hillslopes, particle size distribution, unchannellized floodouts, optically stimulated luminescence.

Acknowledgments

This research thesis was devised and made possible by Professor Terence McCarthy and Dr George Susino, my supervisors. I am indebted to the Jim and Gladys Taylor Trust Fund for their financial assistance. For her endless patience and time, I would like to thank Mrs. D. Hardwick my co-supervisor for helping me with all my ArcGIS questions. I would like to thank the landowner Dr Walter Ward and his farm manager Sakkie Kekana for their generous hospitality and use of the farm on which the research site is located. I would also like to thank Mr. L. Fourie for allowing us access onto his farm adjoining the research site. The use of the laser granulometer was made possible by the metallurgical department of the University of the Witwatersrand. And a special thank you goes out to Mathew Kitching, Lucinda Backwel, Nicolas Grech-Cumbo, Alessandro Craparo, Luisa Ashworth, Jason Ashworth and Karsten Richartz for their extraordinary efforts during field excursions and sample collection.

Contents

List of Figures

List of Tables

List of Abbreviations

OSL	Optically Stimulated Luminescence
GIS	Geographical Information System
DEM	Digital Elevation Model
NDVI	Normalized Difference Vegetation Index
PSD	Particle Size Distribution
M	Graphic Mean
D	Graphic Standard Deviation
S	Graphic Skewness
IDW	Inverse Distance Weighted
IC-PMS	Inductively Coupled Plasma Mass Spectrometry
XRF	X-ray Fluorescence
GPS	Geographical Point System
CAM	A Central Age Model
MAM	A Minimum Age Model

1 Introduction

Processes of sediment production, erosion, transportation and deposition, and their link to landscape evolution, have been the subject of active discussion and research for over a century. The general form of any hillslope is largely determined by the link between slope and valley processes (e.g. Anderson & Anderson, 2010). Depositional environments associated with hillslopes include aeolian, fluvial and slope controlled systems. The processes and products of such systems are dynamic and multidimensional, both in space and time. Although much research has been carried out on diverse sedimentary environments, slope dominated processes have been studied to a lesser degree and almost exclusively in the context of alluvial fans and, the formation of piedmonts. (Krumbein & Sloss, 1951; Blissenbach, 1954; Folk & Ward, 1957; Stanistreet & McCarthy, 1993; Blair & McPherson, 1994; McCarthy & Cadle, 1995; Botha, *et al.,* 2000; 2008; Miall, 1996; Brown, 1997; Blikra & Nemec, 1998; Mason & Knox, 2011).

In the past, much research carried out on sub-aerial depositional processes concerning slope deposition, has been confined largely to arid environments and drylands. Processes operating on slopes existing under more humid and/or mesic conditions are so-called “humid fan” settings (Kochel & Johnson, 1984; Kochel, 1990). Generally, these slopes are referred to as being dominated by colluvial processes and are less well known and more poorly studied.

Changes in slope angle and active surface processes determine changes in grain size distribution and sorting across the length of a hillslope (Botha, 1996). Fluvial environments which experience long periods of warm and dry conditions, followed by periods of intense precipitation generated by low-pressure systems or local convective thunderstorms, may experience a short-term total precipitation which exceeds the long term annual average (Tooth, 2000). In such environments, the erosional effectiveness of individual raindrops is generally very high, even more so where vegetation cover is sparse or intermittent, resulting in increased surface runoff, particle entrainment and subsequent infiltration and evaporation (Tooth, 2000; Thornes, 1994a). Commonly such hillslope flows decrease in volume downstream due to high rates of infiltration and evaporation (Tooth, 2000). This manner of unsteady flow and sediment transport is characteristic of fluvial environments where precipitation is non-uniform, resulting in poorly interconnected drainage networks with surface flow varying from being channeled to being completely unchannneled (Tooth, 2000).

In the Limpopo Province of South Africa, a region known as the Nylsvlei (or Nyl Floodplain) is host to Wonderkrater (or Wonderous crater), one of South Africa's only known peat mounds. The Nyl floodplain and its tributaries are situated on the eastern foothills of the Waterberg mountain range. Tributaries flowing out of the Waterberg range display unusual downstream changes as they approach and converge with the Nyl River and its floodplain (McCarthy, *et. al,.* 2010). The channels of these tributaries decrease in size and depth downstream until, eventually, they disappear completely, forming a piedmont with unchanneled floodouts (Tooth, *et al.,* 2002). On one such floodout, at the toe of an unnamed channel (hereon referred to as the Koodoesfontein channel) on the Dreifontein farm (Fig. 1-1), an actively aggrading piedmont has formed adjacent to the famous Wonderkrater peat mound. The Wonderkrater peat mound is fed by a separate artesian spring-fed steam, and has provided both a climatic record, based on vegetation, and an archaeological record for the Holocene period in Southern Africa (Scott, et al. 2003; 1982; 1989).

The area surrounding this peat mound has been recognized as an actively aggrading piedmont terrain (McCarthy, *et al.,* 2010). The surface morphology and sedimentary processes taking place on the piedmont are the focus of this study. The proximity of the peat mound to its surrounding piedmont surface, suggests that both the peat mound and the piedmont have been actively aggrading for at least 35,000 years (Scott, 1982; 1989; 2003; McCarthy, *pers.comm.,* 2011). The interaction of the aggrading Wonderkrater peat mound, surrounded by the piedmont terrain, thus presents a unique opportunity to study active aggradational processes and products on a distal hill slope deposit (Fig. 1-1).

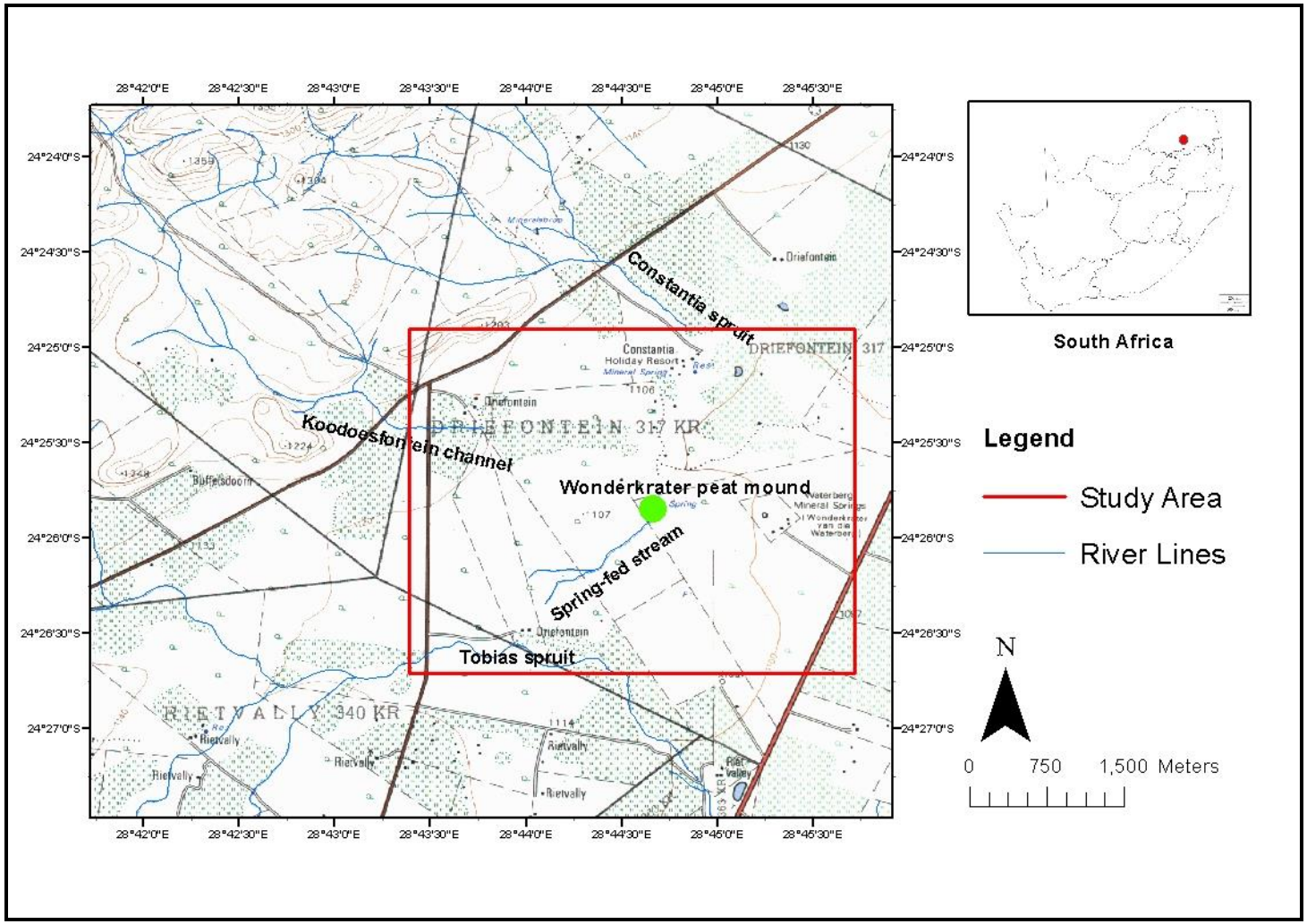

Fig. 1-1: Location and regional topography of the Wonderkrater peat mound and its surrounding piedmont terrain on the Driefontein farm.

The aim of this study is to investigate the morphology and the depositional process taking place on an actively aggrading piedmont terrain along the length of its slope. The presence of the well-dated Wonderkrater peat mound occurring towards the base of the piedmont in question constrains the overall rate of aggradation taking place along the piedmont surface. In order to determine the surface morphology and sedimentary nature, surface samples were collected along transects perpendicular to the surface flow along the length of the piedmont which surrounds the peat mound, and grain size characteristics and distribution were examined.

These were analyzed in the context of the slope, surface flow and current climatic conditions, in order to understand the nature of the aggradational processes taking place on the piedmont. By conducting OSL dating on quartz grains collected from the piedmont adjacent to the Wonderkrater peat mound, an attempt was made to determine the rate of sediment aggradation around the mound, and thereby the rate of aggradation of the piedmont.

2 Literature Review

2.1 Colluvial processes

The process of colluviation are shown to be strongly associated with phases of past humid conditions, during which a slope may stabilize due to the presence of vegetation promoting surface integrity through root-networks and the formation of soil horizons, followed by more arid conditions during which weathered material is transported downslope as sheet wash (Goudie & Bull, 1984; Clarke, *et al.,* 2003). The association of colluvium with the occurrence of unconfined sheet wash and ephemeral gullies may also be ascribed to summer rainfall conditions, and therefore to temperate or even humid climatic conditions (Botha, *et al.,* 1994). Colluvial material, though poorly documented, has been described as being composed of a broad mixture of sand, silt, clay and calcrete nodules, with sedimentary particles

generally ranging approximately from 2000µm - 63µm (Goudie & Bull, 1984, Botha, 1996).

Climate might be one of the most important driving factors in the formation of colluvial material, and downslope piedmonts and basins. During periods of wet climatic conditions, physical and chemical weathering of bedrock increases, resulting in *in situ* colluvium formation along the exposed slope length. As climate transcends towards colder drier periods, hillslope weathering decreases and vegetation is lost. Subsequent increase in intense episodic rainfall, results in rapid erosion of exposed sediments by flash-floods and debris flow, and increased downslope sedimentation of basins as colluvium is stripped (Pederson, *et al.,* 2000). Through the removal of weathered bedrock upslope, and the re-deposition of material on downslope low gradient pediments, large amounts of colluvium may accumulate in this manner during periods of dryer climatic conditions (Price Williams *et al.,* 1982)

Colluvial deposits documented in KwaZulu-natal and the Orange Free State, South Africa, indicate particle transport mechanisms through sheetwash and rilling where channels are formed, as well as through rain-impacted flow where rain drops effect very shallow moving water on low gradient slopes where no channel formation takes place (Botha, 1996). According to Blikra & Nemec (1998) colluvial deposits are easily distinguished on the basis of their steep slopes and avalanche dominated processes, ending in short fans or aprons.

In many colluvial deposits from humid regions, a heavily bioturbated fine-grained soil layer has been recorded as the only migratory layer along the length of the slope surface. A gravel rich horizon marks the boundary between the residual material and the fine-grained migratory soils, which have a tendency to form thick deposits downslope resulting in pedimentation (Thomas, 1994). Scarp retreat has been suggested as being a contributing factor in the formation of colluviums (Moss, 1965). Mass wasting or debris flow can be described as the movement of coarse-grained eroded bedrock and slope material downslope. This movement is largely triggered by

infrequent heavy rain storms (Bertran, *et al.,* 1997). Due to the process of mass wasting and slope erosion, colluvium material is generally poorly sorted (Mason & Knox, 2011). The formation and accumulation of colluvium has been associated with dry, periglacial periods followed by wetter, more humid conditions (Mason & Knox, 2011).

2.2 Alluvial systems

Among the different types of slope-dominated systems, alluvial fans are probably the most widely studied (Miall, 1996). Alluvial fan morphology was first described by Blissenbach in 1954. Alluvial fans have since been described as occurring in areas where the relief is pronounced, gradients are moderate to steep, and erosion and transportation energies are high (Blissenbach, 1954). Blissenbach described fans as consisting of 1) the Apex: the highest elevation along the fan where the stream originates along a watershed and where generally, the sedment deposit is minimal, 2) the Fanhead: the area closest to the apex, 3) the Midfan: halfway between the Fanhead and the furthest lowermost reaches of the fan, and 4) the Fan Base: where the flow competency decelerates and the alluvium sediments are deposited.

Alluvial fans are generally known to form on steeply dipping depositional slopes where, due to the loss of channel confinement, largely unsorted sediments are deposited at the base of the slope. Blissenbach (1954) described dip angles on alluvial fan slopes as rarely exceeding 10° (0.1763), and that such slopes, should be considered as steep. Fans sloping between 5° (0.0874) and 2° (0.0349) were referred to by Blissenbach as being gentle and those fans with angles sloping below 2° (0.0349), as being flat.

Multiple lobes and aprons form at the base of such fans due to channel avulsion (Blissenbach, 1954). Miall (1996) pointed out that a significant difference between alluvial fans and most other fluvial systems, is that other fluvial systems have a ‘concave-up transverse profile’ (pg. 246), with the channel being the lowest point, while fan systems characteristically have a ‘convex-up transverse profile’ (pg. 246)

which can lead to overbank flow and sheet flooding of the bed load. Deposition takes place due to a decrease in flow competence, as flow confinement is lost and flow energy dispersed (McCarthy & Cadle, 1994).

Stanistreet and McCarthy (1993) classified three types of alluvial fans; 1) Debris flow dominated, 2) Braided-river dominated, and 3) Low sinuosity/meandering (or losimean) fans. These three fans were classified on the basis of variation in slope and fan surface steepness, changes in size and activeness of the inner mid and outer sections of the fan, as well as the vegetation density associated with each fan type. The presence or absence, as well as the type, of vegetation found in association with fluvial systems appears to play a major role in the mode of sediment transport and deposition in certain colluvial and/or alluvial systems (McCarthy, *pers. comm*., 2010).

Blair & McPherson (1994) recommend limiting the term ‘alluvial fan’ to systems which have steep slopes (averaging around 25° or 0.4663), are dominated by gravity or debris-flow deposits, and lose their competency as the slope gradient levels out (Miall, 1996). Blair and McPherson (1994) suggested that fine-grained fan deposits and those deposits not associated with uplifted environments should be termed ‘distributary fluvial systems’, ‘terminal fans’ or ‘braided deltas’. However, based on this type of classification, alluvial fans can be identified in the ancient record only by their facies characteristics (Miall, 1996).

Blair and McPherson (1994) went on to describe two varieties of debris-flow-dominated fans:

1. Those constructed mainly through sediment gravity-flow processes along with colluvial slides and rock falls and the secondary processes of overbank sheet flow, wind erosion, weathering, bioturbation, soil development, and case hardening.

2. Those built primarily of sheet flow and hyper concentrated flow deposits where sandy overbank deposits are common and distal sand fringe may be present.

Blair and McPherson (1994) recognized only the debris-flow dominated fan as being a true alluvial fan. McCarthy and Cadle (1995) argued that Blair and McPherson's classification of alluvial fans (1994) is too "restrictive to encompass the wide diversity of natural depositional processes" (pg. 47), and that the different debris-flow dominated fluvial fans identified by Blair and McPherson (1994) are virtually impossible to identify in ancient sedimentary records where the various dispersal patterns of palaeocurrents are almost impossible to define (Miall, 1996).

Miall (1996) pointed out that various fluvial processes might occur in different proportions within a single region, depending on the region's climate and the nature of the source terrains. Miall (1996) suggests a classification system based on three main processes: sedimentary gravity flow, braiding, and meandering. Using these three processes, Miall (1996) recognized three classes of fans: 1) Debris-flow dominated, which are typically small (less than 10km in length) and steep and most common in arid regions, 2) Braided alluvial fans, and 3) Low sinuosity/meandering fluvial fans as identified by Stanistreet and McCarthy (1993). According to Smith (2000), alluvial slopes lacking unconfined fan morphology should be classified as a stream-flow dominated piedmonts. Along the length of alluvial slopes, channeled flow rather than sheetflooding and mass wasting of sedimentary material persists (Smith, 2000).

2.3 Flood-out environments

Terminal or floodout environments describe settings where, at the distal fringe of the fluvial system, flow velocity is lost and streams become ephemeral until eventually, water percolates into the ground or collects as a standing water body (Miall, 1996). Floodouts may be either channeled, unchannelled or a combination of both (Tooth, 1999). The concept of a terminal fan setting, where peripheral flow is lost, has been greatly attributed to arid or semi-arid climatic conditions. There is however,

controversy whether a system which loses its channels downstream may in fact be considered an alluvial fan. North & Warwick (2007) argue that the facies which define an alluvial fan may be lacking in rivers, which terminate in bifurcated sub aerial fan-shaped channels. The mechanical processes involved in the formation of a fan-shaped sedimentary body, must be the same whether these bodies are formed in arid, temperate or humid conditions, on a small scale as peripheral bodies or as large-scale fans or bajadas. So far however, a strict diagnostic lithofacies defining an alluvial fan is missing (North & Warwick, 2007).

2.4 Slope processes

Hillslopes are one of the most prominent and pervasive landforms found on the earth and they differ from other environments in that they encompass a large and variable assemblage of different erosion, transportation and depositional surfaces; with the balance between them varying as their topographic slope gradient varies (Collinson, 1996; Brown, 1997; Smith, 2000). The steepness of slope and the manner of transportation and deposition of sedimentary material, determine the defining shape and geometry of the resulting surface landscape. Along the length of a slope, sediment deposition may occur either as a result of unconstrained debris flow, or due to channel constrained flow (Botha & Partridge, 2000). The geometric features of a slope and its mode of deposition, present a record of past surface events such as droughts, floods and balanced mesic conditions. Surface features formed in the past often influence the manner in which present day systems of erosion, transportation and deposition operate (Brown, 1997).

Environmental factors which shape sedimentary landscapes have long been determined through examining the size and shape of the sedimentary material in question (Krumbein & Schloss, 1951). In sub-aerial studies, current slope and climatic conditions can be used in conjunction with grain parameters in order to establish environmental settings and depositional mode (Blair & McPherson, 1994; McCarthy & Cadle, 1995). The slope along which transportation and deposition takes place, may be either concave, where deposition is confined to the lower talus and

pediment, or convex where active deposition takes place along most of the length the slope (Botha & Partridge, 2000).

3 Study Area

The Nyl river, along with its tributaries, drains parts of the south-eastern and eastern foothills of the Waterberg Range, from where it flows northward across the low-lying Springbok Flats (Frost, 1987; Tooth & McCarthy, 2007). The Nyl floodplain or Nylsvlei (Fig. 3-2), being situated in the semi-arid Limpopo Province of South Africa, hosts a high level of biodiversity and is of both considerable agricultural and conservation value. As a result, a portion of the wetland was declared a RAMSAR site in 1998 (Frost, 1987; Higgins, et., al. 1996). The region also hosts the Wonderkrater peat mound, a site of immense palaeo-climatic and archaeological importance, due to its long and well preserved palynological record (Scott, 1982, 1989; Thackeray and Scott, 1987).

3.1 Regional setting

3.1.1 Geomorphology

The geomorphology of the northwestern margins of Nylsvlei presents a series of drainage networks, with the Wonderkrater peat mound and its surrounding piedmont situated between the expansive Nyl floodplain to the south-east and the Waterberg range to the north-west (Fig. 3-1). Well documented channels flow out of the Waterberg (Reading, 2006; Frost, 1987), and on reaching the piedmont adjacent to the Wonderkrater peat mound, form a dispersed drainage ultimately leading to the aggradational surface which forms the focus of this study (Fig. 1-1).

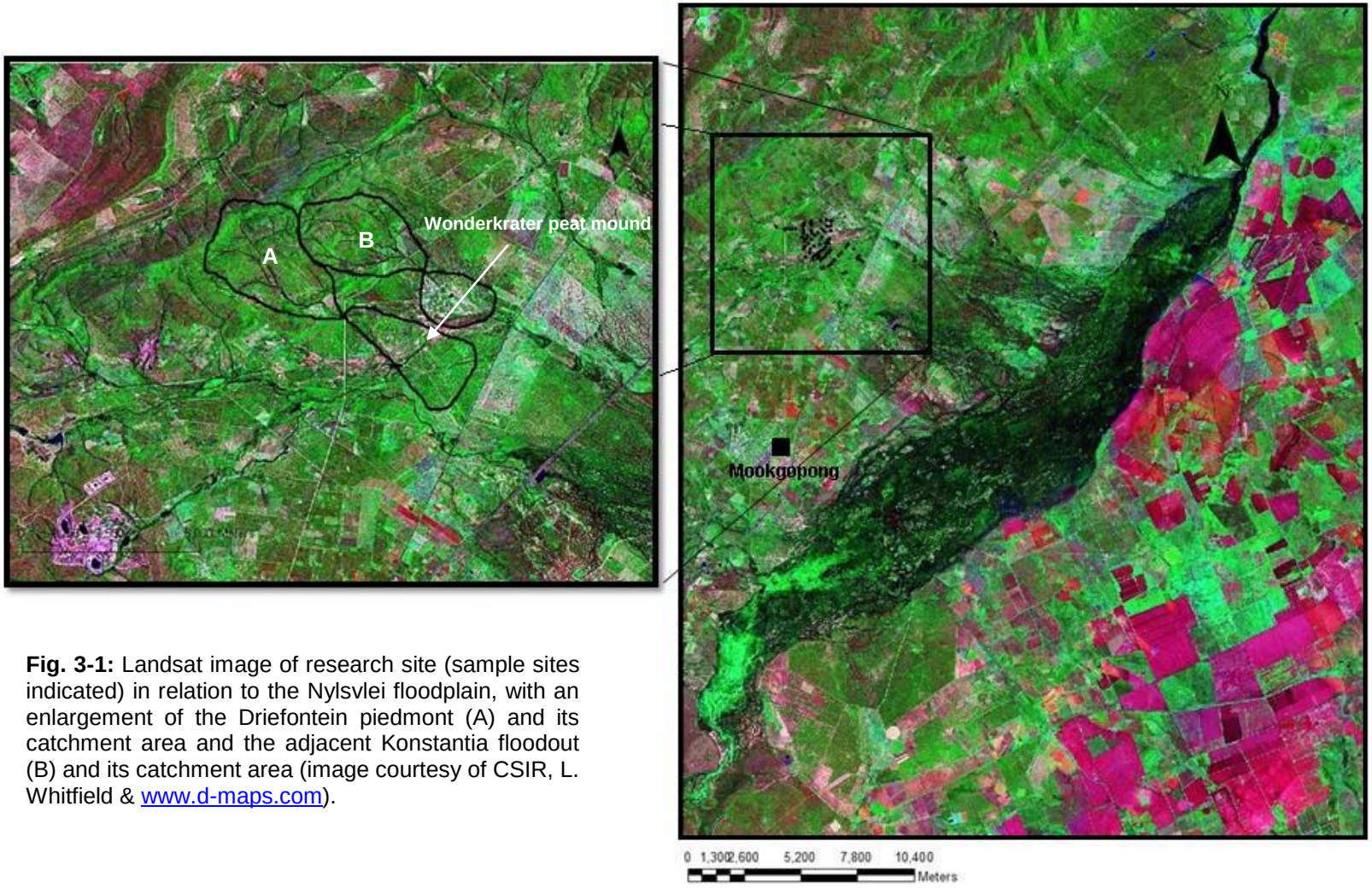

Fig. 3-1: Landsat image of research site (sample sites indicated) in relation to the Nylsvlei floodplain, with an enlargement of the Driefontein piedmont (A) and its catchment area and the adjacent Konstantia floodout (B) and its catchment area (image courtesy of CSIR, L. Whitfield & www.d-maps.com).

Three geographical features dominate the piedmont surrounding the famous Wonderkrater peat mound: 1) the Springbok flats to the south-east, 2) the Nyl River valley running NE along the western edge of the Springbok flats and 3) the Waterberg Range and its foothills to the north-west of the Nyl River (Frost, 1987). It is at the base of these northeastern foothills that the Wonderkrater peat mound and its surrounding piedmont are situated. The aggrading piedmont has a catchment area of roughly 8km^2, and is skirted by the Constantia spruit (or stream) and its floodout to the northeast (Fig. 3-1), and the Tobias spruit and its channels to the southeast. The Koodoesfontein channel which supplies the piedmont, along with the nearby Tobias spruit and Constantia spruit are subject to seasonal rainfall, while the peat mound and its stream are spring fed and thermal.

3.1.2 Hydrology

Along its northward bound course the Nyl River loses confinement near the town of Mookgopong (Naboomspruit) and becomes the unchanneled system known as the Nylsvlei (Frost, 1987; Tooth & McCarthy, 2007). The north bank tributaries of the Nyl River similarly lose confinement and merge with the unchanneled floodplain (Fig. 3-2). The Nylsvlei floodplain itself is underlain by a ~35m thick sedimentary deposit (Tooth et al., 2002). Approximately 25km NE of Mookgopong, the floodplain narrows and the channel reforms as the Mogalakwena River which eventually drains its waters into the eastward flowing Limpopo River (Frost, 1987; Tooth & McCarthy, 2007).

The Nyl River and its tributaries are generally perennial with highly seasonal flow and infrequent flooding events (Tooth & McCarthy, 2007). The north bank tributaries of the Nyl floodplain (or Nylsvlei) arise in the Waterberg Mountains forming incised valleys. As these tributaries approach Nylsvlei, relative relief, channel width and depth decrease, until ultimately, the channels disappear completely, forming broad sedimentary aprons or piedmonts which merge with the unchanneled floodplain (Tooth et al., 2002; McCarthy *pers. comm.,* 2010).

A water mask, based on Landsat images displaying the maximum flood extent of the Nylsvlei region (Fig. 3-2), indicates a westerly extension of the Nyl floodplain towards the eastern ranges of the Waterberg. High water levels indicated on the water mask show distributed surface inundation, rather than strongly inter-connected streams or rivers, contributing to the Nylsvlei volume. This may indicate a prominence of ephemeral streams and/or a loss of surface run-off resulting in temporarily standing bodies of water.

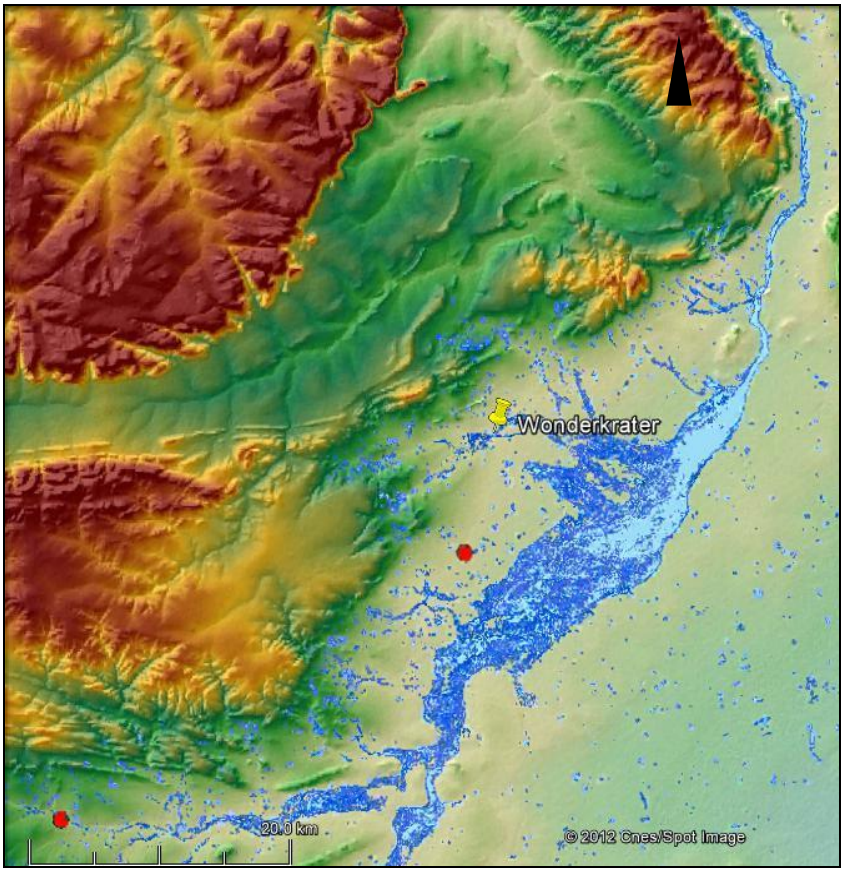

Fig. 3-2: Water mask of the Nylsvlei region, based on Landsat images documenting the maximum extent of flooding (courtesy of Rowberry, *et al.,* 2012).

Recent field observations indicated little or no evidence for channeled movement of sedimentary material across the surface of the above mentioned piedmont. Rather, small ephemeral streams were observed cutting across the surface of the piedmont after heavy rain storms. These small streams were seen to pool and form standing bodies of water which gradually infiltrated into the ground. Summer rain was observed to occur in the late afternoon as intense downpours which lasted for only a short period. This intense episode of rain resulted in the rapid formation of surface water runoff and very little channeled stream formation was observed.

3.1.3 Vegetation

The dominant vegetation type in the Nylsvlei region is characterized as a Broad-leaf Savanna of mixed thorny *Acacia* and *Combretum* woodlands, alternating with C4 grasslands and local marsh communities in waterlogged regions (Werger, 1978; Frost, 1987; Scott, 1981; Scholes and Walker, 1993; McCarthy, et., al. 2010). The strong evapotranspiration from the floodplain promotes subsurface chemical sediment accumulation (Tooth & McCarthy, 2007), while the high porosity of the Waterberg sandstone and to a greater extent the unconsolidated colluvial and alluvial sediments predominating the floodplain and its piedmont, allow for significant water infiltration and potential sub-subsurface water occurrence (Higgins, 1996; Tooth *et, al.,* 2002).

The reconstruction of past vegetation types from the Wonderkrater peat cores has provided evidence for early cool conditions with a mesic Bushveld environment at around ~34ka, followed by a dryer phase which lasted up until about 25ka (e.g. Scott, 1982,1989,1999). A colder phase followed, lasting up until about 11,000 BP. and replacing much of the mesic vegetation with expansive grasslands. This cycle of warmer wet conditions followed by colder dry conditions repeated itself twice more before, such that at about 2000 BP., conditions began to warm up until, at around 1000 BP., the present mesic climatic conditions had established, and gave rise to the modern Broad-leaf Savanna and thorny Acacia Bushveld with intermittent grasslands (Frost, 1987; Scott, 1982, 1989, 1999, Scot *et al.,* 2003; Werger, 1978).

The piedmont plains surrounding Wonderkrater spring are dominated by Acacia woodlands with *Acacia tortilis, A. karoo* and *A. mellifera*, while *Phragmites australis* reeds and hygrophilous grasses and *Carex acutiformis* sedges dominate the artesian spring mound (Scott, 1982; McCarthy *et al.,* 2010). Such Broad-leaf Savanna woodlands generally display high species diversity.

3.1.4 Geology

The Nylsvlei region is underlain by early Proterozoic granites, felsites and minor gabros of the Rooiberg Group which, in the eastern parts, are unconformably overlain by the sandstones, conglomerates and trachytic lavas of the mid-Proterozoic Waterberg Group, which is discordantly overlain by the sandstones, mudstones and basalts of the Permo-Triassic Karoo Supergroup (McCarthy *et al.,* 2010; Higgins, 1996). Regional active tectonism has resulted in large-scale faulting. Several springs occur along these NE-SW trending faults, some of which are classified as thermal springs (Kent, 1949).

The Formations which make up the Waterberg Group are composed of mostly red/purple and brown/orange coloured arenites, with minor conglomerates and siltstones, ranging from very coarse-grained to a fine-grained sedimentary material. The Waterberg Group is divided into three Subgroups: Kransberg, Matlabas and Nylstroom (Fig. 3-3). The Nylstroom Subgroup hosts the Swaerhoek Formation which consists of arenites and rudites at the base of which a thick lava unit occurs. The Swaerhoek Formation is believed to have been deposited as a fan-delta, while the overlying Alma Formation was deposited as bajada-forming alluvial fans, and consists of arkoses, feldspathic arenites, subarenites, and minor lava flows which occur in the south-east (Barker *et al.,* 2006).

The Matlabas Subgroup overlies the Nylstroom Subgroup in a conformable-to-unconformable manner. The Matlabas Subgroup consists of the Skilpadkop Formation, composed of lithic arenites and pebble rudites which were deposited as

braided river systems, while the overlying Aasvoelkop Formation which, due to the lack of chemical sediments, is believed to have been deposited in a shallow lake setting and consist of mainly lutites and arenites.

The Matlabas Subgroup in turn is overlain by the Kransberg Subgroup which, in its south and central region, is composed of the Sandrivierberg, the Clermont and the Vaalwater Formations (Barker *et al.,* 2006). The Sandrivierberg Formation is composed of coarse-grained arenites and rudites, and is thought to have been deposited by large braided rivers. The Clermont Formation overlies the Sandrivierberg Formation, and comprises well-sorted, well-rounded quartz arenites, which are believed to have been deposited in tidally influenced shoreline settings. While the overlying Vaalwater Formation is believed to have been deposited in protected, low-energy environment, and is composed of feldspathic arenites and lutites (Barker *et al.,* 2006). The Nylstoom and Matlabas Subgroups display crude upward-fining cycles. Younger trachyitic lavas are found only in the upper parts of the Swaershoek Formation (Barker *et al.,* 2006).

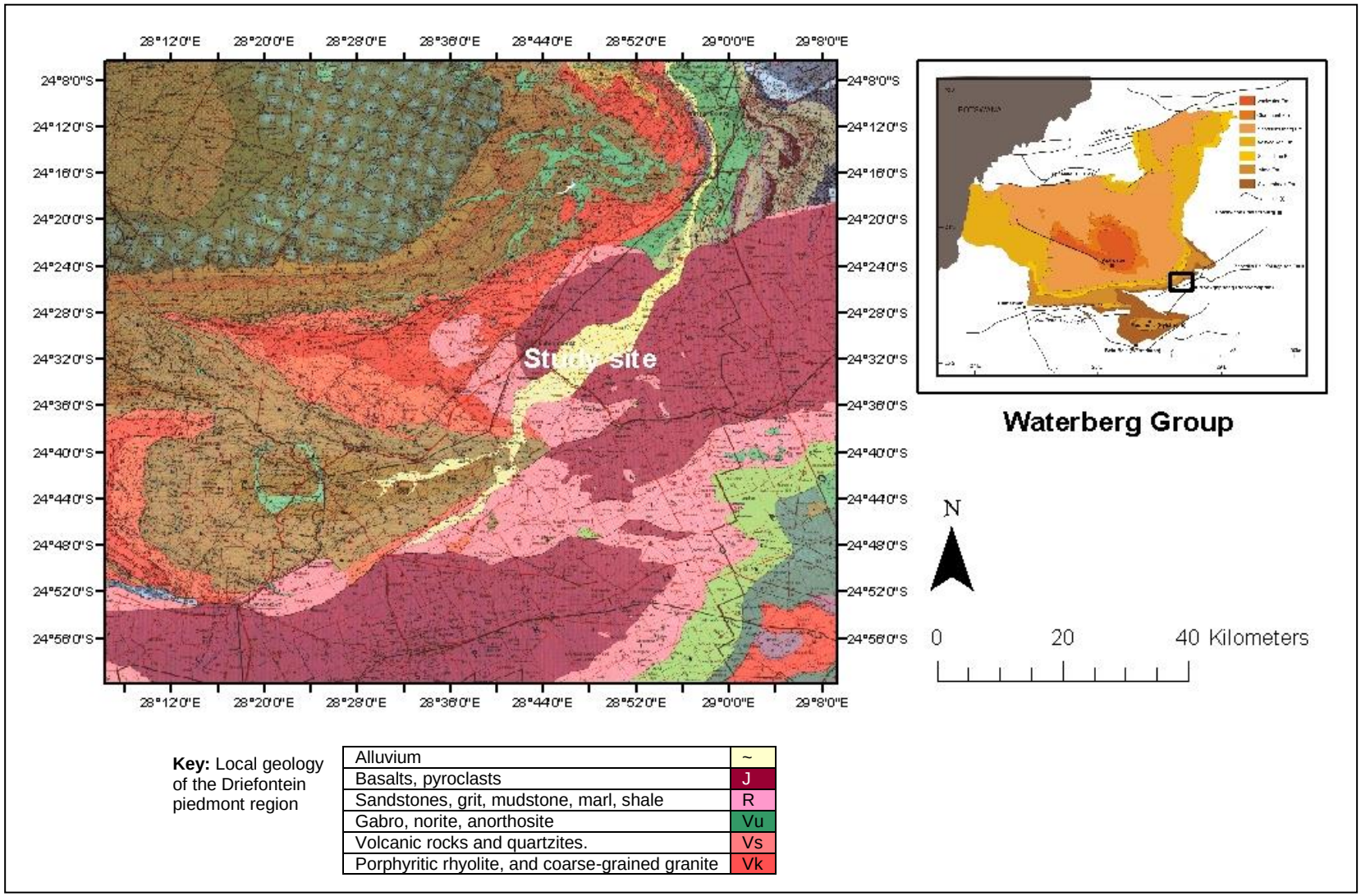

Fig. 3-3: Geological map of the Waterberg Group and its Formations (a) (after Barker *et al.,* 2006; Geological Survey, Pretoria, 1978) with inset of local geology surrounding the Driefontein piedmont and the Wonderkrater peat mound (b) (courtesy of the University of the Witwatersrand School of Geoscience).

The Karoo Supergroup is a significant deposit in Southern Africa and is associated with thick glacial deposits, flood basalts, fossil and plant assemblages, and dolerite dykes and sills. In South Africa the deposits of the Karoo Supergroup cover an area of around 700 000 km^2, of which a smaller but still significant deposit is found skirting the Waterberg Supergroup in the Springbok flats area. The Nylsvlei runs northward through the Springbok Flats basin, which is fault bounded to the north and is composed of the Dwyka, Hammanskrall, Irrigasie and Clarens Formations (Johnson, *et al*., 2006). The Dwyka strata comprise mudrock, diamictite and conglomerate, along with minor coal seems, while the Hammanskraal strata, overlying the Dwyka Formation, is comprised of immature sandstone, and shale with coal. The Irrigasie strata, overlie the Hammanskraal Formation, and comprise of fining-upward sequences ranging from conglomerates through to mudstones. The youngest strata found in the Springbok Flats Karoo basin, is the Clarens Formation which comprises fine-grained, well-sorted pinkish-white quartzose sandstones (Johnson, *et al*., 1997).

The Waterberg mountain range was formed during the subsequent uplift of the fault-bounded Waterberg basin along the tectonically active Melinda fault to the north, and the Zebedila fault to the south (Barker *et al.,* 2006; McCarthy *et al.,* 2009). Subsequent large scale regional faulting and the subsidence of the igneous Bushveld Complex during the Neogene resulted in the downfaulting of the Karoo strata and the formation of a synclinal feature that today hosts the Springbok flats and the Nylsvlei floodplain (McCarthy *et al.,* 2009). The spring feeding the Wonderkrater peat mound is situated on just one of a series of fault splays which fan out from the Zebedila Fault; a major east-west striking fracture zone which coincides with the large Thabazimbi-Murchison Lineament (McCarthy *et al.,* 2009).

3.1.5 Climate of the Nylsvlei region

The present climate associated with the Nylsvlei region is described as being arid to temperate, with winter periods being dry and the majority of rain (~ 85 %) falling as heavy frontal thundershowers during peak summer months, usually from December

through to February (Frost, 1987; McCarthy *et al.,* 2010). This results in a hot, dry savanna-type steppe (Frost, 1987). The long-term average annual rainfall is ca. 620 mm, with a mean annual temperature of 18.6 °C, and a potential evapotranspiration rate of ca. 2400 mm per annum, potentially resulting in a large moisture deficit (Tooth & McCarthy, 2007; Higgins, 1996; Scholes & Walker, 1993; Frost, 1987). In regions of high precipitation variability, the erosive effect of rain drops is generally greater, due to fluctuating vegetation cover and high runoff coefficients (Tooth, 2000; Thorns, 1994a). Pollen records from Wonderkrater cores indicate that climatic conditions for the area ca. 35 000 years ago were much cooler and moister, giving way to much more arid conditions around 11 000 BP (Scott, 1982).

3.2 Selection of study site

This site was selected both for its proximity to the Wonderkrater peat mound because of its well established chronology, as well as being located in an area which remains relatively undisturbed and devoid of intensive surface soil utilization, and cultivation. With the area surrounding the Wonderkrater peat mound remaining relatively undisturbed, its ecology and surface processes remain essentially intact, being influenced almost entirely by natural forces only. A small dam draining the Tobias spruit on the western edge of the piedmont region may affect some of the surface drainage in the south-west region of the piedmont surface. However, this area was not included in the study area. The Driefontein farm is currently a game farm, and any prior use appears to have been primarily for grazing of livestock and there is no evidence that the area was ever cleared of vegetation for crop planting.

The Wonderkrater peat mound itself is located on the Driefontein farm in Limpopo Province, South Africa (24º25’80.60S; 28º44’62.60E), where it rises about 3.5m above the surrounding elevation of an approximate altitude of ~1,100m above sea level (McCarthy, *et al.,* 2010). The piedmont surrounding the Wonderkrater peat mound is referred to as the Driefontein piedmont. The sediments of the aggrading piedmont interlace with the Wonderkrater peat mound, suggesting that as the piedmont aggrades, so too does the peat mound (e.g. Scott, 1982; 1989; 1999; 2002;

Tooth, *et al.,* 2002; McCarthy, *et al.,* 2010, Backwell, *et al.,* 2012). The slope of the Driefontein piedmont at 0.08° (0.14%) is only very slightly inclined. Samples from quartz-rich layers along the edge of the peat mound were dated using OSL, in order to establish the rate of aggradation of the Driefontein piedmont.

4 Methods

Cross-sections, drainage channels and vegetation indices based on topographic maps, orthophotographs and hyperspectral images, were created in order to describe the surface morphology and hydrology of the Driefontein piedmont in detail. Surface soil samples were collected in order to determine particle size distribution which could then be compared to vegetation density and changes in slope elevation. Sedimentary core samples were collected from the edge of the Wonderkrater peat mound for dating using Optically Stimulated Luminescence (OSL), and to determine grain size distribution at depth, and to compare these with results from the Driefontein piedmont surface sediments, as well as various previously described fluvial settings.

4.1 Surface morphology and vegetation

In order to describe the surface morphology of the Driefontein piedmont, the slope aspect was determined by drawing cross-sections based on a 1:10 000 topographic orthophotograph with 5 m contour intervals. Cross-sections were drawn starting from the mountainous Waterberg terrain directly above the head of the piedmont, and fanning south-east across the entire sampled surface of the Driefontein piedmont. Further cross-sections were drawn trending parallel to the Waterberg mountain range.

Channels visible on the orthophotograph, were traced and overlain onto a digital elevation model (DEM) using ArcGIS. A DEM of Wonderkrater and its surrounding piedmont was created using ArcGIS and Grass. Georeferenced maps with 5 m relief

lines (courtesy of the CSIR) were used to create the DEM, which was done using the TopoRaster tool in Grass GIS.

The occurrence and density of vegetation along the length of the slope was examined in relation to the piedmont using multispectral Landsat MSS images. In order to establish the distribution and relative type of vegetation occurring along the Driefontein piedmont surface, a Normalized Difference Vegetation Index (NDVI) was created using a multispectral Landsat MSS image. NDVI values are generated by contrasting the amount of absorbed red light with the amount of reflected near-infrared light. Based on resulting NDVI values, an image can be created to display relative biomass, while at the same time compensating for changing illumination, surface slope, and aspect (Lillesand, *et.al,* 2004).
The following ratio was calculated:

$$NDVI = ((IR - R)/(IR + R)) \quad (1)$$

NDVI values near zero indicate rock or bare soil, while negative values may represent the presence of water or water-stressed vegetation, both of which reflect less near-infrared. Healthy green leaves strongly reflect near-infrared, while absorbing high values of red light due to the presence of chlorophyll. Low positive NDVI values between 0.2 - 0.3 are indicative of shrubs and grasslands, while high values between 0.6 – 0.8 indicate temperate to tropical forests (www.earthobservatory.nasa, 2012).

4.2 Sample collection

Samples were collected in the field on four separate occasions during 2010. The samples for OSL were collected from Pit C (Backwell, *et al.,* 2012) located on the of the Wonderkrater peat mound, and sub-surface analysis were collected in 2010 late January during the wet season to make drilling and excavation easier, while the surface samples were collected during May once the rainy season had come to an end and most of the standing surface water had subsided. All the core and OSL

samples from Pit C, along with the surface samples WK-A through to WK-H, were collected on the Driefontein farm, courtesy of Dr W. Ward (farm owner). The LF samples were collected on the farm directly east of, and adjoining, Driefontein farm courtesy of the Mr. L. Fourie (local farm owner). All of the laboratory and granulometry work was carried out in the OSL laboratory at the School of Geoscience and the School of Precision Engineering (courtesy of Mr. Sigala) of the University of the Witwatersrand.

4.2.1 Surface samples

Surface soil samples were collected in order to determine the nature of sedimentary material on the presently active surface. The samples were collected on successive field trips. 76 surface soil samples were collected along transects (A – H) covering the extent of the active depositional surface of the Driefontein piedmont slope (Fig. 4-1). Transects were arranged perpendicular to the length of the central slope of the Driefontein piedmont, and therefore the general direction of water flow. The nature of the dense Bushveld vegetation and the thick clusters of thorn bushes which dominate the Driefontein piedmont, made sampling along exact transects and with equal distance between the sample points very difficult.

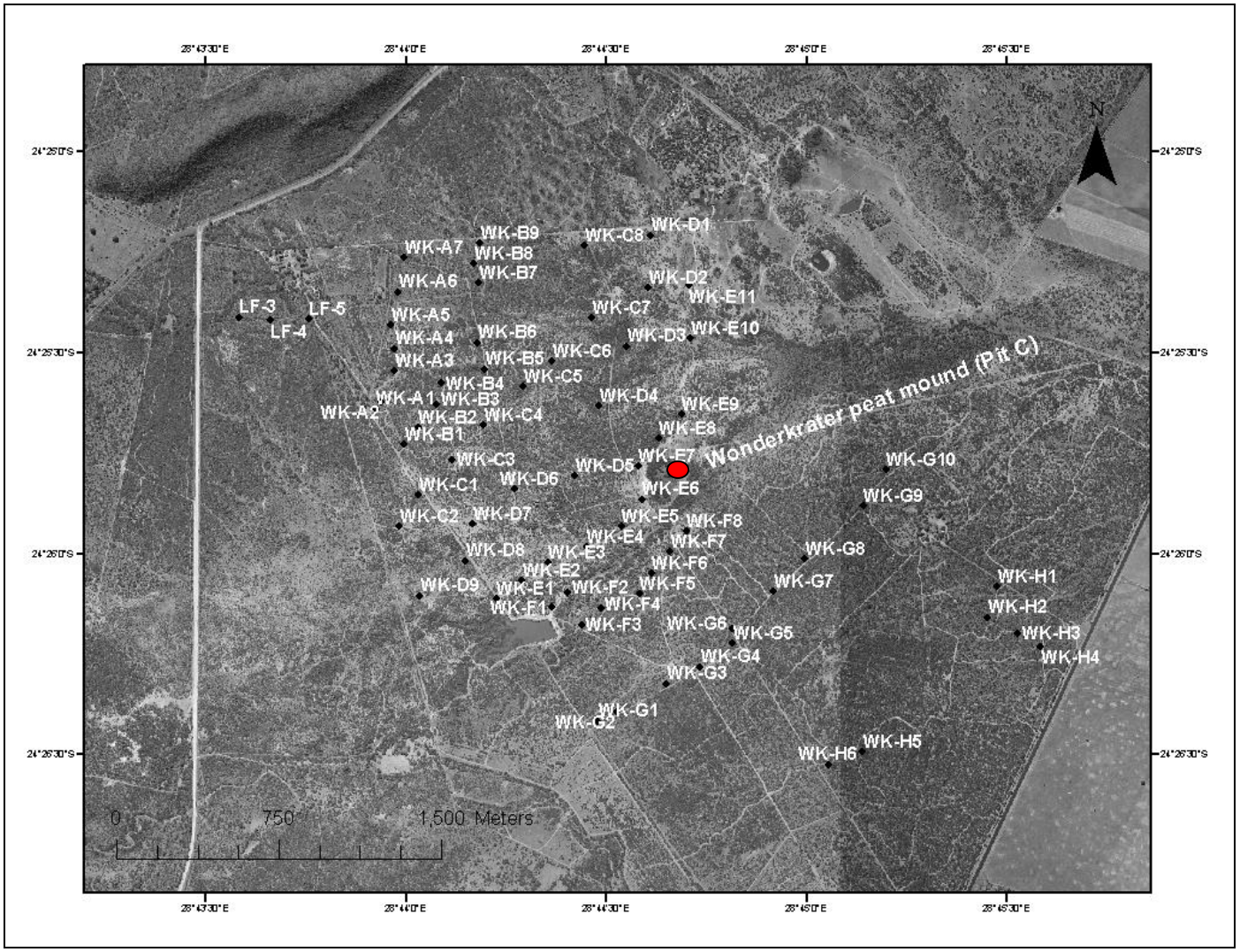

Fig. 4-1: Enlarged orthophotograph of the Driefontein piedmont, indicating the sampled surface transects along with their allocated sample names (courtesy of CSIR and L. Whitfield).

The samples were collected at approximately 100 m intervals from each other. A small shovel was used to collect the soil samples reaching a maximum depth of 10 – 15 cm. The individual sample localities were recorded using a Garmin eTrex GPS. Surface samples (LF) were also collected on a subsequent field trip along the length of the main feeder channel upstream from the point of dispersal where the channel empies onto the surface of the Driefontein piedmont (LF-3, -4, and -5, see Fig. 4-1). These samples were collected along the length of the channel as well as within the channel itself, which was dry at the time of sampling (see APPENDIX I, Table A-1 for coordinates of sample collected along the Driefontein piedmont).

4.2.2 Sediment sampling from depth

Samples for OSL dating were collected from Pit C (Backwell, *et al.,* 2012) located on the edge of the Wonderkrater peat mound during late January 2010 (Fig. 4-1). Pit C was dug out using a back-actor in order to expose a clean vertical stratigraphic face (Fig. 4-2). Five OSL samples, WK1-125, WK1-135, WK1-155, WK1-180 and WK1-220, were collected at depths of 125cm, 135cm, 155cm, 180cm and 220cm from surface (Fig. 4-3 a and b).

Fig. 4-2: Excavation of Pit C in order to expose a clean vertical stratigraphic face for OSL sampling.

With each OSL sample core, two additional cores were taken from within 40cm of the OSL sample core location in order to determine the palaeodose or background radiation which is generated through the U, Th and K content of the soil. The sample tubes, upon removal from the exposed face, were sealed and wrapped up in thick black plastic bags and then placed within black plastic containers for transport in order to insure that the sediment was not exposed to sunlight during the process of collection. The samples were only opened again once they were within the red light illuminated OSL laboratory.

Fig. 4-3: a) Hammering in of OSL sample tubes into sand lenses of Pit C. b) Vertical measurement of sample depths from surface.

An approximately 7m deep sediment core (WK2) was drilled directly behind the exposed vertical face in Pit C, from where the OSL samples were retrieved. The core was drilled using a percussion drill. Prior to removal from the drill core, the sediment samples were separated into 10cm interval segments. Colour and composition was documented (Fig. 4-4 a, b and c), and samples were sealed into plastic bags for transport and subsequent particle size analysis. Due to the nature of the wet peat and sediments, some core was lost due to slumping or compaction during drilling.

Fig. 4-4: a) Drilling of WK2 using a hand held percussion drill. b) Extraction of WK2. c) Onsite sample documentation and d) cutting of samples into 10cm intervals prior to packing.

Of the WK-2 core, 55cm was lost to compaction or slumping making an accurate correlation with the OSL samples difficult. Representative samples from sandy layers in the WK2 core were treated and sieved using the same methods as for the surface samples. The representative core samples were sieved such that everything smaller than 2000µm was analyzed using laser diffraction (Malvern Mastersizer). The particle size distribution of WK2 was interpreted using Gradistat, while the composition of WK2 was plotted up using a core logging tool called STRATER.

An attempt was made during later field trips, to drill to the bedrock in order to determine the thickness and particle size distribution of the alluvial-colluvial cover along the length of the Driefontein piedmont. However, these attempts were unsuccessful. Due to the dry conditions later in the year, and the very fine-grained

nature of the sedimentary material, large amounts of core was lost down-hole during extraction, making it impossible to collect sufficient material in order to establish a continuous stratigraphy.

4.3 Laboratory work

All of the samples collected in the field were opened, treated and analyzed in the red-light illuminated dark-room of the sedimentary laboratory at the University of the Witwatersrand. All the collected soil samples were treated and cleaned prior to analyzing. The water content of the OSL samples was established by determining the net weight of each sample prior to and after drying in an oven at 50ºC over night.

Once dried, the samples were cleaned using a treatment of 32 % hydrochloric acid (HCl) followed by a treatment of hydrogen peroxide (H_2O_2). Following cleaning, the grains were dispersed using potassium pyrophosphate in preparation for particle distribution analysis and OSL dating: Dried samples were first placed into beakers, where they were submerged in the hydrochloric acid in order to remove any carbonates occurring within the sediments. All of the samples were stirred periodically over a minimum period of four hours or otherwise until any reaction within the beaker had ceased. The samples were then rinsed several times with distilled water and dried again at 50°C. Following this, the samples were submerged in hydrogen peroxide in order to remove any organic matter. The hydrogen peroxide treatment also lasted a minimum of four hours. After rinsing each sample carefully again with distilled water, the grains were dispersed using potassium pyrophosphate-97%, after which they were rinsed repeatedly until clean and then dried for the last time at 50ºC. A portion of each of the clean WK1 samples was sent off to the OSL laboratory at the University of the Witwatersrand where further treatment of the grains was carried out prior to determining the OSL ages.

4.3.1 Granulometry

The size and shape of a particle occurring within any sedimentary deposit is of a direct result of the 'entrainment, transport and depositional conditions' under which the sediments were deposited (Pye & Blott, 2004, pg. 19). Therefore, the Particle Size Distribution (PSD) is a viable indicator of the nature and environment under which deposition took place. The sediments collected from the Driefontein piedmont and Pit C along the edge of the Wonderkrater peat mound, were analyzed to determine their particle size and frequency using sieving methods as well as laser granulometry. Luminescence dating was carried out on samples taken from Pit C.

The use of standard sedimentological sieves is still one of the most common methods of determining particle size of sediments. The mass percentage of grains present within each sieve size interval can be determined either in weight percent or volume percent (Blott & Pye, 2004; Krumbein & Sloss, 1951). Sieving is suitable mainly for the analysis of material greater than 63 micron in diameter (sand and gravel). Modern laser granulometry instruments are capable of analyzing particle sizes ranging from 0.04–2000 µm (Pye & Blott, 2004). Understanding the particle size distribution of a sample, as well as describing the grains texturally, facilitates the interpretation and comparison of the particle's behaviour during erosion, transportation and deposition (Krumbein & Sloss, 1951). Mean, standard deviation (or sorting) and skewness were plotted for the grain size distributions using SigmaPlot 11 (a graphic statistical tool). Size distributions are described numerically or graphically, which commonly includes the use of histograms and cumulative frequency curves.

Laser granulometry instruments are able to accurately analyze a wide range of unconsolidated particles, while requiring only minimal sample material (Blott & Pye, 2004). However, due to the manner in which grain size frequencies are measured, results obtained using different methods should not be combined if the samples are of non-uniform composition. The laser granulometry method determines particle size using a mathematical approximation model, whereby comparing the manner in which

the laser scatters or diffracts when chancing upon the sample particles (http://www.malvern.com). The resulting particle size distribution is calculated as a volume % rather than a mass %, which is common in standard sieving methods (Blott & Pye, 2004; Allen & Thornley, 2004).

The WK1 sediment samples from Pit C were cleaned and then sieved, using both standard sedimentology sieves at ¼ Φ intervals and lasergranulometry. The standard sieves are cut off at 63 µm or 4 Φ, and none of the WK1 samples had any notable silt fraction. The piedmont surface samples however, were found to be much finer-grained than the WK1 samples. For these surface samples, the loss of the clay and silt fraction was avoided by analyzing each surface sample using the Mastersizer 2000 granulometer, Version 5.40. To ensure that none of the grains were greater than 2800µm (-1.5 Φ), samples were sieved at 2800µm, but the majority of samples contained little of such material. The fraction smaller than 2800 µm was analyzed using a laser granulometer set to analyze PSD from 2800µm - 0.010µm (-1.5 Φ – 16.6 Φ). Repeat analyses were made at intervals in order to ensure test-reproducibility. Due to the mixed mineralogy of the samples, the density of the different size fractions might vary, making the combination of results from the laser granulometer with the sieving method inadvisable.

Results from both the sieving and the laser granulometery were analyzed using Gradistat, a particle size distribution and statistics package for the analysis of unconsolidated sediments (Blott & Pye, 2001) which can be applied to any of the standard measuring techniques e.g. sieving and laser granulometry. Gradisat was used to calculate and plot mean, mode, sorting and skewness both arithmetically and geometrically (in metric units) and logarithmically (in phi units) using moment and Folk and Ward graphical methods (Folk & Ward, 1957; Blott & Pye, 2001).

Conversion from diameter (D) in metric units to phi units (Φ):

$$\Phi = \frac{-\text{Log}(D/1)}{\text{Log } 2} \quad \text{where } D = \mu m/1000 \qquad (2)$$

Graphs of mean grain size vs. skewness, kurtosis vs. skewness and standard deviation vs. skewness were plotted after Friedman (1961) for the Driefontein piedmont surface samples, as well as the OSL samples from Pit C. Each moment for each sample was calculated after Folk and Ward (1975), using cumulative frequency curves on the phi (Φ) scale results:

$$\text{Graphic Mean: } M = \frac{\Phi 16 + \Phi 50 + \Phi 84}{3} \qquad (3)$$

Where the graphic mean (*M*) is the average particle size category, and 'takes into account the physical effects of the magnitude of the particle diameter' (Koldijk, 1968, pp 58)

$$\text{Graphic Standard Deviation: } D = \frac{\Phi 84 + \Phi 16}{4} \qquad (4)$$

The standard deviation (*D*), when calculated from the entire grain-size distribution, is a measure of the sorting degree, also known as the sorting index, and accurately describes the variation in grain size (Koldijk, 1968)

.

$$\text{Graphic Skewness: } S = \frac{\Phi 84 - \Phi 16 - 2(\Phi 50)}{2(\Phi 84 - \Phi 16)} + \frac{\Phi 95 + \Phi 5 - 2(\Phi 50)}{2(\Phi 95 - \Phi 5)} \qquad (5)$$

Graphic skewness (*S*) indicates whether the grain size distribution is bell shaped or skewed to right or the left, depending on the tails of the frequency distribution curve. Skewness has been demonstrated to be the most sensitive parameter in discriminating between sediment types when plotted against standard deviation (Friedman, 1967; Koldijk, 1968).

From the WK2 core, ten representative samples were chosen for granulometry. Samples were chosen where major mineralogical changes were observed. The samples were taken from depths of 105cm, 180cm, 225cm, 290cm, 345cm, 370cm, 405cm, 450cm, 565cm and 625cm respectively. All the WK2 core samples were cleaned and prepared as in section 3.3, and analyzed for particle size distribution using the same methods as those applied for the Driefontein piedmont surface samples. Results from the laser granulometer were analyzed using Gradistat.

4.4 Grain size contour intervals and surface flow

A contour map of the mean grain size (in phi) of the surface samples was drawn up using the GIS program ArcMap. The contour intervals were based on approximate ¼ phi intervals from the laser granulometer results, and show the mean grain size variation across the surface of the piedmont slope. The contour interval map was generated by creating an Excel spreadsheet which related the grain size results to the X- and Y-coordinates obtained from the GPS waypoints for each surface sample (refer to APPENDIX I, Table A-1). From this Excel spreadsheet, a shapefile was created in ArcCat which was imported into ArcMap10 and a feature class was created from the spreadsheet based on the X- and Y-coordinates. With the aid of the geostatistical analysis tool in ArcMap, grain-size contour lines were created. The contour lines were created using the Inverse Distance Weighted (IDW) interpolation.

A digital elevation model, or DEM, was created for the Driefontein piedmont research site using ArcMap10 and Grass. The DEM was generated using a 5m interval contour map with accurate relief lines and relief points (courtesy of Wits Geography Department). The visible surface channels found in the Driefontein piedmont region

were traced using a 1:10 000 orthophotograph and, once georeferenced, were overlain onto a DEM image as a shapefile using ArcGIS.

4.5 Roundness index

Once the sediment samples were clean, dried, and sieved, the roundness index (based on Powers, 1953, Table 3.1) was determined for the WK1 samples from pit C, as well as for three representative surface samples (L-7, WK-C4, and WK-G4) selected to represent the entire length of the piedmont (see APPENDIX I, Figure A-1). A comparative roundness index chart (Table Table 4-1) was used (abbreviated from Powers, 1953; Briggs, 1977) to compare the grains which were viewed using a 60 x magnification. For each sample a random selection of forty or twenty individual grains, depending sample size, were examined from grain size intervals of 2800-1400 µm, 1400-1000 µm, 1000-700 µm, and 700-500 µm (or from 1.5-0 Φ). The grains were analyzed microscopically, and roundness, sphericity, and composition were determined optically for each sample size interval.

Table 4-1: Comparison chart for visual roundness index (Briggs, 1977; Powers, 1953)

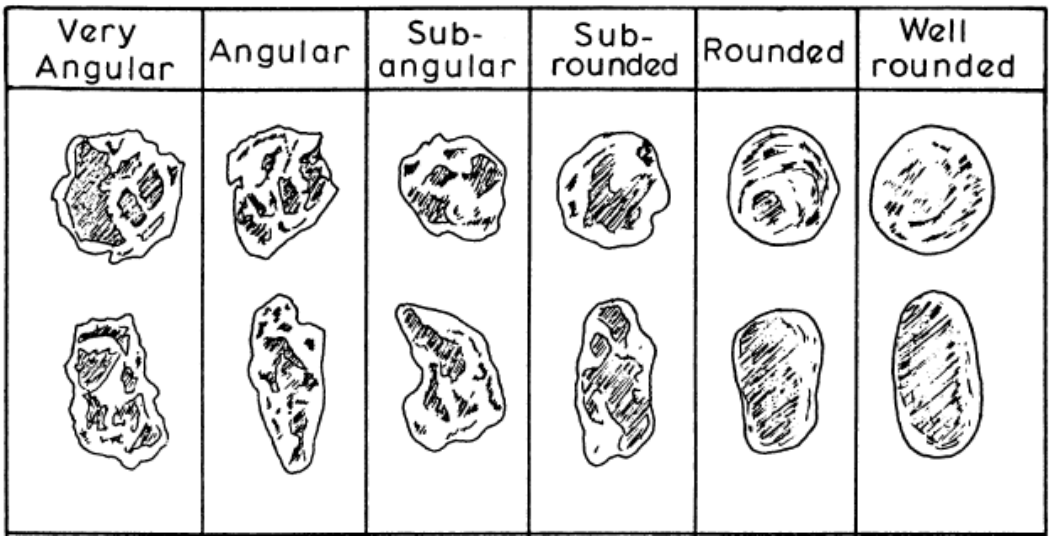

4.6 Grain composition

The mineral grain composition of the WK1 samples and three representative surface samples (L-7, WK-C4, and WK-G4) were also determined optically. The grain samples chosen for each grain size interval, used in determining the roundness index, were simultaneously analyzed for their mineral composition. The clean grains were identified as Quartz, feldspar and carbonates, based on optical properties such as cleavage, colour and luster. Any volcanic or micaceous material would have been removed from the samples during HCl treatment. The grain composition for the surface and sub-surface samples were plotted on a ternary diagram as percentage of total sample using SigmaPlot11.

4.7 OSL dating

Optically simulated luminescence (OSL) is an absolute dating method used to determine the time of deposition of quartz-rich sediments. This method involves the use of quartz grains, which prior to analysis, are separated from heavy minerals, feldspars, and other contaminants using density separation and chemical treatment. The method involves a datable signal which is obtained from the grains by shining a beam of light onto them. Luminescence is emitted by the grains, which is measured by a light sensitive device (e.g. a photomultiplier). This emitted signal is a measurement of the last time the grains were exposed to sunlight, either during transportation or deposition, and prior to burial. This exposure to light is known as the bleaching event (Aitken, 1998). This bleaching event sets the quartz grain's latent luminescence signal, acquired during periods of deposition when they are no longer exposed to sunlight, to zero, as the photon 'traps' found within imperfections of the quartz grains' crystal lattice are emptied of any nuclear radiation. The efficiency with which these traps are 'emptied' however is variable, depending on the effectiveness with which each grain was exposed to sunlight during transportation and deposition; the remaining radiation trapped within the grains is known as the residual signal.

Once buried and no longer exposed to sunlight, the latent signal of the grains begins to build up due to the presence of the weak ionizing radiation of thorium, uranium and potassium-40, found in all sedimentary material in varying proportions depending on the parent material and the age of the deposit. The ionizing radiation from the surrounding sediment is known as the *dose-rate,* which will vary from site to site and must thus be measured for each OSL sample taken. In order to determine the age signal of any quartz grain, the nuclear radiation dose, which induced the bleaching event prior to burial, must be experimentally determined in a laboratory using a calibrated source; this dose is known as the *palaeodose* (Aitken, 1998). The OSL age (in years) is determined by dividing the *equivalent dose (D_e)(Gy)* (or total energy accumulated during burial) by the *dose rate (Gy/year)* (or the energy delivered each year from radioactive decay in the surrounding soil) (Duller, 2008):

$$\text{Age} = \frac{\text{Palaeodose (Gy)}}{\text{Dose-rate (Gy/annum)}} \qquad (6)$$

However, in practice, there are many complications to consider when calculating the dose-rate and the palaeodose of each OSL sample. In light of this, multiple sample runs are usually carried out. The most suitable grain size range for OSL dating is 100-200µm (Susino, pers. com., 2010) which narrows down the sample size markedly. Due to long-term variations in the earth's geomagnetic field and the continuous variation in cosmic ray intensity across the surface of the earth, accurate altitude, latitude and depth measurements need to be taken from the OSL sample site. Suitable adjustments need to be made according to the location of the sample site in order to determine the intensity, and hence the contribution of cosmic radiation to the final dose rate of the samples (Prescott & Hutton, 1994, Fig 2). Inhomogeneity of ionizing elements found in the material surrounding the OSL samples, as well as the level of water saturation, can skew the dose-rate and as a result the final age determination (Susino, *pers. com*., 2011). Sample preparation proceedings carried

out by the University of the Witwatersrand were recorded on an Excel spread sheet as part of the laboratory records (Table 4-2).

Table 4-2: Step by step procedure of WK1 sample preparation and treatment prior to OSL analysis, courtesy of the University of the Witwatersrand OSL laboratory

Date: 08/02/2010

Samples No.1,2,3,5, Re-etched 07/07/2011

No.	sample code	water content					etching					sieving							etching				
		empty beaker (g)	beaker & wet sample (g)	dry in oven	beaker & dried sample (g)	W (%)	HCL	H_2O_2	$K_4P_2O_7$	rinse with D.W.	dry in oven	- um	90 - 106 um	180 - 212 um	rinse with D.W.	dry in oven	H.M. separation	dry in oven	H_2SiF_6	HF(40min)	rinse with HCL	dry in oven	pack to container
1	WK1/125	184.312	602.356	x	515.288	26.31	x	x	x	x	x		x	x	x	x	x	x		x	x	x	x
2	WK1/135	184.555	695.578	x	609.871	20.15	x	x	x	x	x		x	x	x	x	x	x		x	x	x	x
3	WK1/155	178.246	606.175	x	494.384	35.36	x	x	x	x	x		x	x	x	x	x	x		x	x	x	x
4	WK1/180	262.329	675.338	x	526.518	58.33	x	x	x	x	x		x	x	x	x	x	x		x	x	x	x
5	WK1/220	272.077	781.551	x	709.208	16.55	x	x	x	x	x		x	x	x	x	x	x		x	x	x	x

In order to determine the dose rate for the samples, ^{238}U and ^{232}Th concentrations were determined by ICP-MS at the University of Cape Town. ^{238}U and ^{232}Th concentrations and radiation intensity were calculated in Bq/kg. K_2O concentrations were measured at the School of Geoscience of the University of the Witwatersrand, using XRF from which % ^{40}K per sample was calculated. These radioactive isotope measurements were used in determining the environmental dose rate of the Wonderkrater OSL samples.

The prepared grains were analyzed by the OSL laboratory of the University of the Witwatersrand, where aliquot and single grain analysis was carried out. The measurements were made using a Risø TL/OSL-DA-15 automated reader which enables both optical and thermal stimulation. The amount of radiation a sample has been exposed to since its burial along with the rate at which this dose is transmitted, enables the age determination.

The dose rate is the total amount of energy which a sample received from the surrounding environment while it was buried. The dose rate (Gy/year) is determined from the measured abundance of ^{238}U, ^{232}Th and ^{40}K (expressed as bequerrels/kilogram (Bq/kg)). The equivalent dose (D_e) is determined in the laboratory using either the *additive dose* method or the *regeneration* method (Duller, 2008). Recovery test results obtained from the OSL laboratory of the University of the Witwatersrand School of Geoscience are shown in Appendix II.

5 Results

The gently dipping surface of the Driefontein Piedmont is characterized by the channeled flow from the Koodoesfontein stream, its main depositional surface along the Wonderkrater peat mound, and the floodout plain beyond the peat mound where all surface flow is lost.

5.1 Surface morphology of the Driefontein piedmont

Using the ArchGIS tool, the surface geomorphology and spatial dynamics currently active along the length of the Driefontein piedmont was mapped. For all the site-specific sample names, their GPS coordinates, and their respective grain size frequency curves, see Appendix I.

5.1.1 Surface topography of the Driefontein Piedmont

Surface cross-sections of the Driefontein piedmont were drawn as both radial transects that fan out from the Koodoesfontein stream at the head of the piedmont and across the surface of the piedmont, as well as transects running parallel to the Waterberg range across the piedmont surface, from where the piedmont was narrowest in the north-west and widened towards the south-east (Fig. 5-1).

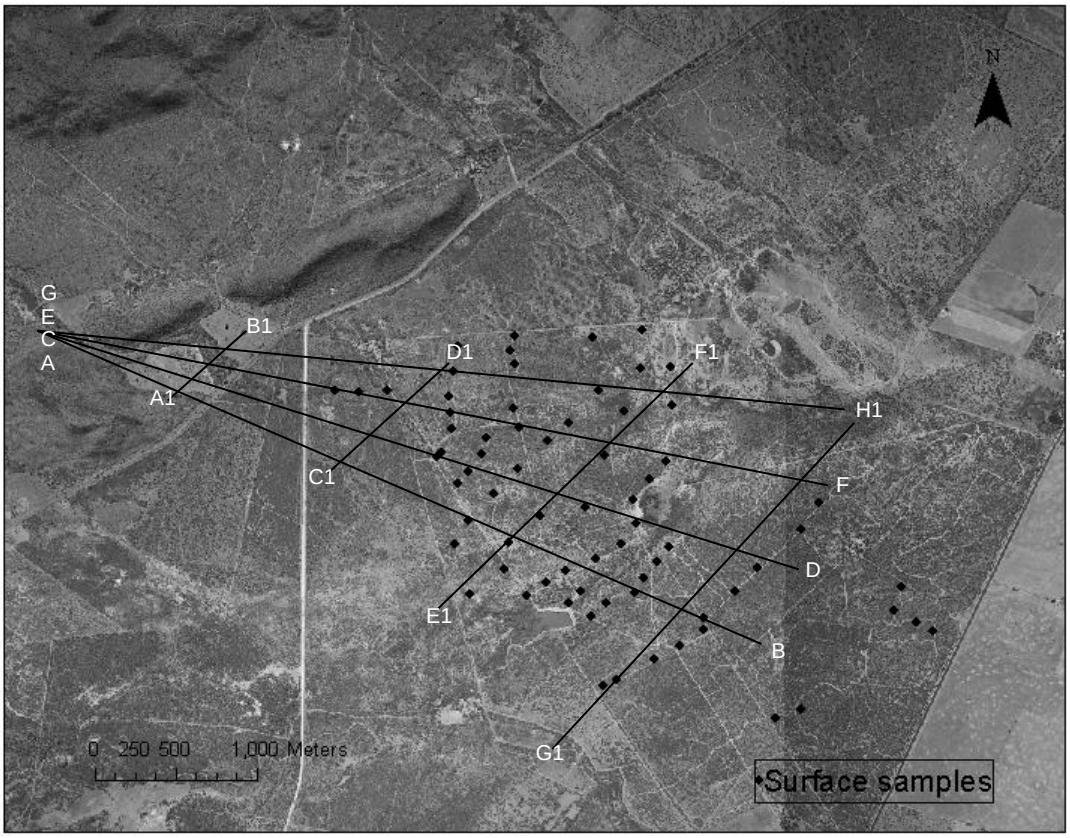

Fig. 5-1: Location of cross sections indicated on an orthophotograph: four cross-sections radiating out from the piedmont source (A-H), and four cross-sections running parallel to the Waterberg range across the surface of the piedmont (A1-H1). Sampled surface sites are indicated as waypoints.

Each cross section fanning out radially along the length of the piedmont is approximately 3500 km long (Fig. 5-2). The radial cross section curves are concave up, and change from an elevation of 1155m at the top, to 1105m near Wonderkrater, and 1095m along the depositional surface south east of Wonderkrater. A small step near the Wonderkrater peat mound is seen on the C-D cross section, which is not present in the other curves (Fig. 5-2). A distinct loss in inclination near the base of the slope is seen in all of the longitudinal cross-sections, especially in the C-D and E-F cross-sections which intercept the Wonderkrater peat mound and its feeder channel.

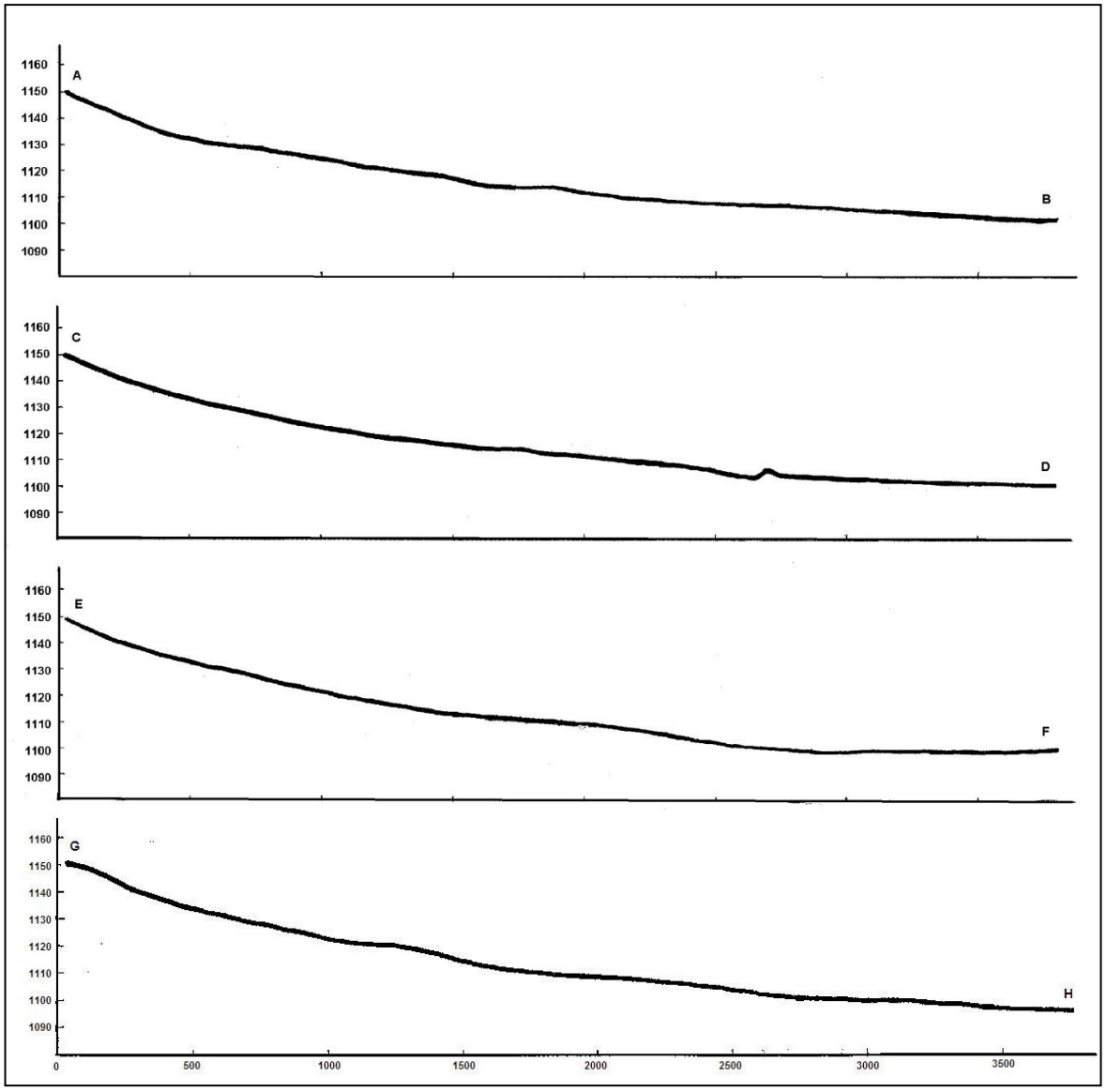

Fig. 5-2: Longitudinal cross-sections A to H fanning out radially from the piedmont apex across the length of the Driefontein piedmont (see orthophotograph, Fig**. 5-1**).

Cross-sections trending parallel to the Waterberg Range show that the piedmont slopes gently downwards towards the north-eastern sections of the Driefontein piedmont (Fig. 5-3). Parallel cross-sections C1-D1 and G1-H1 also indicate that both the upper and lower reaches of the piedmont tend to be slightly convex up (Fig. 5-3).

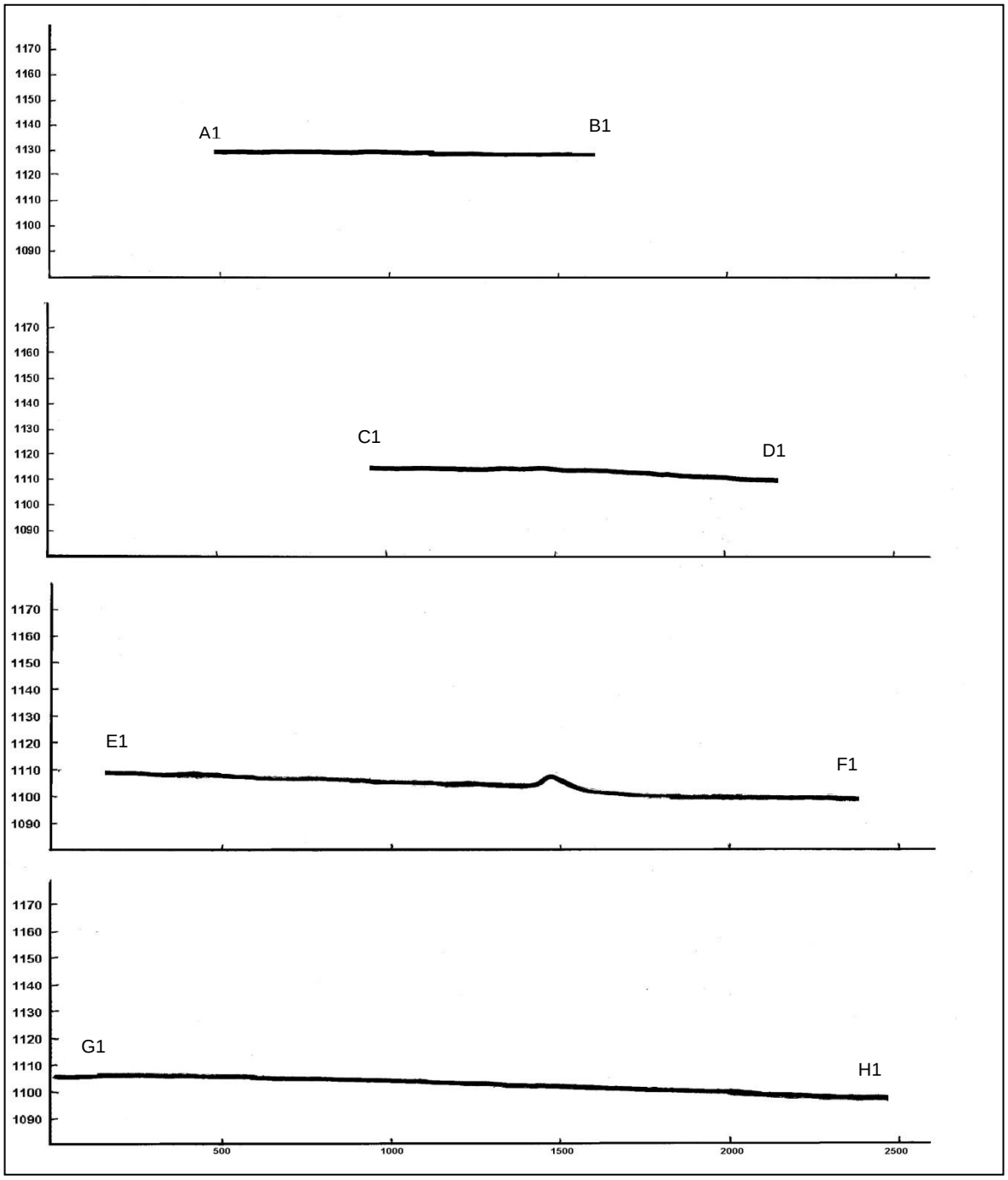

Fig. 5-3: Four cross-sections (A1-H1) trending parallel to the Waterberg range across the width of the Driefontein piedmont surface (see orthophotograph, Fig**. 5-1**). Cross section A1-B1 spans the narrowest part of the piedmont to the northwest, while cross section G1-H1 describes the piedmont surface at its widest to the southeast.

5.1.2 Surface drainage along the length of the Driefontein piedmont

The DEM shown in FigureFig. 5-4 illustrates changes in altitude based on a 5m interval contour map. Areas of high elevation are shown in green, changing through to yellow and then red with decreasing elevation. Superimposed flowlines indicate surface channels traced from a 1:10 000 orthophotograph of the Driefontein piedmont and its surrounding region. Dominant flow-direction is north-west to south-east across the piedmont surface. Channeled flow is absent in the south-eastern regions of the piedmont, where the slope gradient becomes increasingly gentle such that in the south-east it is almost flat.

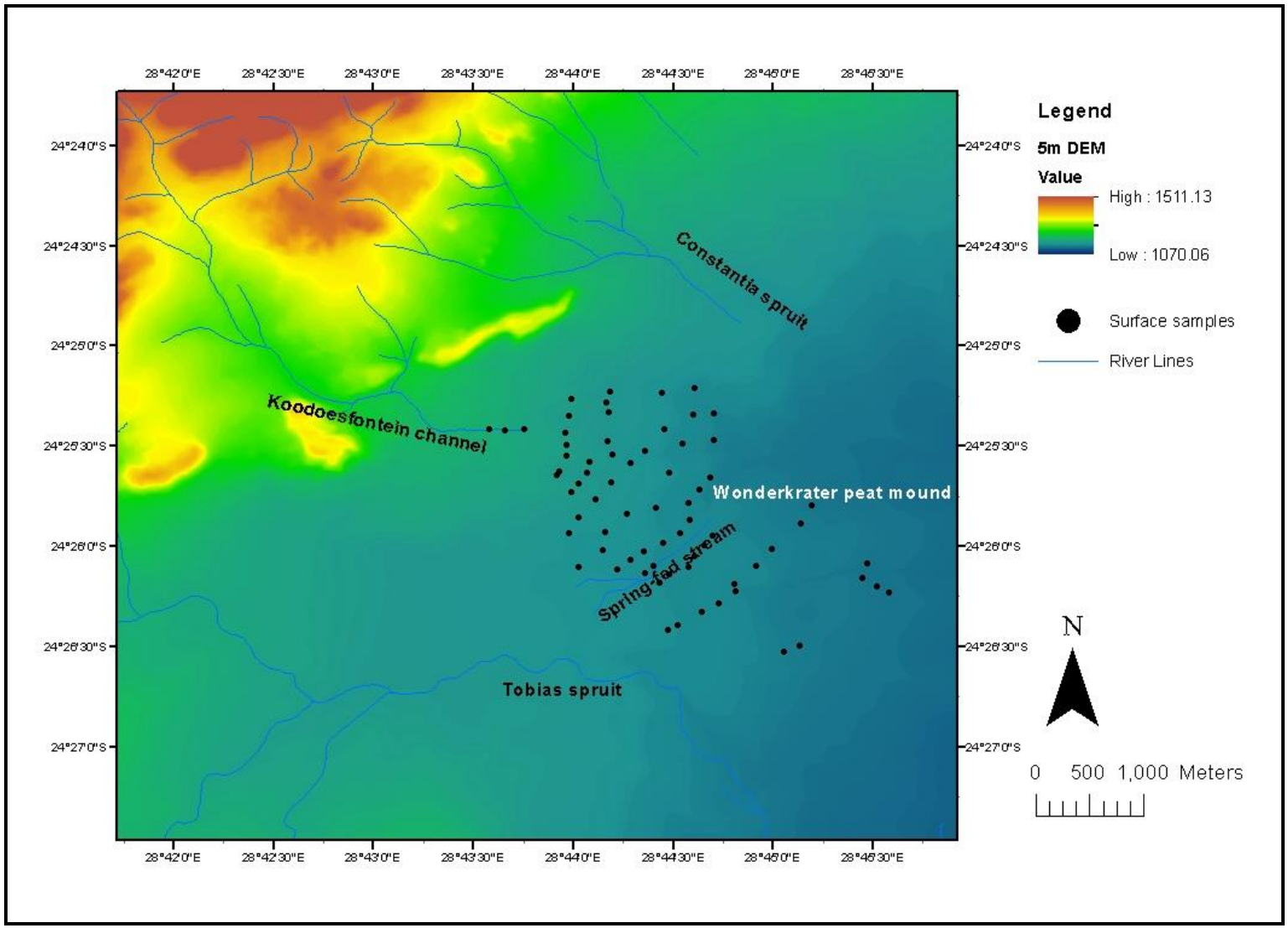

Fig. 5-4: Channels draining the Driefontein piedmont were traced from a 1:10 000 orthophotograph and were overlain on to a 5m digital elevation model of the area. Sample sites are shown as black diamonds.

5.1.3 Vegetation analysis of the Driefontein piedmont area

NDVI results for the Wonderkrater peat mound and its surrounding terrain indicate a vegetation index ranging from -0.53 to +0.77 (Fig. 5-5 a). Vegetation cover across the piedmont surface is observed to range from very sparse in the northeastern Constantia region, to very dense around Wonderkrater and the south-eastern floodout, where slope gradient is low and channeled surface flow disperses.

The NDVI results in FigureFig. 5-5a indicate temperate to tropical vegetation indices at the head of the piedmont and surrounding the peat mound, while lower indices (between 0.2 and 0.3) indicate grasslands or thorny shrubs. Values around zero are indicative of sandy patches devoid of vegetation, while negative values suggest the presence of standing surface water bodies, or regions of high soil moisture content. When relating the NDVI results of FigureFig. 5-5a to the satellite image of Fig. 5-5 b, which accentuates the vegetated regions in green, a good correlation is observed. Most of the piedmont study area is well vegetated with thorn shrubs and grassland.

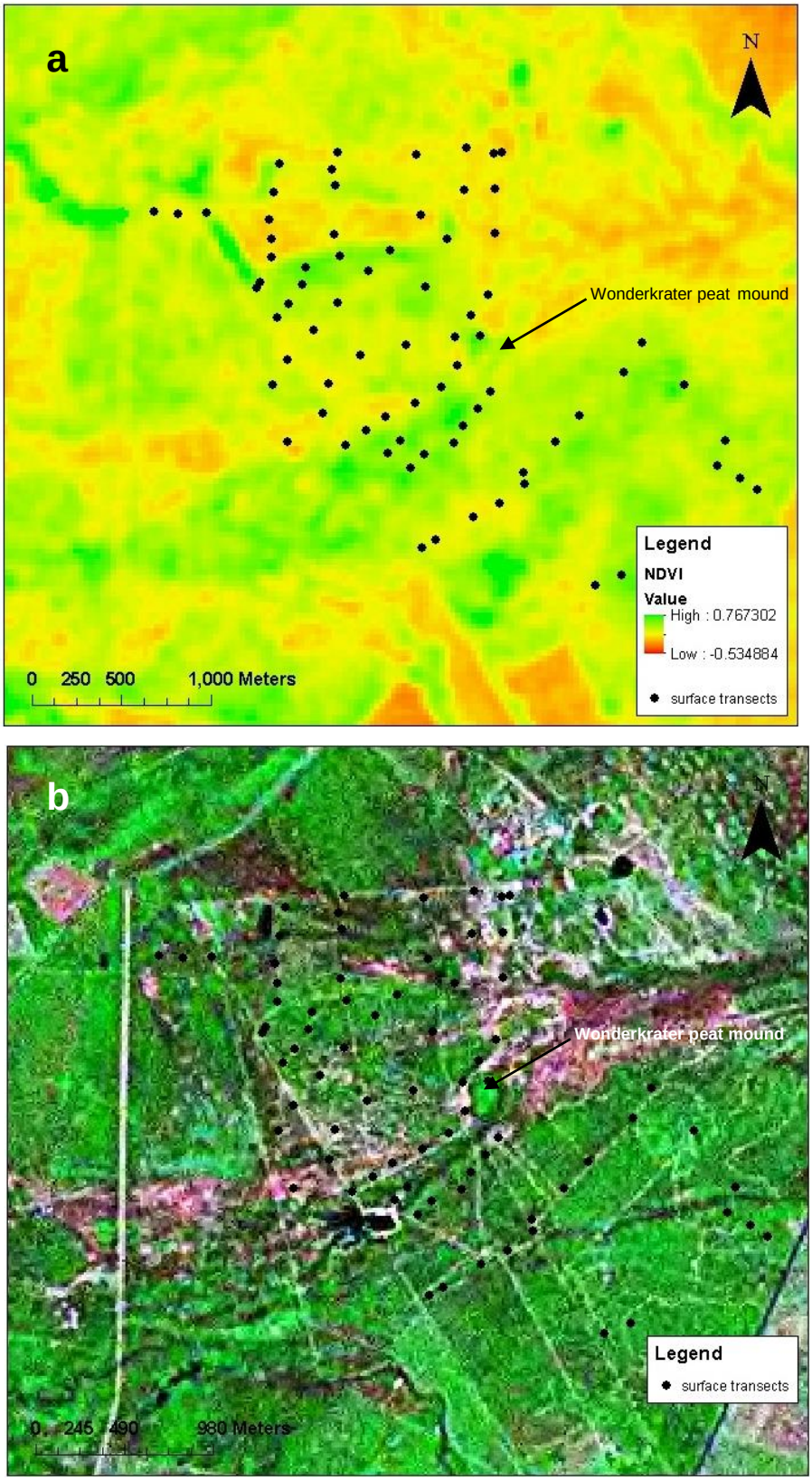

Fig. 5-5: Visual relation of NDVI results from the Driefontein piedmont and its surrounding terrain (a) with vegetation occurrence as seen on a coloured Spot satellite image (b) (courtesy of CSIR & USGS, 2012).

During field trips in 2011, the vegetation across the Driefontein piedmont surface was observed as being patchy, alternating from dense *Acacia*, to open grasslands and barren sandy sites (Fig. 5-6). Many of the sandy sites occur where there has been disturbance such as roads or animal paths. Tracks orientated in a NW-SE direction of the fan often show evidence of enhanced runoff in the form of shallow erosion gullies.

Fig. 5-6: Photograph of piedmont surface adjacent to the Wonderkrater peat mound. Patch-work of thick accacia bush alternating with open grassland areas and sandy sites.

5.2 Surface sediment characteristics

5.2.1 Grain size, sorting and spatial variation

The average grain size of surface samples ranged from 1.4 Φ in the Koodoesfontein stream, to 4.3 Φ directly south-east of the Wonderkrater peat mound. The general modality of the Driefontein piedmont surface samples tend to be either bi- or tri-modal (see Appendix I). However, south-east of the Wonderkrater peat mound where

surface flow is dispersed, the average grain-size was found to decrease noticeably and grain modality becomes more multi-modal (see Appendix I).

The average grain size of surface samples was found to be coarse grained (1.4 – 2.2 Φ or ~370 - 210 µm) in the source channels near the piedmont apex (see surface channels, Fig. 5-4), with possible influences from the Constantia and Tobias spruit regions along the north-eastern and south-western regions of the study area. Grain size becomes increasingly finer-grained down the slope of the piedmont. From the point of channel dispersion to the Wonderkrater peat mound, the mean grain size is seen to decrease from 2.2 Φ (~210 µm) to approximately 3.0 Φ (~120 µm). To the south-east of the Wonderkrater peat mound and the spring-fed steam, very fine-grained material (3.0 – 4.3 Φ or ~120 – 47 µm) appears to 'fan out' as surface flow disperses on to a depositional floodout. The grain size contours are observed to decrease in grain size from north-west to south-east across the Driefontein piedmont surface, with the exception of a localized increase in grain size in the southern region of the piedmont (Fig. 5-7).

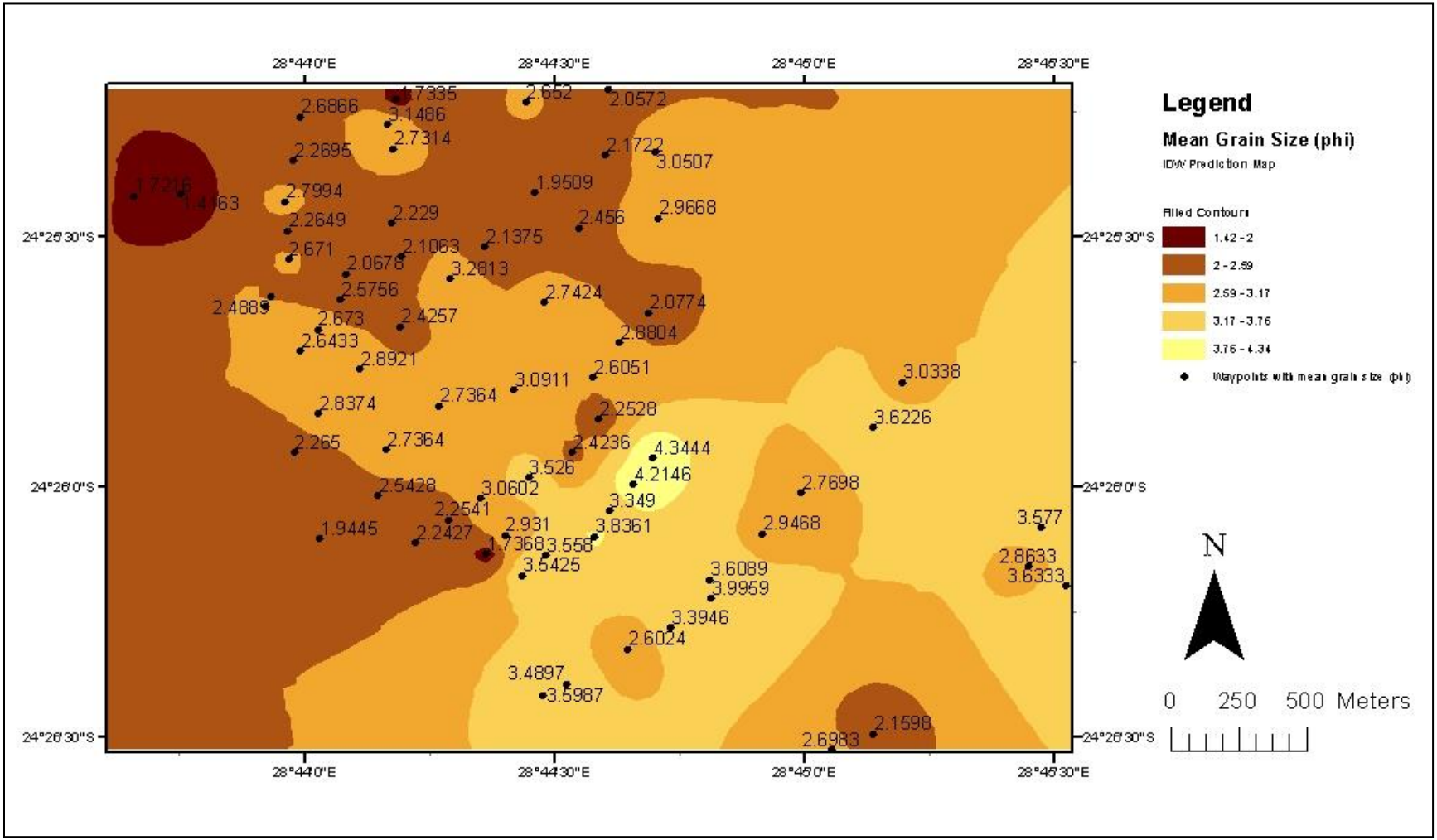

Fig. 5-7: Prediction contour map of mean grain size distribution across the Driefontein piedmont surface.

The average standard deviation, or sorting, of the Driefontein surface samples grains is 1.5 Φ (~350 µm). The standard deviation was found to decrease across the Driefontein piedmont to 1.1 Φ (~450 µm) approaching the Wonderkrater peat mound and increase again to 1.5 Φ (~350 µm) south east of the possible fault line across the floodout south east of Wonderkrater (Fig. 5-8).

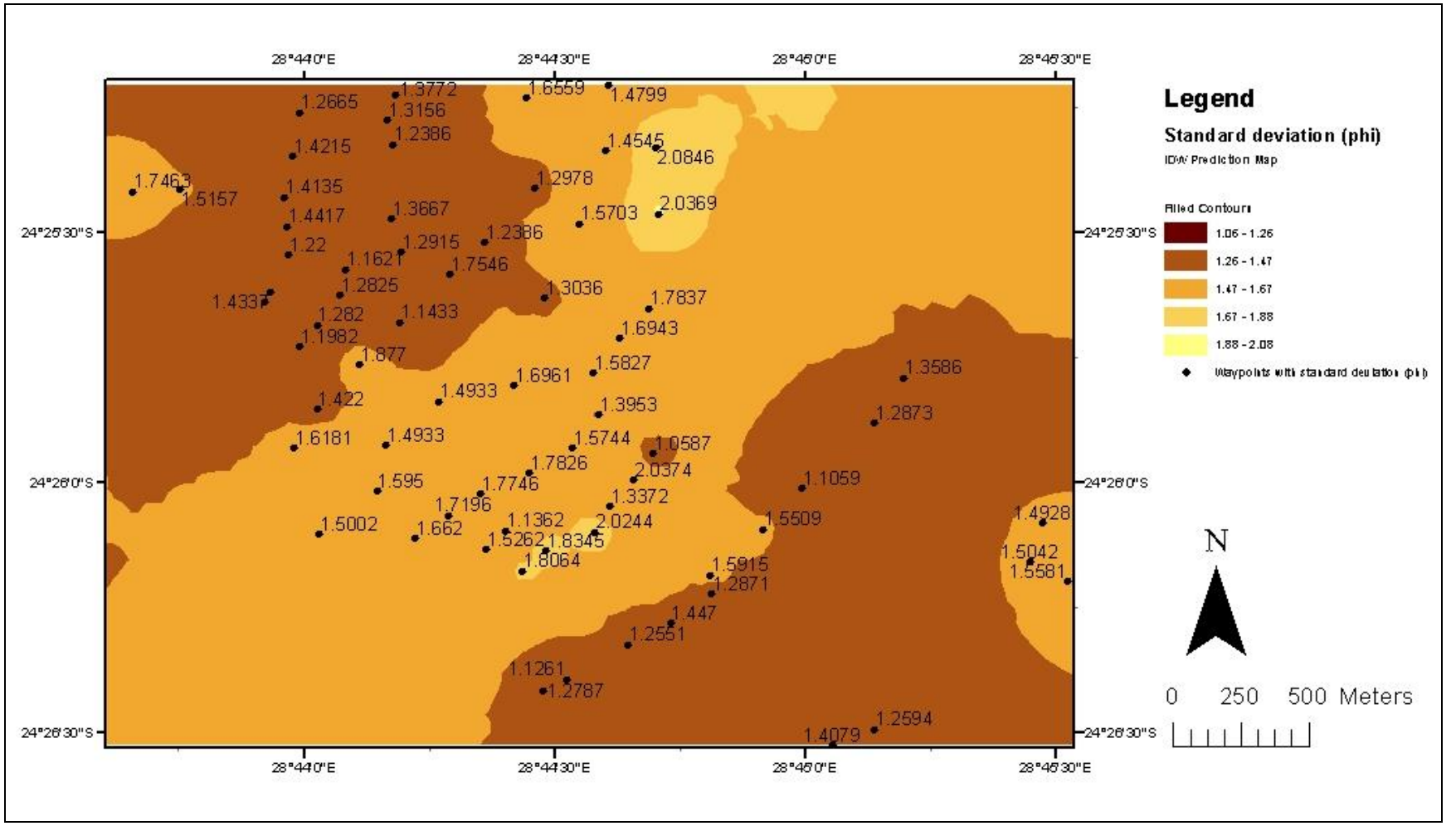

Fig. 5-8: Prediction contour map of standard deviation (sorting) of grain size across the Driefontein piedmont surface.

5.2.2 Roundness index of surface grains

Microscope results were plotted on a stacked histogram for tree selected surface samples (LF-7, WK-C4, and WK-G4). The surface samples (Fig. 5-9) indicate predominance of very angular to angular grains near the source of the piedmont (sample LF-7), becoming more sub-angular to angular near the center of the piedmont (sample WK-C4), and finally becoming almost entirely sub-rounded to rounded on the south-eastern regions of the piedmont where surface flow is lost (sample WK-G4).

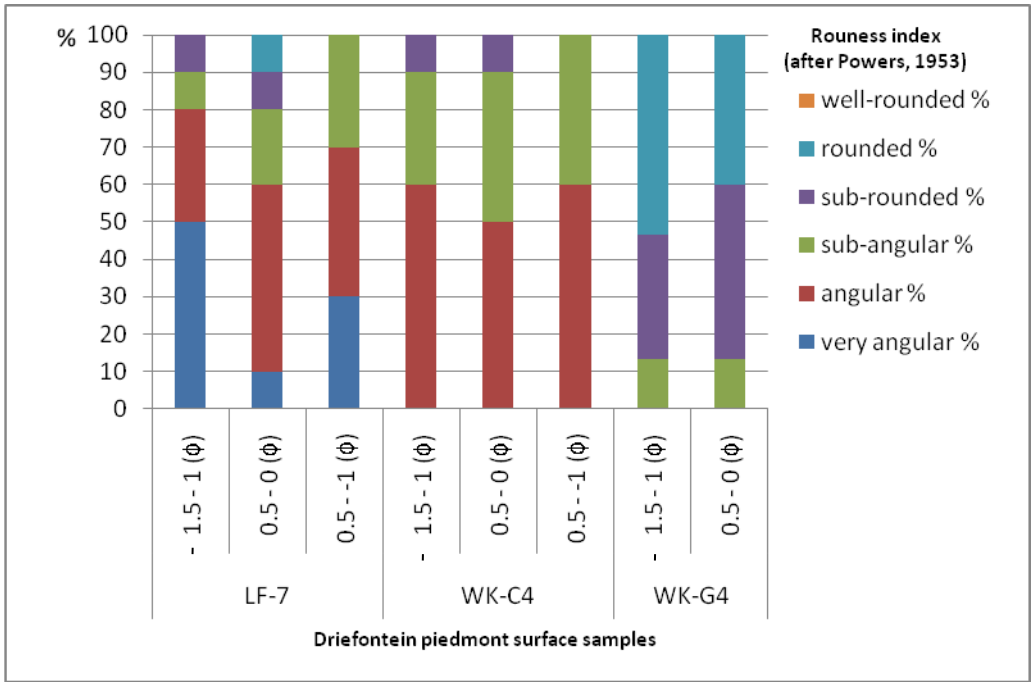

Fig. 5-9: Roundness index (after Briggs, 1977; abbreviated from Powers, 1953) of selected surface samples across the length of the piedmont from north-west to south-east: LF-7 was sampled at the source of the piedmont, WK-C4 sampled near the Wonderkrater peat mound, and WK-G4 sampled on the distal south-eastern reaches of the piedmont surface (see Appendix I).

5.2.3 Mineral grain composition of surface samples

Grain composition results for representative surface samples were plotted up on ternary diagrams (Fig. 5-10). Surface samples (samples LF-7, WK-C4 & WK-G4) from along the length of the piedmont indicate a general predominance of quartz grains, with up to 50% feldspar in the northwestern source regions of the piedmont, and highs of between 60-90% rock fragments occurring along the center of the Driefontein piedmont (please refer Fig. 4-1 for sample location). This trend of declining feldspar and rock fragments along the length of the hillslope away from the source indicates the loss of mineralogically softer grains, in the 2800 - 500µm range, due to abrasion and chemical weathering.

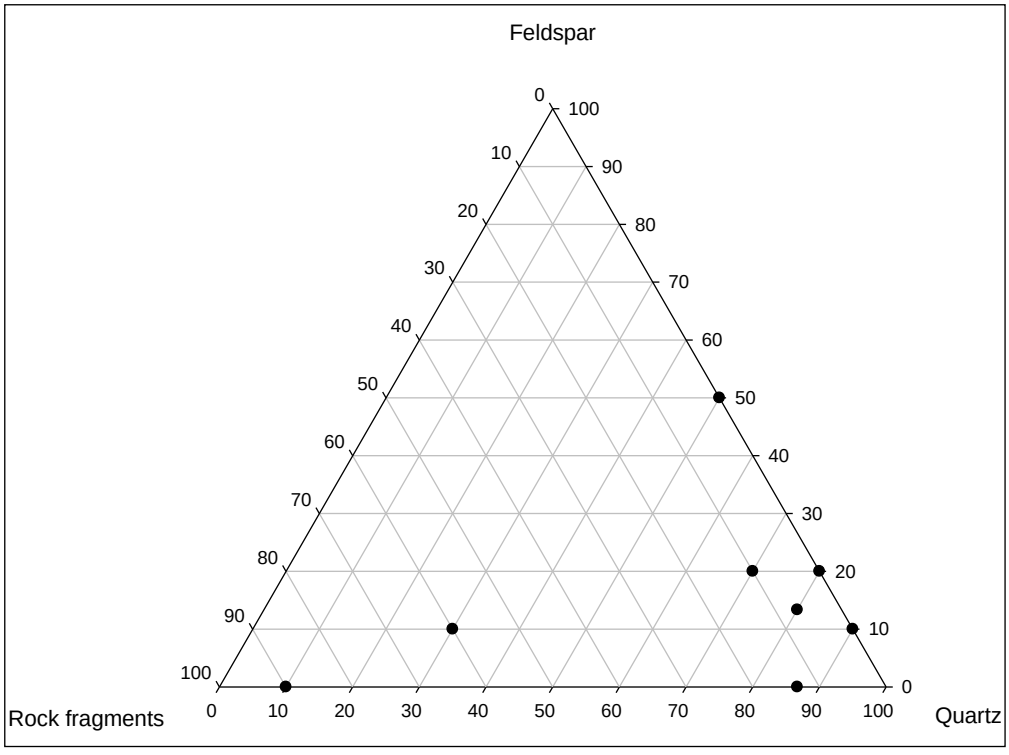

Fig. 5-10: Ternary diagram of mineral composition of representative surface samples from across the Driefontein piedmont (samples LF-7, WK-C4, and WK-G4).

5.3 Sediment characteristics of samples from Pit C

5.3.1 Grain size variation and sorting with depth

Although the WK2 core samples were analyzed for particle size distribution using laser granulometry, while standard sieving techniques were used for the samples from Pit C, the mean grain sizes of each of the two sample sites were compared graphically in order to get a sense of changing grain size with depth (Fig. 5-11).

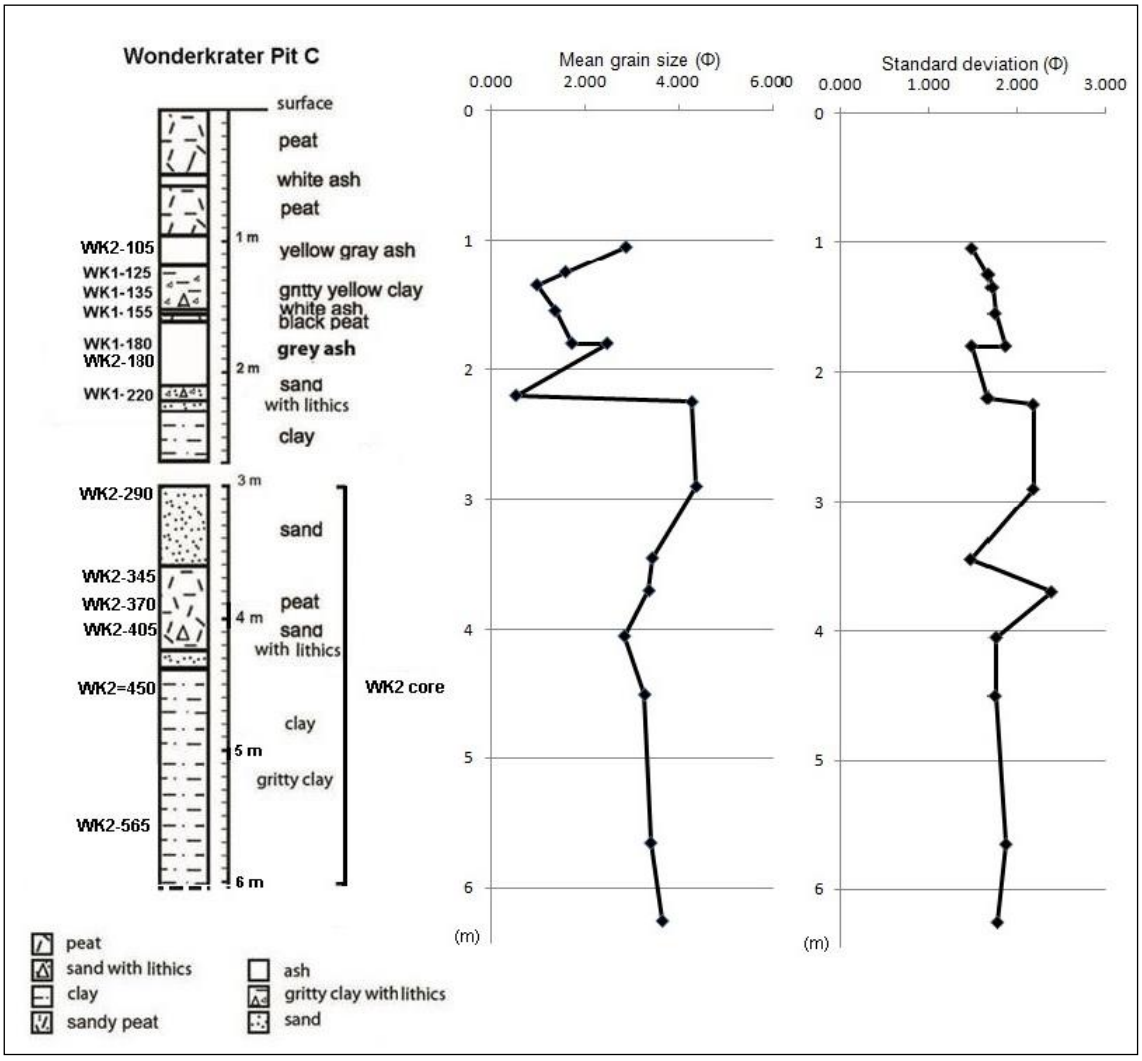

Fig. 5-11: Stratigraphic colum from Wonderkrater's Pit C (WK1 and WK2 combined), showing mean grain size and standard deviation (sorting) for each sample with increasing depth. (WK1 log curtesy of Backwell, *et al.,* 2012).

When plotting the mean grain sizes of the Pit C samples, abrupt variation in average grain size was observed within the first two meters from the surface. Mean grain size at 105 cm depth was fine-grained 2.9 Φ (~137 µm), becoming coarser grained at 135 cm depth. Between 155 and 180 cm depth, the grain size was seen to become increasingly finer-grained, ranging from 1.4 to 2.4 Φ (~391 - 181 µm), becoming coarse grained again at 220 cm depth. At 225 cm mean grain size abruptly became fine-grained again, ranging from 4.3 Φ (~52 µm) at 225 cm to 2.8 Φ (~140.5 µm) at 405 cm, and then coarsening again to 3.6 Φ (~80.2 µm) at 625 cm depth (see Appendix I for WK1 grain size distribution curves).

Although WK2 was drilled to 7m depth, there was approximately 55cm of core loss, due to slumping and/or compression of material as a result of the very wet conditions during which the samples were taken. The approximate point at which the core was either lost or compressed is estimated to have occurred just short of 3 m depth.

Overall, the sediment characteristics of the WK1 and WK2 grains were observed as being generally poorly sorted (Fig. 5-11). Between 105 and 155 cm depth, the standard deviation (or sorting index) of the sedimentary samples was observed to range between 1.5 – 1.9 Φ (~2.8 – 3.4 µm). The standard deviation was observed to vary greatest between 180 and 405 cm depth, ranging between 1.5 – 2.4 Φ (~2.8 – 5.2 µm). At depth below 405 cm, the samples were observed to display very little, if any, variation in sorting, remaining at or close to 1.8 Φ (~3.7 µm).

5.3.2 Roundness index of grains from Pit C

The roundness results of the WK1 samples from Pit C, were plotted up on a stacked histogram (Fig. 5-12). The overall roundness index of the WK1 samples was found to range from angular to sub-rounded, with the greater majority of the grains being sub-angular. Between 20 – 40% of the remaining sample tended to be either angular or sub-rounded. A slight increase in angularity, both in the finer and courser sedimentary material fraction, with increasing depth was observed in the WK1 samples. With the exception of an increase in roundness observed in the courser

grain fraction of sample WK1-180 at 180 cm depth. Overall, the variation in roundness measured in the WK1 samples, appears to be cyclic.

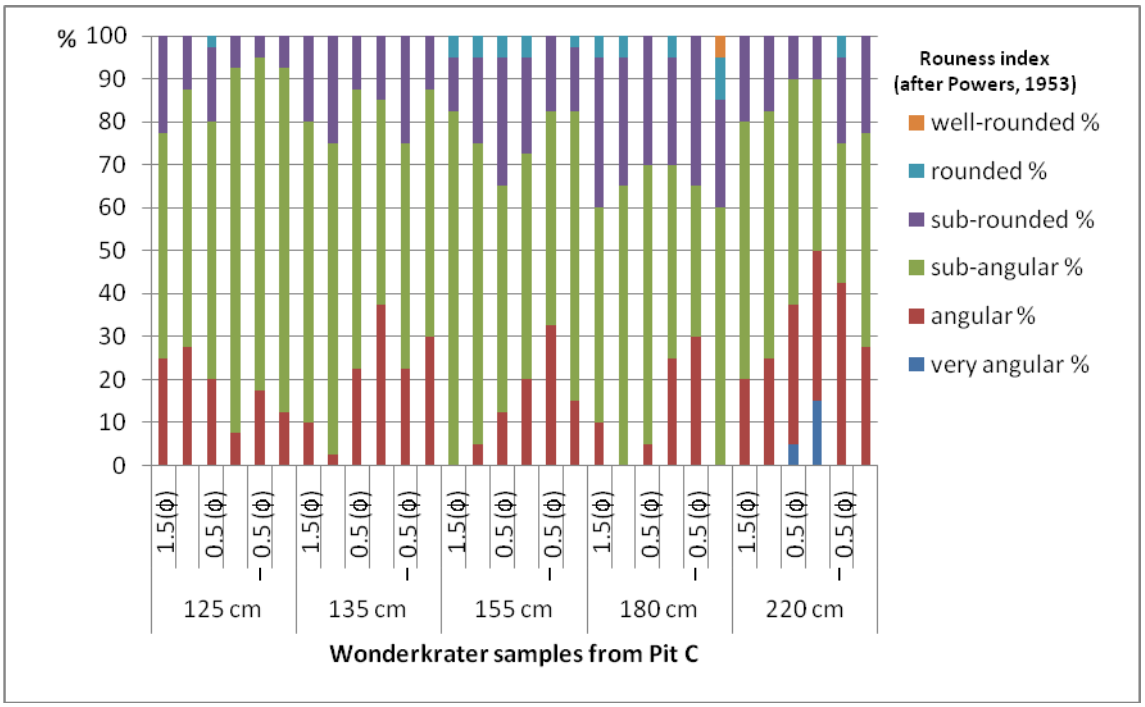

Fig. 5-12: Roundness index for the WK1 sample grains from Pit C, indicating increasing angularity with depth (from 125cm to 220cm), with a possible hiatus occurring at 180cm where well rounded grains occur in the courser grain fraction (roundness index after Briggs, 1977; abbreviated from Powers, 1953).

5.3.3 Mineral proportions at depth

Any mineral grain found occurring within the region of Wonderkrater and its piedmont should, in accordance with the local geology and parent material, consist predominantly of felsites and sandstones along with minor mafic material. During sample preparation, mineral separation separated out minor micas and heavy minerals. Optical analysis of the cleaned WK1 and surface sample grains, revealed the major mineral composition to be made up of quartz, feldspars (mostly orthoclase) and carbonates bound to rock fragments. Results for the WK1 sediment samples were plotted up on ternary diagram (Fig. 5-13).

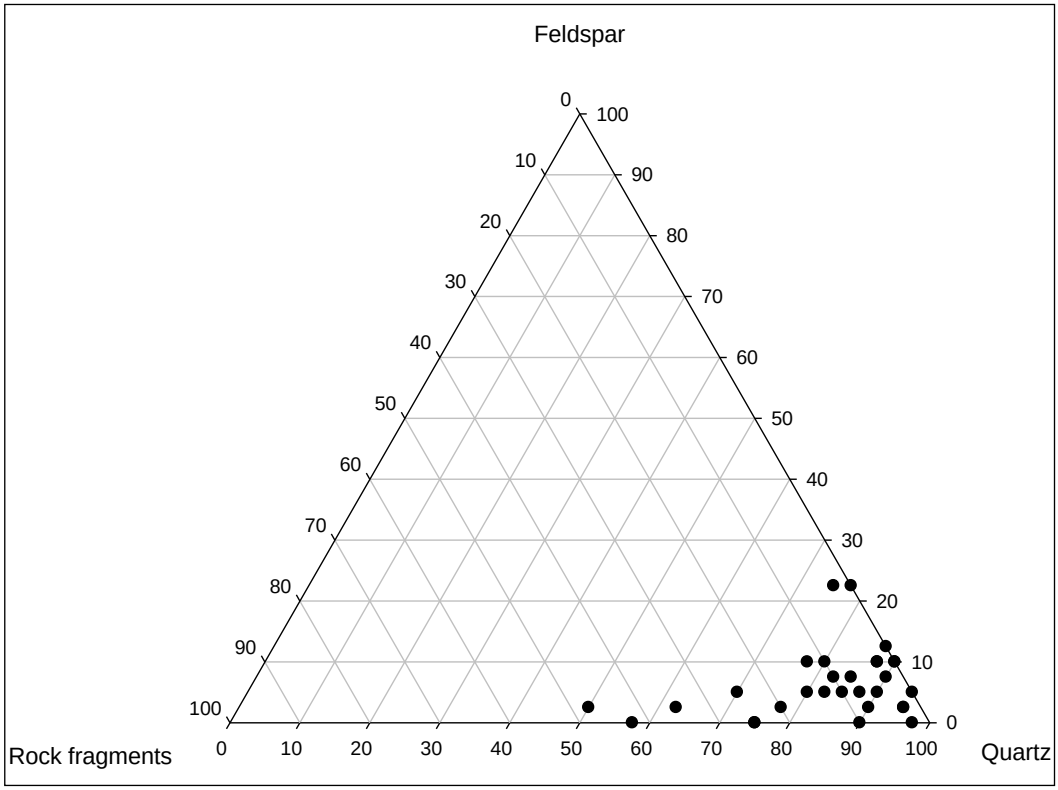

Fig. 5-13: Ternary diagram of mineral composition the WK1 samples from Pit C after the removal of heavy and light minerals using SPT.

For the WK1 samples from Pit C, between 50-90% of the grains were found to be composed of quartz, while up to 50% of the grains were composed of frock fragments with minor carbonates attached to them, and up to 24% of the observed grains were found to be feldspathic (Fig. 5-13). The WK1 samples display a relatively low percentage of feldspars and rock-fragments when compared to near-source piedmont surface samples.

5.4 OSL dates

5.4.1 Aliquot results

Aliquots from samples WK1-125, 135, 155, 180 and 220 were assessed using the OSL rejection criteria. Dose recovery tests were carried out on the WK1 aliquots (see Appendix II). However, only WK1-180 produced reliable dose recovery ratios.

A Central Age Model (CAM) was determined based on the WK1 aliquot results (Table 5-1). The results indicate an age discontinuity at WK1-155. Due to poor luminescence in four out of the five samples, aliquot results were compared with results obtained using single grain analysis.

Table 5-1: Central Age Model for the WK1 samples based on aliquot results (courtesy of OSL laboratory of the University of the Witwatersrand)

Sample	Depth	Water	Cosmic ray	Total dose	De CAM	Age CAM
	cm	Content %	Gy/kg	Gy/kg	Gy	ka
WK1-125	125	26.3	1.382 ± 0.025	2.223 ± 0.04	190.726 ± 6.82	85.78 ± 3.76
WK1-135	135	20.2	1.379 ± 0.025	3.082 ± 0.13	192.732 ± 4.86	62.55 ± 3.27
WK1-155	155	35.4	1.374 ± 0.024	2.149 ± 0.02	258.867 ± 8.63	118.16 ± 4.88
WK1-180	180	56.3	1.372 ± 0.024	1.531 ± 0.02	130.259 ± 3.44	78.59 ± 2.76
WK1-220	220	16.6	1.358 ± 0.023	1.899 ± 0.03	229.305 ± 9.38	120.76 ± 5.76

5.4.2 Single grain results

Due to the nature of the grains being analyzed, it is not uncommon for single-grain measurements to emit the same amount of luminescence as aliquot measurements, making it difficult to obtain sufficient luminescence to determine D_e. Single-grain analysis was carried out on the WK1 samples and D_e was determined with a relative maximum error of 20% (Fig. 5-14).

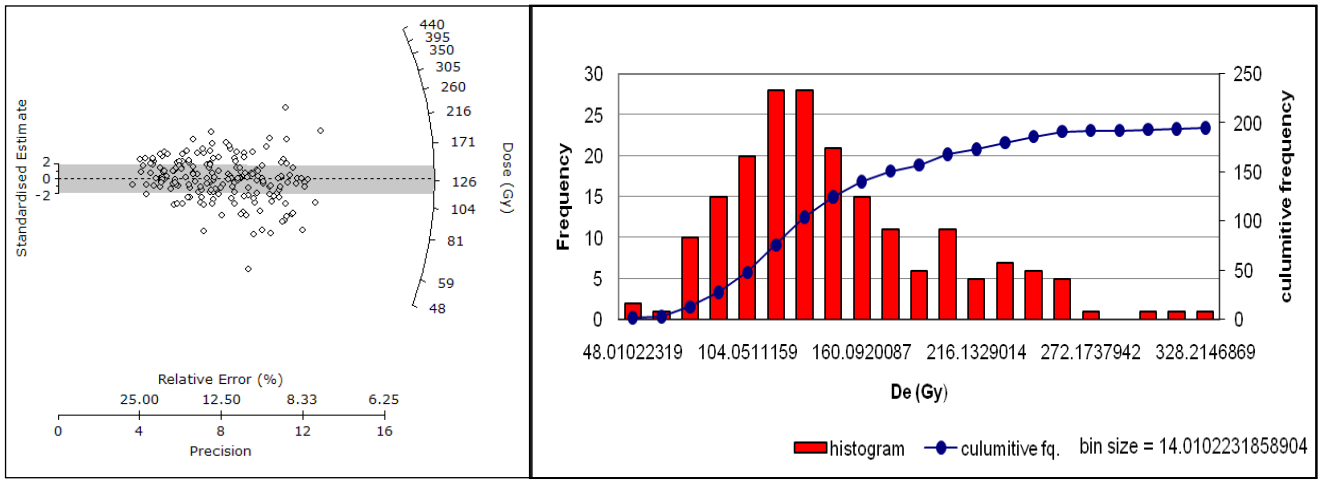

Fig. 5-14: Example of a radial plot for D_e values from a single-grain analysis carried out on the WK1 samples, as determined by the OSL laboratory of the University of the Witwatersrand. The plots indicate scatter for D_e for the grain samples WK1-180, with a relative error of 25% or less.

A Minimum Age Model (or MAM) (Table Table 5-2), as determined by the OSL laboratory of the University of the Witwatersrand, was compared with a determined central age model in order to create a preferred age model for the Wonderkrater deposit. The preferred OSL ages for the Wonderkrater samples are based on combined aliquot and single grain analysis results (Table Table 5-3).

Table 5-2: Minimum age model for the WK1 samples based on aliquot results, with ages indicated in thousand years (ka). Preferred ages are based on the minimum age model (courtesy of Susino, 2012)

Sample	Depth	Water	Cosmic ray	Total dose	De MAM	Age MAM
	cm	Content %	Gy/kg	Gy/kg	Gy	ka
WK1-125	125	26.3	1.382 ± 0.025	2.223 ± 0.04	104.81 ± 12.68	37.33 ± 4.61
WK1-135	135	20.2	1.379 ± 0.025	3.082 ± 0.13	136.8 ± 10.52	46.47 ± 3.73
WK1-155	155	35.4	1.374 ± 0.024	2.149 ± 0.02	148.1 ± 11.82	50.49 ± 4.21
WK1-180	180	56.3	1.372 ± 0.024	1.531 ± 0.02	72.29 ± 4.99	50.94 ± 3.72
WK1-220	220	16.6	1.358 ± 0.023	1.899 ± 0.03	110.4 ± 13.81	58.66 ± 7.46

Table 5-3: Preferred age based on minimum age model (courtesy of Susino, 2012)

Depth	Age MAM (ka)
125 cm	37.33 ± 4.61
135 cm	46.47 ± 3.73
155 cm	50.49 ± 4.21
180 cm	50.94 ± 3.72
220 cm	58.66 ± 7.46

Luminescent dates are calculated in 'years before the date of measurement', which for the Pit C (WK1) samples is 04/02/11. Field water content was used to assess the water content for Equivalent dose (De) calculations of the five OSL samples from Wonderkrater's Pit C.

6 Discussion

The Driefontein piedmont provides a unique opportunity to study active aggradation where colluvial, alluvial and floodout environments co-exist within a setting suggestive of continuous aggradation extending back to the Holocene. By comparing the results from the Driefontein piedmont with other fluvial deposits, an attempt was made to obtain more insight into the depositional processes active along its surface, and the characteristics of the sediments deposited.

The varying degrees and interaction of erosion, transportation and deposition, determine past and present geomorphological processes (Reading, 1996). Erosion may occur on a small scale where loose sediments are scoured from near surface environments through the actions of wind or water, or on a large scale where high energy floods or winds will activate the movement of vast volumes of coarse-grained terrestrial material and flood waters may cut deep erosive channels. Transportation of sedimentary material may take place in the form of debris flows, bedload,

suspended load, or through wind action (Reading, 1996; Collinson, 1996; Brown, 1997). Transportation and deposition is always dependent on the amount of energy involved in the transporting mechanism.

In general, sediment transported down slope, by means of channeled flow, and deposited as fans and lobes where competency and channel confinement is lost in a valley and delta setting, is termed alluvium, and the resulting landscape an alluvial fan. Sediment transported through mass wasting and sheet wash, and deposited along low-angle slopes, it is termed colluvium (Botha, *et al.,* 1994; Miall, 1996). The Driefontein piedmont was found to display both alluvial and colluvial characteristics.

In order to classify the Driefontein piedmont samples, they were compared with Blair & McPherson's classic alluvial fan samples. As with Blair and McPherson's 1994 samples, a longitudinal section across the Driefontein piedmont was taken and divided into 500m intervals (Fig. 6-1). For each 500m interval, proximal or intersecting surface samples, were selected and plotted to represent characteristic grain-size for that particular slope interval.

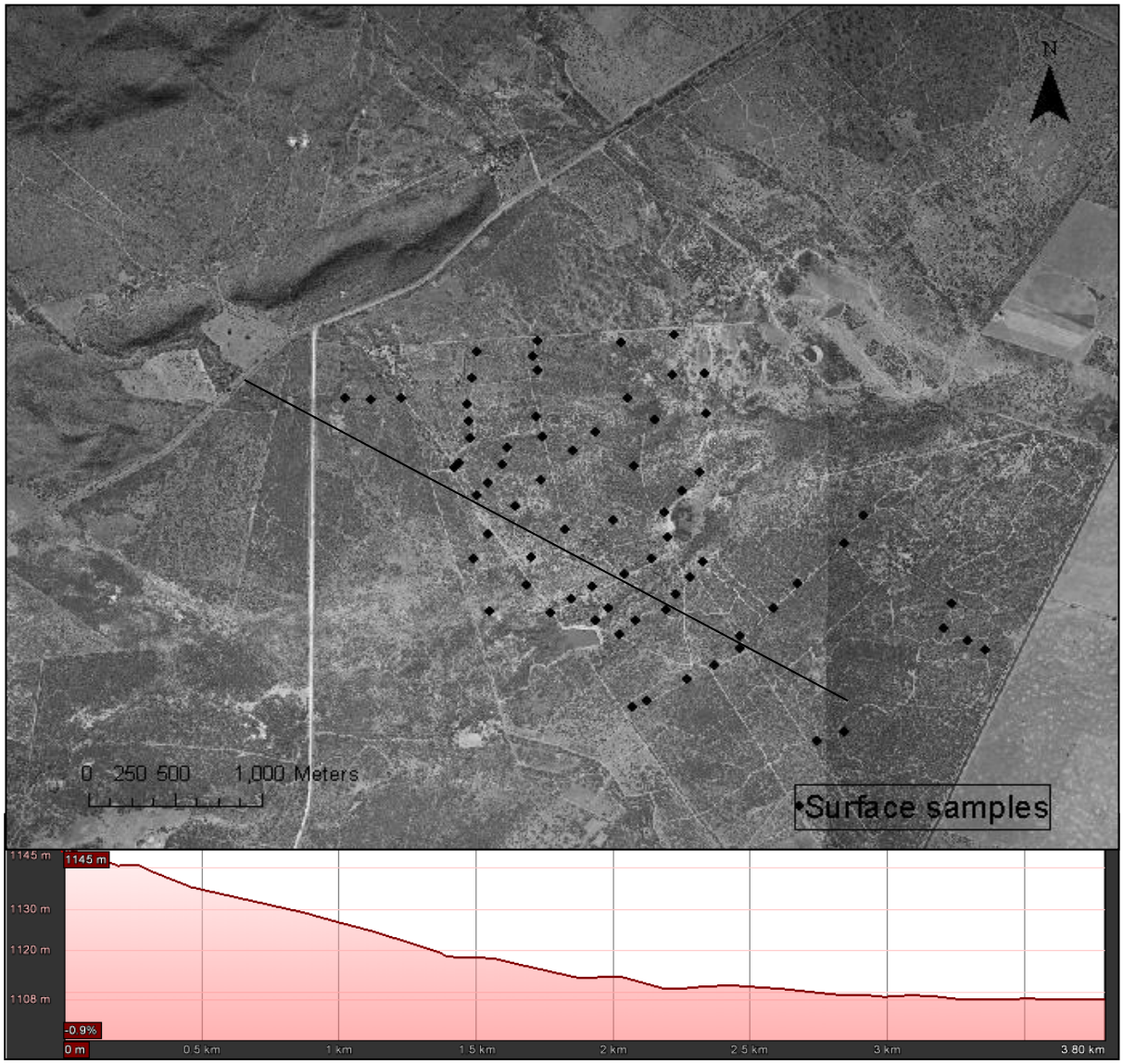

Fig. 6-1: Longitudinal section of Driefontein piedmont slope where intersecting surface samples (at 500m intervals) were plotted on McCarthy and Cadle's 1995 semiquantative graph (elevation cross-section was determined using GoogleEarth).

The mean grain size of the surface samples, either intersecting or within a close proximity to the Drifontein piedmont cross-section (Fig. 6-2), were plotted on Blair and McPherson's 1994 comparative slope vs. grain size graph as adapted by McCarthy & Cadle (1995). The modal grain size intervals are based on an approximate log-scale (after Wentworth, 1919), and the slope interval was measured on a scale of 1/10 000m. When plotted alongside other subaerial fan slope examples, the Driefontein surface samples (circled in red) are found to lie within Blair &

McPherson's "natural depositional slope gap", and on the fine-grained silty sand end of the modal grain size scale, rather than following the characteristic slope-grain size trend-line of alluvial fan morphologies (Fig. 6-2). Alluvial fans with medium slopes (0.58 to 1.58 %) have been found to correspond to Blair and McPherson's 1994 depositional gap (Saito & Oguchi, 2005). With a slope of 0.14% the Driefontein piedmont falls into this depositional gap.

When comparing grain size and slope relationships, as drawn by Blair and McPherson (1994, Fig. 5), it must be noted that Blair & McPherson's (1994) sample points each represent a different fan (Fig. 6-2), while the Blissenbach, Bluck, Scott and Yana samples, used by McCarthy and Caddle (1995), represent a spectrum of samples across the entire reach of individual fans. The Driefontein samples also represent a range of sub-aerial material sampled across the surface of a single piedmont. The Blissenbach and Bluck samples represent arid alluvial fans (Blissenbach, 1954; Bluck, 1964), while the samples from Yana stem from glacial outwash fans (Boothroyd & Ashley, 1975).

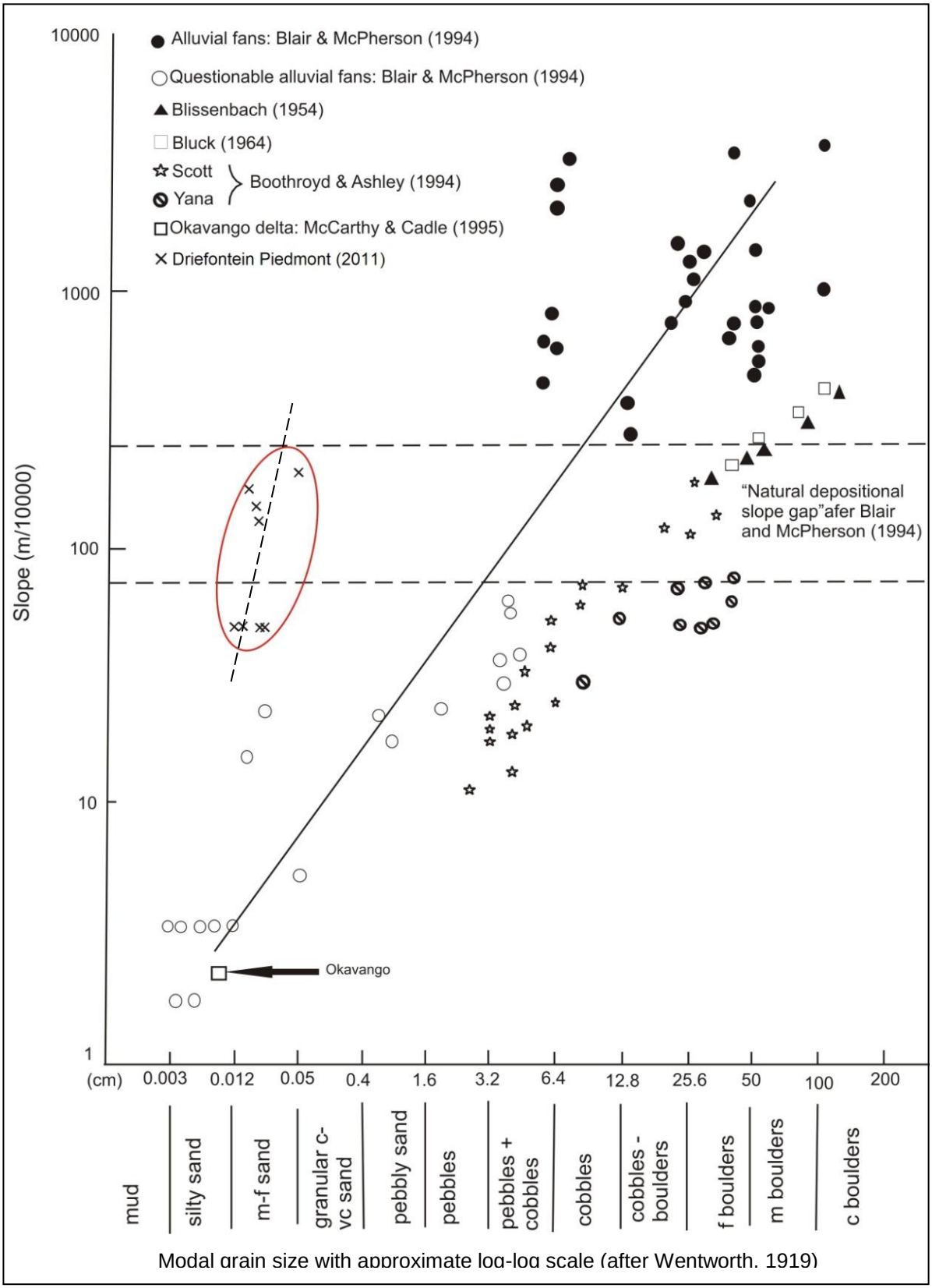

Fig. 6-2: Blair & McPerson's (1994) semiquantative graph, as abbreviated by McCarthy and Cadle (1995) showing grain size vs. slope relationships, and a regression line, with the Driefontein piedmont samples circled in red.

The slope of the Driefontein piedmont is not steep enough, nor is its grain-size course enough for it to fall within Blair & McPherson's definition of an alluvial fan. According to the plot in Fig. 6-2, the slope of the Driefontein piedmont should be too steep to support such fine-grained material, or the sedimentary particles too fine for such a steep slope. Moreover there appears to be a rough correlation between slope and mean grain size for the Driefontein samples, but the gradient of the trend is considerably steeper than for any other fans. The shape of the Driefontein fan could be described to look like an alluvial fan, but the slope/grain size characteristics are very different.

Examinations of aerial photographs and site investigations indicate that although well-defined channels occur in the upper-most reaches of the Driefontein piedmont, they become smaller and disappear rapidly, with flow becoming unchannelled across the piedmont. The DEM, with its potential drainage lines determined for the Driefontein piedmont region, indicates little channeled surface drainage in regions of where gradient is low. It is within this area of lowered elevation and gradient, that a complete loss of surface flow was observed. The observed loss of surface flow corresponds to very fine-grained surface sediments sampled from this region.

6.1 The sedimentary nature of the Driefontein piedmont

6.1.1 Surface sediments

By superimposing the surface drainage channels, based on the 1:10 000 topographic map of the Driefontein region, onto a 5m interval DEM, a correlation between slope gradient and active channel flow was observed. A stronger correlation is suggested for areas with little or no vegetation (coloured red or white), while areas of dense vegetation suggest the potential presence of surface, or near-surface water. Vegetation density appears to have an effect on the near surface sedimentary distribution, or lack thereof, especially during periods of heightened precipitation and runoff.

The NDVI results from the Wonderkrater peat mound and its surrounding piedmont terrain shows sparse vegetation cover in the northern sections of the piedmont, becoming increasingly denser and more broad-leafed in the southern region. The vegetation index was found to correspond to the grain size distribution. Regions with high vegetation index values (0.5 – 0.7) correspond with finer grained surface sediments, while regions indicating lower vegetation index values (0.0 – 0.3) predominate in areas of coarser grained surface material. The presence of vegetation may therefore act as a retaining agent for fine-grained material along slopes where incline should be too steep to support the fine-grained sedimentary material which was sampled along the length of the Driefontein piedmont.

Interpolation methods generally do not take into account any changes in elevation between one sample and the next, and directional adjustments may be required in order to determine a precise interpolation. Although the calculations for IDW interpolation do not have any directionality associated to them, when compared to the DEM they relate grain-size changes to changes in elevation and slope gradient fairly faithfully, with minor exceptions along the peripheral regions of the study site, where surface sediments were disturbed and sampling was limited.

The grain-size contours indicate a prominent NW-SE trending depositional system, which appears to fan out south of the NE-SW trending spring-fed stream and its associated fault system (see Figure A1.1, Appendix I). It is significant to note that there is little or no change in grain size south-east of the probable ‘fault line’ over a distance of almost 3km. Apart from the channeled stream feeding the head of the piedmont, overall surface drainage along the Driefontein piedmont was observed as occurring either as very small, shallow depression, activated only during thunderstorms, or as sheet runnoff. The standard deviation of the surface samples is seen to increase near the Wonderkrater peat mound and along the short NE-SW trending channel running off the mound itself and along the likely fault line. This might suggest a ‘trapping’ of sediments up along the length of the spring-fed stream.

Representative surface sample grains from the Dreifontein piedmont are predominantly very angular to angular near the source region of the hillslope, becoming more sub-angular further downslope near the peat mound, and sub-rounded to rounded in the south-east of the Driefontein piedmont. This suggests progressive sediment transportation across the surface of the piedmont, and would support the filtering of larger more angular material along the spring-fed stream, such that it acts as a minor barrier to the grains which are slowly moved and re-worked along the length of the piedmont slope.

The mineralogy of the grain samples across the Driefontein piedmont surface is suggestive of the sample's location along the length of the piedmont. Samples from the northwestern regions of the hillslope are coarser grained and indicate a higher percentage of feldspars than samples from those sites sampled further downslope. The percentage of rock fragments (composed of cemented carbonate, quartz and feldspars) is seen to increase near the center of the piedmont, and then decrease further downslope. Progressive surface and chemical weathering of the feldspar grains would account for their increased paucity in the south-eastern parts of the Driefontein piedmont.

The movement of grains downslope across the surface of the Driefontein piedmont appears to be taking place episodically and over multiple seasons, as sheet floods or occasional debris flows, resulting in asymmetrical grain size distributions, poor effective abrasion and generally fine-grained immature sediments. The transportation mechanisms observed at Driefontein capable of such an energy regime, are the short but intense summer thundershowers which rapidly mobilize surface material to then be deposited rather quickly once the rain ceases, and the potential transport energy subsides.

6.1.2 Sediment characteristics of samples from Pit C

The roundness index results for the WK1 sediments samples from sand-rich lenses, indicate that the majority of the grains are sub-angular, and to a lesser degree either angular or sub-rounded. The lack of roundness observed in the WK1 grains suggests a short, potentially high energy, regime of transportation through whatever medium or mechanism responsible for mobilizing and transporting the particles along the length of the Driefontein piedmont slope. It further suggests very little re-working post burial. If the grains had been transported along the Driefontein piedmont with enough energy over extended periods of time, the majority of the grains would tend to be well-rounded. If there had been short, rapid episodes of high-energy particle-mobilization, the majority of grains would be more angular and coarser grained. The sub-angular nature of the sampled grains from the Driefontein piedmont are indicative of a medium, or episodic energy regime; enough energy to cause sub-rounding during transportation and sediment relocation, but not enough for large particle to be entrained. In addition, in situ post depositional chemical weathering may be taking place in the lower regions of the piedmont. Abrupt increase in roundness could be explained by a hiatus of higher rainfall, and resultant abrasive action of grains during deposition, such as the sediments found at 180cm depth.

The composition of the WK1 grain samples from Pit C, were composed mostly of quartz (up to 98%), intermediate to high amounts of rock fragments (composed of cemented carbonate, quartz and feldspars), and minor orthoclase feldspars (up to 22%), and are similar to the present surface compositions. However, a lower percentage of feldspars and rock fragments were found in the WK1 samples, demonstrating a lack of mineralogically softer grains at depth in the central piedmont region, were surface grains still display a high percentage of rock fragments. The lack of roundness in the WK1 grains suggests higher levels of abrasion at the time of deposition, than what is currently found along the surface of the Driefontein piedmont.

The particle size distribution of the WK1 and WK2 samples indicate relatively poor sorting with depth, being often bi-, or tri-modal in their distribution (see Appendix II). This multi-modality of sediments can be explained as a mixture of multiple log-normal distributions within a single grain population resulting from the effect of abrasion on different grain mineralogies, through the mechanical action of weathering, or through the effect of bioturbation (Folk & Ward, 1957; Spencer, 1963). The development of skewness and kurtosis is strongly affected by the multi-modality of grain populations, and hence the mineral composition and the effective abrasion of grains. The median size of any sediment could be described as a measure of the energy conditions of deposition, as well as the environment in which it is deposited. In a low energy environment multi-modal populations are more common, due to the contribution of fine-grained material, which renders the grain size median less useful as an indicator for the energy conditions during deposition (Spencer, 1963). When compared to other fluvial settings, the coarse-grained WK1 samples show a grain size distribution not unlike the colluvial grains sampled by Botha (1996).

On the whole, over a six meter depth range, the WK2 samples show distinctly bi-, tri- and even multi-modality in their distribution, and they display a general positive skeweness with a few exceptions tending towards being symmetrical (see Appendix I). This predominant positive asymmetry is indicative of the limiting competency found in dune and river environments (Friedman, 1961).

Fining-upward sequences have been described in distal alluvial fan environments, as topography becomes progressively buried and depositional locations become ever more distal (Harvey *et al.,* 2005). The sampled WK1 sediments were generally finer-grained, but alternate with depth in their being either skewed to the left or to the right (see Appendix I). The WK1 samples were seen to increase slightly in coarseness between 125cm and 135cm depth, becoming increasingly finer-grained from 135 cm to 180cm, where clay and peat lenses were thicker. From 180cm to 220cm depths, mean grain size was observed to become rapidly coarser-grained, while the WK2 samples were in general finer grained. This difference seen in the WK1 and WK2

samples may be as a result of the different methods used to determine grain size distributions. These changes in grain size within the WK1 material, may suggests that layers of different material occurs within the upper reaches of Pit C.

Comparing the lithology of Pit C alongside the grain characteristic of the WK1 and WK2 sediment samples, a stratigraphic record and relative climatic condition of the aggrading Wonderkrater peat mound and the surrounding Driefontein piedmont could be established. Where peat and clay occurred, depositional conditions would have been wet and conducive to the growth of vegetation and slow moving or standing bodies of water. Peat layers were at times interspersed with gray ash layers, indicative of the burning of peat, most likely during dryer windier months. Below the peat layers, coarse grained sand was sampled, suggesting that dryer conditions prevailed during the time of deposition, coupled with the shrinking of the peat mound. When taking into consideration the expanse of elapsed time suggested by the C^{14} and OSL ages, these lithologyical records of wet and dry cycles appear to be indicators of changing climatic conditions, rather than those of seasonal changes.

6.1.3 Environmental correlation

Grain size comparisons of standard deviation vs. mean, mean vs. skewness, and standard deviation vs. skewness were carried out using the Driefontein piedmont surface samples and the Wonderkrater samples from Pit C, in comparison to aeolian samples from the Kalahari and the Namib desert (Lancaster, 1981; 1986), colluvial samples from Swaziland (Botha, 1996), and fluvial samples from the Okavango channels (Stanistreet & McCarthy, 1993). The results shown in Fig. 6-3 a, b and c, and were plotted using Friedman's parameters as environmental field discriminations (Friedman, 1961).

Sample skewness, according to Friedman (1961), is indicative of its depositional environment, regardless of the mineralogy of the individual sand grains. Sorting index, mean size and skewness comparisons of the surface samples indicate that the Dreifontein piedmont samples lie largely within what Friedman (1961) described as

being a ‘fluvial environment’. When comparing standard deviation with mean size, most of the Driefontein surface samples occur within Friedman’s ‘River Sand field’. Approximately a quarter of the surface samples, along with all of the sediment samples from Pit C, lie within Friedman’s combined ‘Dune and River sand field’. Though poorly sorted, the Driefontein piedmont surface samples show a high degree of symmetry, thus being neither strongly associated with dune or beach depositional environments.

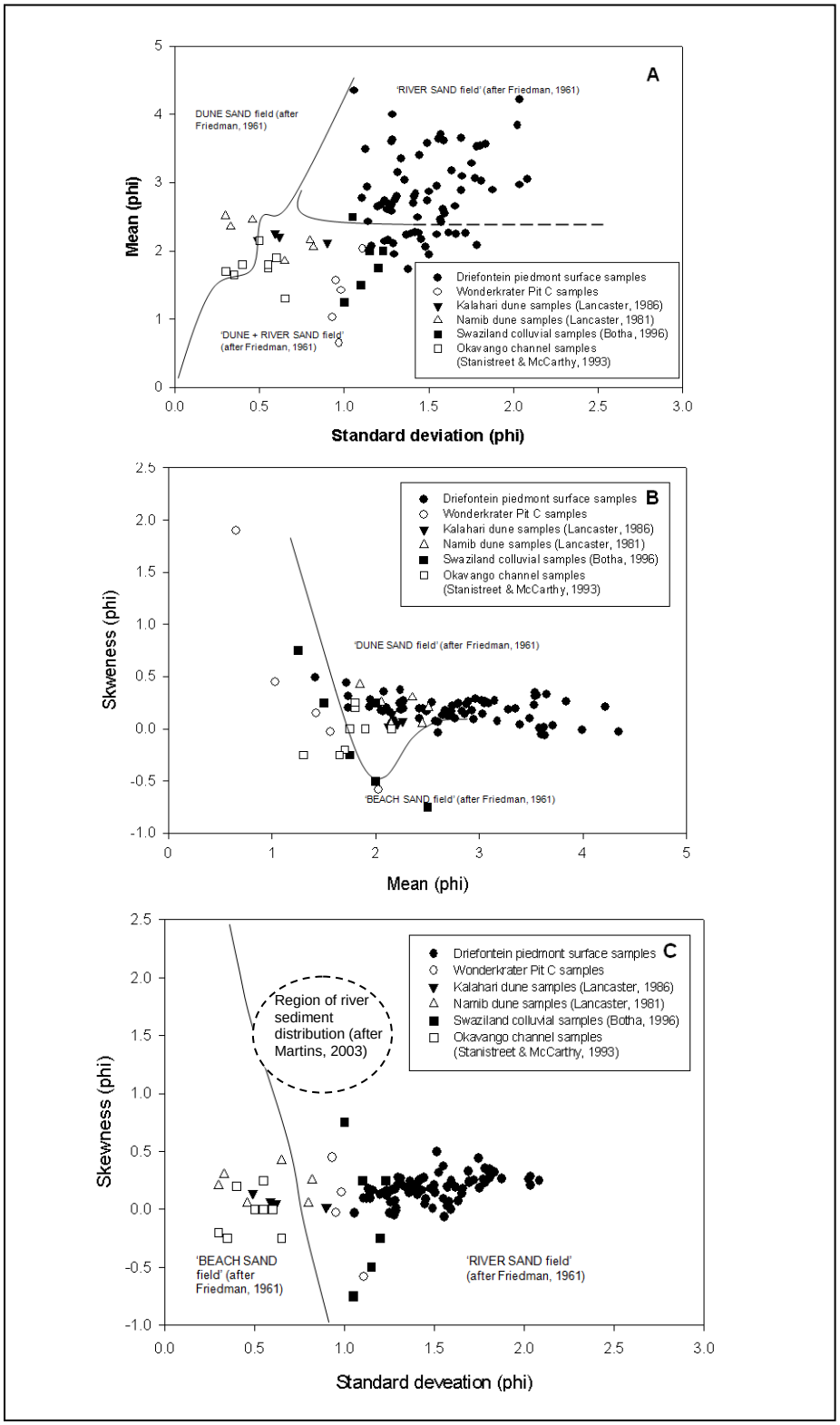

Fig. 6-3: A comparison of the Driefontein piedmont surface samples and the Wonderkrater Pit C samples with aeolian Kalahari and Namib samples (Lancaster, 1981; 1986), colluvial samples from Swaziland (Botha, 1996), and Okavango channel samples (Stanistreet & McCarthy, 1993). Discriminating environmental fields (after Friedman, 1961) using standard deviation (sorting index) vs. mean (A), mean vs. skewness (B), and standard deviation vs. skewness (C) where river sediments (after Martins, 2003) are indicated.

When comparing standard deviation with skewness, all the samples from the Driefontein piedmont, including those samples from Pit C, were seen to lie firmly within Friedman's 'River Sand field'. In the absence of absolute values, the collective region of the grain size distribution of 20 different rivers sampled from around the world is indicated in Fig. 6-3 c, as comparative reference (Martins, 2003).

When plotting the mean, standard deviation (sorting) and skewness of the Driefontein piedmont samples, the samples fall outside of Friedman's original boundaries of dune environment, and plot within the reaches of Friedman's field of "river sand" environments. However, they are very much finer-grained than any samples plotted by Friedman in 1961. When plotting Driefontein samples, they are most like the Kalahari samples, in their sorting, suggesting that some of the Driefontein material might have been windblown. A distinct difference in grain-size can be seen between the samples from the Driefontein piedmont and the aeolian samples from the Kalahari and the Namib Desert (Lancaster, 1986; 1981).

Overall, the Driefontein piedmont displays downslope changes in sorting and grain maturity, correlating to both changes in gradient and the presence or absence of channeled streams and vegetation. Sedimentary particles were observed to change with depth, indicative of changes in slope due to basin fill and pediment retreat (Fig. 6-4). Changes in sedimentary grain characteristics with depth may also be related to climatic hiatus, determined using OSL and C^{14} ages, and highlighting the climatic changes from the Holocene to the present. A fourth type of fan classification is suggested here in order to adequately describe the sedimentary characteristics and setting of the Driefontein piedmont. This fourth type should be described as a 'slow creep fan', with characteristically fine-grained and poorly-sorted sediments, occurring along a well vegetated slope characteristic of Blair and McPherson's 1994 slope depositional gap.

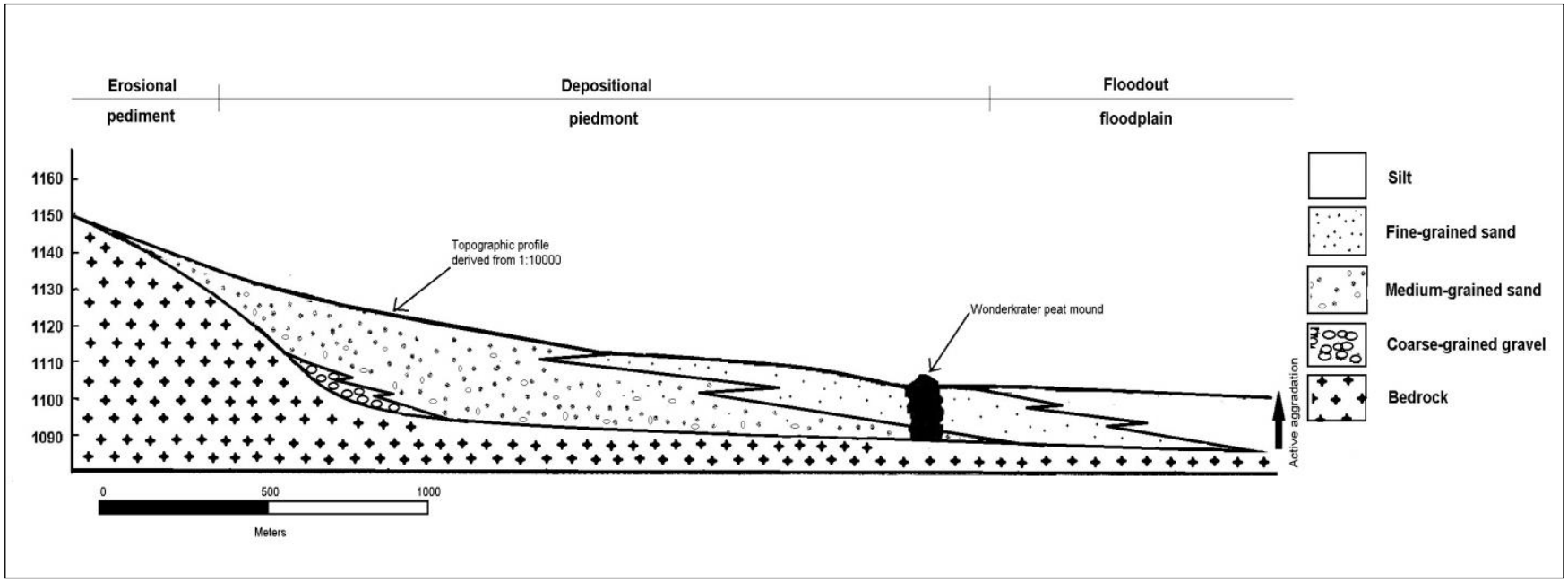

Fig. 6-4: Depositional processes along the Driefontein piedmont, based on surface morphology, grain size distribution, and the presence of the Wonderkrater peat mound.

6.2 OSL ages from Pit C

Determining the exact age of sedimentary events beyond the radiocarbon reliability range is often problematic. Two different methods of dating are commonly used when dating sedimentary sequences (Brown, 1997):

- Relative methods; require deductive reasoning through the matching and correlating of stratigraphic sequences with like properties, using such indicators as fossils, pollen, minerals, weathering patterns (Brown, 1997; Susino, 1999).
- Chronometric or absolute methods; which provide independent age estimates based on physical, chemical or biological time clocks. These methods provide numerical or calibrated data. Examples of absolute dating methods include radiocarbon, thermoluminescence, potassium-argon and the uranium series (Brown, 1997; Susino, 1999).

Different absolute dating results can sometimes be calibrated against each other. However, often the calibration calculations are very complex, especially when trying to reconcile the results of different dating techniques (Susino, 1999). Direct age determinations of colluvial-alluvial settings are rare (Mills, 1988).

Luminescence techniques provide a method of age determination that allows for sedimentary environments, such as alluvial fans to be used as proxies in the reconstruction of Quaternary fluvial depositional conditions (Fuller, *et al.,* 1998). Robinson, *et.al,* (2005) determined that the shallow unconfined flows found along the length alluvial fans in Argentina, along with associated windblown and fluvial environments found on such slopes, provide efficient bleaching opportunities for quartz grains, making these sub aerial environments highly suitable for OSL dating. OSL dating done on colluvial material from the eastern Grand Canyon, provided evidence which indicates that changes in climate rather than changes in base level or tectonism, acted as the main controlling agent in the formation of local surface deposits (Anders, *et al.,* 2005).

Attempts have been made to compare sedimentary age results gained using optically stimulated luminescence with results gained from stratigraphically related radiocarbon dates (Pinaar, *et al.,* 2008). Such correlations need to be carried out with great caution, as the environments which are suitable for the formation of carbon-rich deposits generally require high levels of water and water fluctuation sometime during the process of sediment deposition. This presence of water has a negative implication for accurate OSL dating. Fluctuating water tables may affect the OSL dose rate by mobilizing radioactive elements within the soil. The re-mobilization and mixing potential associated with fluctuating water tables may result in post-depositional bleaching of quartz grains (Pinaar, *et al.,* 2008). Another difficulty when correlating radiocarbon ages with OSL dates lies in the calibration of the radiocabon age. The radiocarbon age is measured relative to the year AD 1950 and is based on the half-life of ^{14}C which has a known error of approximately 3%, while OSL dates are calculated using true calendar years (Pinaar, *et al.,* 2008). In order to make a correlation possible, radiocarbon dates must be carefully calibrated to the year in which the OSL samples were taken (Taylor, *et al.,* 1996; Pinaar, *et al.,* 2008).

OSL results taken from the dry margin of the peat mound may provide insights into past surface processes as well as an indication of the rate of aggradation of the piedmont landscape. The upper ca. 4-5m of peat from the Wonderkrater peat mound provides a reliable record going back about 15,000 years, with deeper sequences providing dates ranging between about ca.15,000 BP and 34,000 BP. Combining the Tswaing and Wonderkrater results has provided a more continuous reconstruction, suggesting that two cool and two moderately warmer phases took place between 190,000 and 150,000 years BP (Holmgren, *et al.,* 2003). The average rate of aggradation, based on radiocarbon ages taken from the centre of the peat mound, was found to approximate a rather slow accumulation rate of 0.17 m every 1000 years (Scott, *et al.,* 2003; Backwell, *et al.,* 2012)

An attempt was made to correlate past thermoluminescent (IRSL) and radiocarbon results from Wonderkrater peat samples with OSL age estimates recovered from Pit C by Backwell *et al.,* 2012 (Fig. 6-5). The water content of the OSL samples presented a major problem in determining an accurate age model for the Driefontein piedmont, as did the reduced bleaching event of the sampled quartz grains.

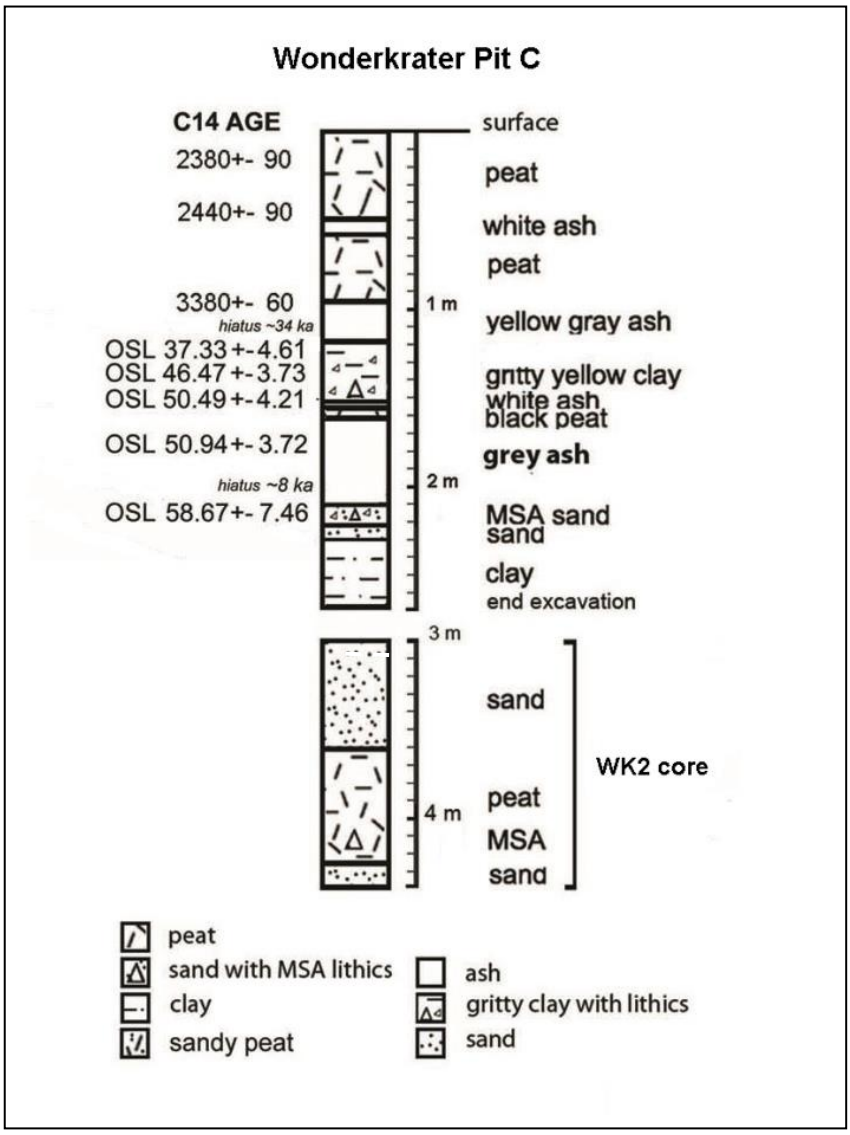

Fig. 6-5: Age model for the Wonderkrater peat mound and its proximal piedmont, based on previously correlated radiocarbon and IRSL dates along with new OSL results taken from the edge of the peat mound in Pit C. Dose rate corrections (DRC) were used to establish IRSL age estimates, and OSL age estimates (based on minimum age model results) (Huntley & Lamothe, 2001; Scott *et. al*,. 2003; Lamothe *et al.,* 2003; Backwell, *et al.,* 2012).

Dating samples with high peat contents is problematic. The slow circulation of water in peat-rich environments may cause disequilibrium in the decay series, as uranium is selectively removed by the percolating water (Duller. 2008). Estimating the water content over time in a peat mound is difficult, and care must be taken to take into account the effects of compression and dewatering which may have taken place in the past (Duller, 2008). The large hiatus of approximately 34 thousand years between the C14 results of the peat layers and the OSL results of the underlying sandy layers is problematic, and might suggest a time break in the depositional process such as heightened levels of erosion, or more likely a problem with the OSL age results. Either way, the OSL results from Pit C should be treated with caution.

Irrespective of the OSL results from Pit C, evidence of changing climatic conditions during the aggradation of the Driefontein piedmont has been provided by previous authors who did work on the Wonderkrater peat mound (Scott, 1982; 1989; 1999; 2002; Tooth, *et al.,* 2002; McCarthy, *et al.,* 2010, Backwell, *et al.,* 2012). Evidence suggests that around 45 ka the Wonderkrater peat mound and its surrounding piedmont terrain experienced heightened aridity which would promote periodic sheet flooding or debris flows, followed by wetter conditions by around 30 ka and the growth and spread of savanna woodlands and grasslands.

7 Conclusion

The physical, chemical, and biological characteristics of any depositional environment, determines the depositional setting and the generation of its sedimentary nature (Bloggs, 1995). The present surface conditions of the Driefontein piedmont, its slope inclination, the type and vegetation density, and the climatic conditions, all contribute to its characteristic morphology and depositional history.

The Driefontein piedmont slope, being very shallow in its slope inclination and slightly concave-up in the longitudinal direction should, according to Botha and Partrige

(2000), have its major deposition confined to the lower pediment. The parallel cross-sections indicate the slightly convex-up characteristics typical of an alluvial fan setting. According to Smith (2000), the persistence of channeled flow across piedmonts, as opposed to unconfined flow common along alluvial fan surfaces, distinguishes such piedmonts as alluvial-slope rather than alluvial-fan facies. Such alluvial slopes are more likely to form where mountains lack abrupt structural and topographic relief (Smith, 2000).

The Driefontein piedmont slope has been shown to be either too steep or too shallow for 'characteristic' alluvial grain sizes, such as those described by McCarthy and Cadle (1995) and Blair and McPherson (1994). A 'lag' of fine-grained sedimentary material was observed, which is explained by the presence of the savanna-type shrub and grassland vegetation providing soil support and acting in a 'retaining' manner, whether through root action or the presence leaf matter, or a combination of both. Down-stream movement of fine-grained sands and silts, is effectively hindered along the length of the relatively steeply inclined slope of the Driefontein piedmont.

When comparing the environmental characteristics of the Driefontein piedmont with other fluvial grain size distributions and parameters, the grain parameters suggest the dominant environmental settings of Driefontein piedmont to be unchanneled floodouts, with colluvial processes having taken place in the past. With the slope of the Driefontein pediment not being steep enough to result in precipitation-induced slope failure and subsequent debris-flow (Blair, 1999), but still displaying downward, though largely unchannelled, movement of sediment transport in water flow over time, a fourth of fan type is needed to discribe the Driefontein piedmont.

Present day mechanisms capable of entrainment, transport and deposition of surface sediments along the Driefontein piedmont, are cyclic or episodic, moderate-to-high energy regimes. Seasonal summer storms alternating with semi-arid winter conditions would be the most likely candidate capable of such transport of sedimentary material along the length of the piedmont surface. Occasional flash

floods and debris flows following heightened periods of drought, may at times have deposited larger and coarser grained material along the piedmont slope.

Age estimate correlations suggests that the OSL results taken from Pit C have a sedimentary age ranging from ~30ka in the upper layers to ~45 ka in the lower sequences. The stratigraphy also indicates that there are two sedimentary events present in this sequence, interrupted by a layer of peat and ash. Increasing angularity and coarseness of grain size at a depth of 220cm would suggest a period of increased aridity followed by heightened levels of flooding during the time of deposition estimated at around 45 ka, which is in accordance with other proxy records from central southern Africa (Shaw, 1988; Brook *et al.,* 1998; Thomas *et al.,* 2003; Chase, 2009).

A decline in feldspar and rock fragments away from the source and along the length of the hillslope surface, suggests the loss of compositionally softer grains, due to abrasion and chemical weathering. Increasing angularity and coarseness of grain size with depth is suggestive of pediment retreat and the abrupt lack of peat in Pit C at this depth, indicates periods of increased aridity during the time of deposition, which is estimated to having taken place around 45,000 years ago. The process of colluviation is shown to be strongly associated with phases of past humid conditions, during which a slope may stabilize due to the presence of vegetation, promoting surface integrity through root-networks and the formation of soil horizons, followed by arid or glacial conditions during which weathered material is transported downslope as sheet wash (Goudie & Bull, 1984; Clarke, *et al.,* 2003). Evidence suggests that the change in grain maturity along the Driefontein piedmont is as a result of the combined effect of vegetation distribution, slope inclination and regional climate, as well as past colluviation, retreating pediment slope and active aggradation as the Nylsvlei basin fills with sediment.

The Driefontein piedmont was observed to display minor channeled flow at the foothill of the Waterberg Range, transcending to unconfined surface flow on its lower slope, suggesting that the sampled piedmont region presents a continuum of depositional slope environments, ranging from alluvial-slope to alluvial-fan facies. As the Driefontein piedmont does not confine to any of the proposed alluvial fan classes, a fourth type of fan class is needed in order to describe the characteristics of the Driefontein piedmont. This fourth type is here described as a ‘slow creep fan’, with characteristically fine-grained and poorly-sorted grains, occurring along a well vegetated, low inclination slope. The sedimentary deposition of such a ‘slow creep fan’ would span over multiple seasons in a semi-arid environment, during which transportation energies range from episodic sheet floods and occasional debris flows, to windblown entrainment as a result of local long-term, seasonally-alternating wet and dry conditions, coupled with regional climate change and long-term pediment retreat.

8 Reference

Aitken, M.J. (1998) *An introduction to optical dating: the dating of Quaternary sediments by the use of photon-simulated luminescence.* Oxford University Press, New York.

Allen, J.R.L. & Thornley, D.M. (2004) Laser granulometry of Holocene estuarine silts: effects of hydrogen peroxide treatment. *The Holocene* **14,** 290-295

Backwell, L.R., McCarthy, T.S., Wadley, L., Henderson, Z., Lamothe, M.. Barré, M., Steininger, C., Sievers, C., Chase, B.M., deKlerk, B., Pollarolo, L., Woodborne, S., Scott, L., Brink, J., Bamford, M., Rossouw, L., d'Errico, F. & G. Susino (2012) *Multiproxy record of late Quaternary climate change and Middle Stone Age human occupation at Wonderkrater, South Africa* Unpublished research report. University of the Witwatersrand.

Barker, O.B., Brandl, G., Callaghan, C.C., Eriksson, P.G. and van der Neut, M. (2006) The Soutpansberg and Waterberg Groups and the Blouberg Formation. *In:* Johnson, M.R., Anhaeusser, C.R. & Thomas, R.J. (Eds.). *The Geology of South Africa.* Geological Society of South Africa, Johannesburg/Council for Geoscience, Pretoria. 309-318.

Bertran, P., Hetu, B., Texier, J. & Van Steijn, H. (1997) Fabric characteristics of subaerial slope deposits. *Sedimentology.* **44,** 1-16.

Blair, T.C. & McPherson, J.G. (1994) Alluvial fans and their natural distinction from rivers based on morphology, hydraulic processes, sedimentary processes, and facies assemblages. *Journal of Sedimentary Research,* **3**, 450-489.

Blair, T.C. (1999) Cause of dominance by sheetflood vs. debris-flow processes on two adjoining alluvial fans, Death Valley, California. *Sedimentology* **46**, 1015-1028

Blikra, L.H. & Nemec, W. (1998) Postglacial colluviums in western Norway: depositional processes, facies and palaeoclimatic record. *Sedimentology* **45,** 450-489.

Blissenbach, E. (1954) The geology of alluvial fans in semiarid regions. *Bulletin of the Geological Society of America,* **65,** 175-190.

Bloggs, S (1995) *Principles of sedimentology and stratigraphy, 2nd ed.* Prentice-Hall Inc. New Jersey.

Blott, S.J. & Pye, K. (2001) Gradistat: A grain size distribution and statistics package for the analysis of unconsolidated sediments. *Earth Surface Processes and Landforms* **26**, 1237–1248.

Botha, G.A., Wintle, A.G. & Vogel. J.C. (1994) Episodic late Quaternary alaeogully erosion in northern KwaZulu-Natal, South Africa. *Catena* **23,** 327-340.

Botha, G.A. (1996) Memoir of the geological survey of South Africa 83. Council for Geoscience, Pretoria.

Botha, G.A. (2000) Colluvial deposition, In: Partridge, T.C. & Maud, . (Eds.) *Cenozoic of South Africa*. Oxford University Press, New York.

Brook, G.A. Cowart, J.B. & Brandt, S.A. (1998) Comparison of Quaternary environmental change in eastern and southern Africa using cave speleothem, tufa and rock shelter data. In: Alsharhan, A.S., Glennie, K.W., Whittle, G.L. & Kendall, C.GSt.C. (Eds), *Quaternary Deserts and climate Change*, 239-249. Rotterdam, Balkema.

Brown, A. G. (1997) *Alluvial geoarchaeology: floodplain archaeology and environmental change.* Cambridge University Press, Great Britain.

Chase, B.M. 2009. Evaluating the use of dune sediments as a proxy for palaeo-aridity: a southern African case study. *Earth-Science Reviews* **93**, 31-45

Collinson, J.D. (1996) Alluvial sediments, in Reading. H.G. (eds) *Sedimentary Environments: Processes, facies and stratigraphy.* Blackwell Publishing, UK.

Folk, R.L. & Ward, W.C. (1957) Brazos River bar: a study in the significance of grain size parameters. *Journal of Sedimentary Petrology* **27**, 3–26.

Friedman, G.M. (1961) Distinction between dune, beach, and river sands from their textural characteristics. *Journal of Sedimentary Petrology.* **31,** 514-529.

Frost, P.G.H. (1987) The regional landscape: Nylsvley in perspective. *South African National Scientific Programmes Report no.133*, Council for Scientific and Industrial Research, Pretoria.

Fuller, I.C., Macklin, M.G., Lewin, J., Passmore, D.G. & Wintle, A.G. (1998) River response to high-frequency climate oscillations in southern Europe over the past 200k.y. *Geology.* **26** (3), 275-278.

Gabris, G. & Nagy, B. (2005) Climate and tectonically controlled river style changes on the Sajo-Hernad alluvial fan (Hungary). *In*: Harvey, A.M., Mather, A.E. & Stokes, M. (eds) *Alluvial fans: Geomorphology, Sedimentology, Dynamics.* Geological Society, London, Special Publications, **251,** 61-67.

Harvey, A.M., Mather, A.E. & Stokes, M. (2005) Alluvial fans: geomorphology, sedimentology, dynamics - introduction. A review of alluvial-fan research. *Geological Society,* London, Special Publications, **251**, 1-7

Huntley, D.J. & Lamothe, M. (2001) Ubiquity of anomalous fading in K-feldspars being measured in optical dating or thermoluminescence dating. *Ancient TL,* **15**, 11-13.

Holmgren, K., Lee-Thorp, J.A., Cooper, G.R.J., Lundblad, K., Partridge, T.C., Scott, L. Sithaldeen, R., Talma, A.S. & Tyson, P.D. (2003) Persistent millennial-scale variability over the past 25,000 years in South Africa. *Quaternary Science.* **22,** 2311-2326.

Higgins, S.I., Coetzee, M.A.S. Marneweck, G.C. & Rogers, K.H. (1996) The Nyl River floodplain, South Africa, as a functional unit of the landscape: A review of current information. *African Journal of Ecology.* **34,** 131-145.

Jackson, S.T. & Charman, D. (2010) Editorial: Peatlands – palaeoenvironments and carbon dynamics. *In*: Jackson, S.T., Charman, D., Newman, L. & Kiefer, T. (eds.) Peatlands: Palaeoenvironments and Carbon dynamics. *Pages News.* **18** (1), 3-4.

Johnson, M.R., Van Vuuren, C.J., Visser, J.N.J., Cole, D.I., Wickens,H.de V., Christie, A.D.M. & Roberts, D.L. (1997) The foreland Karoo Basin, South Africa. *In:* Selley, R.C. (Ed.), *Sedimentary Basins of Africa.* Elsevier, Amsterdam, 269-317.

Johnson, M.R., Van Vuuren, C.J., Visser, J.N.J., Cole, D.I., Wickens ,H. de V., Christie, A.D.M. ,Roberts, D.L. & Brandl, G (2006) Sedimentary rocks of the Karoo Supergroup. *In:* Johnson, M.R., Anhaeusser, C.R. & Thomas, R.J.

(Eds), *The Geology of South Africa.* Geological Society of South Africa, Johannesburg/Council for Geoscience, Pretoria, 461-499.

Kent, L.E. (1949) The thermal waters of the Union of South Africa and South West Africa. *Trans. Geol. Soc. S. Afr.* **52** 231-264.

Kochel, R.C. & Johnson, R.A. (1984) Geomorphology and sedimentology of humid-temperate alluvial fans, central Virginia. In Koster, E. & Steel, R. (Eds), Gravels and conglomerates. *Canadian Society of Petroleum Geologists Momoir,* **10**, 109-122

Kochel, R.C. (1990) Humid Fans of the Appalachian Mountains. *In:* Rachocki, A.H & Church, M (Eds) *Alluvial Fan: A Field Approach.* Southern Illinois University, Carbondale.

Koldijk, W. S. (1968) On environment-sensitive grain-size parameters. *Sedimentology* **10,** 57-69.

Krumbein, W. C. & Sloss, L. L. (1951) *Stratigraphy and sedimentation.* W. H. Freeman and Company. London and San Francisco.

Lancaster, N (1981) Grain-size characteristics of Namib desert linear dunes. *Sedimentology.* **28,** 115-122.

Lancaster, N (1986) Grain-size characteristics of linear dunes in the southwestern Kalahari. *Journal of Sedimentary Petrology.* **56 (3),** 395-400.

Lillesand, T.M., Kiefer, R.W. & Chipman, J.W. (2004) Remote sensing and image interpretation, 5th ed. John Wiley & Sons, United States of America.

Maslin, M.A. & Christensen, B. (2007) Tectonics, orbital forcing, global climate change, and human evolution in Africa: introduction to the African palaeoclimate special volume. *Journal of Human Evolution.* **53,** 443-464.

Martins, L.R. (2003) Recent sediments and grain-size analysis. *Sedimentological Research Group.* **1,** 90-105.

Mason, J.A. & Knox, J.C. (2011) Age of colluvium indicates accelerated late Wisconsinan hillslope erosion in the Upper Mississippi Valley. *Geology.* **25** (3), 267-270.

McCarthy, T.S., Elley, W.N., Backwell, L., Marren, P., de Klerk, B., Tooth, S., Brandt, D. & Woodborne, S. (2010) The character, origin and palaeoenviromental

significance of the Wonderkrater Spring Mound, South Africa*. Journal of African Earth Science*. **58**, 115-126.

McCarthy, T.S, & Cadle, A.B. (1995) Discussion: Alluvial fans and their natural distinction from rivers based on morphology, hydraulic processes, sedimentary processes, and facies assemblage. *Journal of Sedimentary Research,* **3**, 581-583.

Miall, A.D. (1996) *The geology of fluvial deposits: sedimentary facies, basin analysis, and petroleum geology*. Springer, Germany.

Mills, H.H. (1988) Surficial geology and geomorphology of the Mountain Lake area, Giles County, Virginia, including sedimentological studies of colluvium and boulder streams. *U.S. Geological Survey Professional Paper* **1469***,* 57.

Moss, R.P. (1965) Slope development and soil morphology in a part of south-west Nigeria. *Journal of Soil Sciences,* **16** (2), 192-209.

Olivier, J., van Niekerk, H.J. & van der Walt, I.J. (2008) *Physical and chemical characteristics of thermal springs in the Waterberg area in Limpopo Province, South Africa.* Water SA, **34.**

Owen, R.B., Renaut, R. W., Hover, V.C., Ashley, G.M. & Muasya, A.M. (2004) Swamps, springs and diatoms: wetlands in the semi-arid Bogoria-Baringo Rift, Kenya. *Hydrobiologia.* **518,** 58-78.

Pederson, J., Pazzagalia, F. & Smith, G. (2000) Ancient hillslope deposits: Missing links in the study of climate controls on sedimentation. *Geology.* **28** (1), 27-30.

Pentecost. A., Jones, B., & Renaut, R.W. (2003) What is a hot spring? *Can. J. Earth Sci.* **40** (11) 1443-1446.

Powers, M.C. (1953) A new roundness scale for sedimentary particles. *Journal of Sedimentary Petrology*. **23** (2), 117-119

Prescott, J.R. & Hutton, J.T. (1994) Cosmic ray contribution to dose rates for luminescence and ESR dating: large depths and long-term time variations. *Radiation Measurements.* **23** (213), 497-500.

Price Williams, D., Watson, A. & Goudie, A.S. (1982) Quaternary colluvial stratigraphy, archaeological sequences and palaeoenvironment in Swaziland, Southern Africa. *The Geographic Journal*. **148** (1), 50-67.

Pye, K. & Blott, S.J. (2004) Particle size distribution of sediments, soils and related particulate materials for forensic purposes using laser granulometry. *Forensic Science International* **144,** 19-27.

Reading, H. G. (1996) *Sedimentary Environments: processes, facies and stratigraphy,3rd ed.* Blackwell Publishing. Oxford University.

Robinson, R.A.J., Spencer, J.Q.G., Strecker, M.R., Richter, A. & Alonso, R.N. (2005) Luminescence dating of alluvial fans in intramontane basins of NW Argentina. *In*: Harvey, A.M. Mather, A.E. & Stokes, M. (eds) *Alluvial Fans: Geomorphology, Sedimentology, Dynamics.* Geological Society, London. Special Publications, **251**, 153-168.

Rowberry, M.D., McCarthy, T.S., Tompson, M., Nomnganga, A. & Moyo, A. (2012) The spatial and temporal characterization of flooding within the floodplain wetland of the Nyl River, Limpopo province, South Africa. *Water SA.* **37(4)**, 445-451.

Saito, K. &. Oguchi, T. (2005) Slope of alluvial fans in humid regions of Japan, Taiwan and the Philippines. *Geomorphology,* **70**, 147–162

Scholes, R.J. & Walker, B.H. (1993) *An African Savanna: Synthesis of the Nylsvlei study.* Cambridge University Press, Great Britain.

Scott, L. (1982) A Late Quaternary pollen record from the Transvaal Bushveld, South Africa. *Quaternary Research*, **17**, 339-370.

Scott, L. (1989) The climatic conditions in southern Africa since the Last Glacial Maximum, inferred from pollen analysis. *Palaeogeography, Palaeoclimatology, Palaeoecology,* **70**, 345-353

Scott, L. (1999) The vegetation history and climate in the Savanna Biome, South Africa, since 190,000ka: a comparison of pollen data from the Twaing Crater (Pretoria saltpan) and Wonderkrater. *Quaternary International.* **57-58,** 215-223.

Scott, L., Holmgren, K. Talma, A.S. Woodborne, S. & Voegel, J.C. (2003) Age interpretation of the Wonderkrater spring sediments and vegetation change in the Savanna Biome, Limpopo province, South Africa. *South African Journal of Science,* **99,** 484-488.

Shaw, P.A. 1988. After the flood: the fluvio-lacustrine landforms of northern Botswana. *Earth-Science Reviews*. **25**, 449-456.

Smith, G.A. (2000) Recognition and significance of streamflow-dominated piedmont facies in extensional basins. *Basin Research.* **12,** 399-411.

Spencer, D.W. (1963) The interpretation of grain size distribution curves of clastic sediments. *Journal of Sedimentary Petrology,* **33 (1)**, 180-190.

Susino, G.J. (1999) Microdebitage and the archaeology of rock art: an experimental approach. MSc thesis. School of Archaeology, University of Sydney.

Susino, G.J. (2010) *The OSL lab Blurb2.* Geo-luminescence Laboratory, University of Witwatersrand, School of Geoscience.

Stanistreet, I.G. & McCarthy, T.S. (1993) The Okavango fan and the classification of subaerial fan systems. *Sedimentary Geology,* **85**, 115-113.

Thomas, M.F. (1994) *Geomorphology of the Tropics: a study of weathering and denudation in low latitudes.* John Wiley & Sons, England.

Thomas, D.S.G., Brook, G., Shaw, P., Bateman, M., Haberyan, K., Appleton, C., Nash, D., McLaren, S., Davies, F. 2003. Late Pleistocene wetting and drying in the NW Kalahari: an integrated study from the Tsodilo Hills, Botswana. *Quaternary International*. **104**, 53-67.

Thornes, J.B. (1994a) Catchment and channel hydrology. In: Abrahams, A.D., Psarsons, A.J. (Eds.), *Geomorphology of Desert Environments*. Chapman and Hall, London. 257-287.

Taylor, R.E., Stuiver, M. & Reimer, P.J. (1996) Development and extension of the calibration of the radiocarbon time scale: archaeological applications. *Quaternary Science Reviews.* **15,** 655-668.

Tooth, S. (2000) Process, form and change in dryland rivers: a review of recent research. *Earth-Science Reviews.* **51** 67–107.

Tooth, S., McCarthy, T.S., Hancox, P.J., Brandt, D., Buckley, K., Nortje, E. & McQuade, S. (2002) The geomorphology of the Nyl River and floodlain in the semi-arid Northern Province, South Africa. *South African Geographical Journal*. **84,** 226-237.

Tooth, S. & McCarthy, T.S. (2007) Wetlands in Drylands: geomorphological and sedimentological characteristics, with emphasis on examples from southern Africa. *Progress in Physical Geography* **31(1)**, 3-41

Wallinga, J., Murry, A.S. & Bøtter-Jensen, L. (2002) Measurement of the dose in quarts in the presence of feldspar contamination. *Radiation Protection Dosimetry.* **101** (1-4), 367-370.

Wentworth, C.K. (1919) A laboratory and field study of cobble abrasion. *Journal of Geoloogy.* **27**, 507-521.

Werger, M. J. A. (1978) Biogeographical division of Southern Africa. In: M. J. A. Werger (Ed*), Biogeography and Ecology of Southern Africa*. Junk, The Hague, pp. 145 170.

http://www.malvern.com (23/03/2010, 11:30)

http://d-maps.com/pays.php?num_pay=7&lang=en (26/05/10, 13:15)

http://www.sa-venues.com/game-reserves/np_nylsvley.htm (11/02/11, 11:15)

http://www.usgs.gov/pubprod/aerial.html#satellite (02/05/12, 20:25)

http://earthobservatory.nasa.gov/Features/MeasuringVegetation/measuring_vegetation_2.php (04/06/12, 20:56)

GoogleEarth (2012) Cnes/Spot image.

Appendix I

Fig. A.1.1 Enlarged orthophoto of the Driefontein piedmont site indicating 1) the pediment region, 2) the piedmont, 3) spring-fed stream along a possible geological fault line, and 4) the floodout to the south east. Sampled surface sites are shown along with their allocated sample names (courtesy of CSIR and L. Whitfield).

Table A-1: Name, location, mean, standard deviation, skewness and kurtosis of surface samples collected along the Driefontein piedmont

Name	X	Y	Mean phi	Standard dev.	Skewness	Kurtosis
WK-A1	28,73207	-24,4273	2,7955	1,3093	0,2306	1,3085
WK-A2	28,73227	-24,427	2,4889	1,4337	0,1611	1,2767
WK-A3	28,73285	-24,4258	2,671	1,22	0,1405	1,288
WK-A4	28,73283	-24,4248	2,2649	1,4417	0,2712	1,4331
WK-A5	28,7327	-24,4239	2,7994	1,4135	0,2384	1,2318
WK-A6	28,73298	-24,4225	2,2695	1,4215	0,2567	1,3016
WK-A7	28,73323	-24,4211	2,6866	1,2665	0,1669	1,3289
WK-B1	28,73323	-24,4288	2,6433	1,1982	0,1277	1,3265
WK-B2	28,73382	-24,4281	2,673	1,282	0,1737	1,4233
WK-B3	28,73458	-24,4271	2,5756	1,2825	0,0758	1,2756
WK-B4	28,73477	-24,4263	2,0678	1,1621	0,1614	1,1285
WK-B5	28,73662	-24,4257	2,1063	1,2915	0,2029	1,2596
WK-B6	28,7363	-24,4246	2,229	1,3667	0,2436	1,4474
WK-B7	28,73635	-24,4221	2,7314	1,2386	0,1198	1,1083
WK-B8	28,73615	-24,4213	3,1486	1,3156	0,2666	1,3906
WK-B9	28,73642	-24,4205	1,7335	1,3772	0,1998	1,0043
WK-C1	28,73383	-24,4309	2,8374	1,422	0,1631	1,2606
WK-C2	28,73303	-24,4322	2,265	1,6181	0,1918	1,2119
WK-C3	28,73523	-24,4294	2,8921	1,877	0,2617	1,2243
WK-C4	28,73655	-24,428	2,4257	1,1433	0,0946	1,1065
WK-C5	28,7382	-24,4264	3,2813	1,7546	0,1808	1,1128
WK-C6	28,73938	-24,4254	2,1375	1,2386	0,1594	1,2288
WK-C7	28,74103	-24,4236	1,9509	1,2978	0,2746	1,0794
WK-C8	28,74075	-24,4206	2,652	1,6559	0,1338	1,0712
WK-D1	28,74348	-24,4201	2,0572	1,4799	0,1777	1,2926
WK-D2	28,74342	-24,4223	2,1722	1,4545	0,084	0,9331
WK-D3	28,7425	-24,4247	2,456	1,5703	0,1937	1,2744
WK-D4	28,74137	-24,4272	2,7424	1,3036	0,215	1,3993
WK-D5	28,74033	-24,4301	3,0911	1,6961	0,2399	1,224
WK-D6	28,73783	-24,4307	2,7364	1,4933	0,1665	1,1585
WK-D7	28,73608	-24,4321	2,7364	1,4933	0,1665	1,1585
WK-D8	28,73582	-24,4336	2,5428	1,595	0,2478	1,2017
WK-D9	28,73388	-24,4351	1,9445	1,5002	0,2054	1,1724
WK-E1	28,73708	-24,4352	2,2427	1,662	0,179	1,2219
WK-E2	28,73817	-24,4345	2,2541	1,7196	0,2515	1,1597

WK-E3	28,73923	-24,4337	3,0602	1,7746	0,2586	1,2342
WK-E4	28,74085	-24,4331	3,526	1,7826	0,2264	1,2034
WK-E5	28,74228	-24,4322	2,4236	1,5744	0,1874	1,3011
WK-E6	28,74315	-24,4311	2,2528	1,3953	0,1792	1,2755
WK-E7	28,743	-24,4297	2,6051	1,5827	0,0636	1,0498
WK-E8	28,74387	-24,4286	2,8804	1,6943	0,2306	1,2182
WK-E9	28,74482	-24,4276	2,0774	1,7837	0,3519	1,0746
WK-E10	28,74515	-24,4244	2,9668	2,0369	0,284	0,9762
WK-E11	28,74508	-24,4222	3,0507	2,0846	0,2444	0,9385
WK-F1	28,73942	-24,4356	1,7368	1,5262	0,314	0,971
WK-F2	28,74005	-24,435	2,931	1,1362	0,1766	1,189
WK-F3	28,74063	-24,4363	3,5425	1,8064	0,311	1,1451
WK-F4	28,74143	-24,4356	3,558	1,8345	0,3163	1,2115
WK-F5	28,74305	-24,435	3,8361	2,0244	0,2583	1,1308
WK-F6	28,74353	-24,4342	3,349	1,3372	0,1943	1,3335
WK-F7	28,74432	-24,4333	4,2146	2,0374	0,2077	1,198
WK-F8	28,74498	-24,4324	4,3444	1,0587	-0,0331	1,0659
WK-G1	28,74132	-24,4403	3,5987	1,2787	-0,0555	1,0756
WK-G2	28,74208	-24,4399	3,4897	1,1261	0,0937	1,1001
WK-G3	28,74413	-24,4388	2,6024	1,2551	-0,0351	1,1807
WK-G4	28,74555	-24,438	3,3946	1,447	0,0417	0,996
WK-G5	28,74692	-24,4371	3,9959	1,2871	-0,0138	1,1264
WK-G6	28,74688	-24,4364	3,6089	1,5915	-0,001865	0,9084
WK-G7	28,74862	-24,4349	2,9468	1,5509	0,0901	1,2047
WK-G8	28,74992	-24,4336	2,7698	1,1059	0,0945	1,333
WK-G9	28,75233	-24,4314	3,6226	1,2873	0,009328	1,0698
WK-G10	28,75328	-24,4299	3,0338	1,3586	0,1419	1,1319
WK-H1	28,75792	-24,4347	3,577	1,4928	0,006509	1,1226
WK-H2	28,75752	-24,436	2,8633	1,5042	0,1407	1,018
WK-H3	28,75875	-24,4366	3,6333	1,5581	-0,066	1,1685
WK-H4	28,7597	-24,4372	3,7069	1,5718	0,0254	1,0655
WK-H5	28,75232	-24,4416	2,1598	1,2594	0,0573	1,1159
WK-H6	28,75092	-24,4421	2,6983	1,4079	0,1239	1,1885
LF-3	28,72638	-24,4235	2,2382	1,5501	0,3697	1,7288
LF-4	28,7277	-24,4237	1,7216	1,7463	0,4381	1,8427
LF-5	28,72927	-24,4236	1,4163	1,5157	0,4936	1,818

Sedimentary sample laboratory treatment procedure:

- Water content: weight of wet sample – weight of dry sample
- Oven dry at 50º (earth maximum temperature)
- Etching in HCl and H_2O_2 and in order to remove organic and carbonate contaminants. Each treatment lasted a minimum of 4 hours and each sample was rinsed with deionized water and dried between treatments.
- Sieving of samples at ¼ Φ intervals using standard sedimentary sieves for OSL samples and lasergranulometry for core and surface samples.
- Heavy metal separation using Sodium polytungstate (SPT) and a FRANZT machine with setting: slope = 21º, tilt = 17º, and amperage = 1.4 - 1.5
- Further etching for OSL samples using H_2SiF_6
- Final oven drying before packing in plastic bags and light proof containers for OSL samples.

Grain size distribution: Surface samples LF and WK - A to - H:

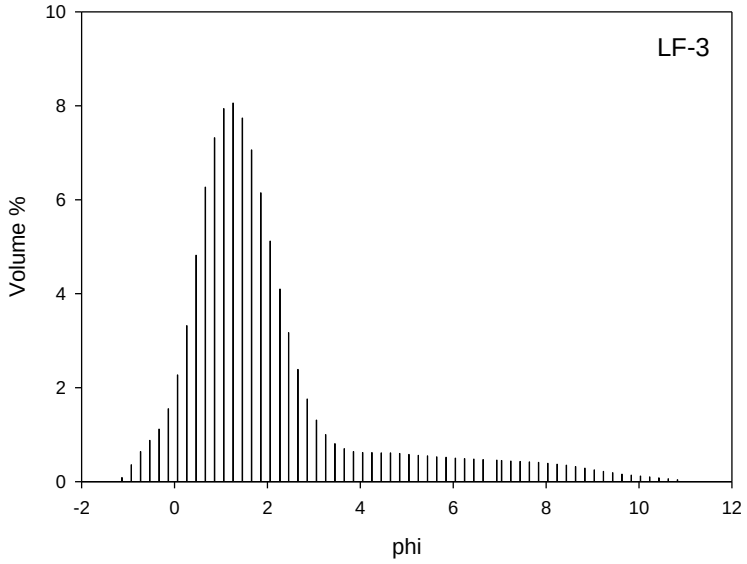

Fig. A1.2 Frequency distribution curve for Wonderkrater surface sample LF-3

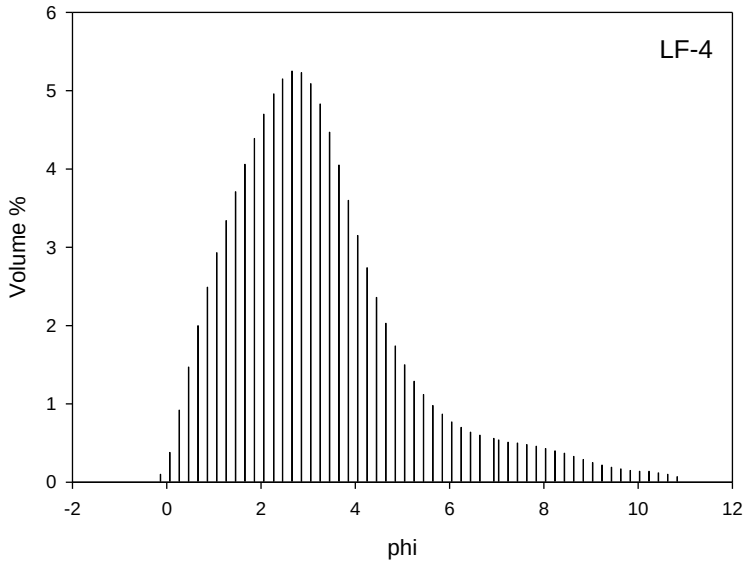

Fig. A1.3 Frequency distribution curve for Wonderkrater surface sample LF-4

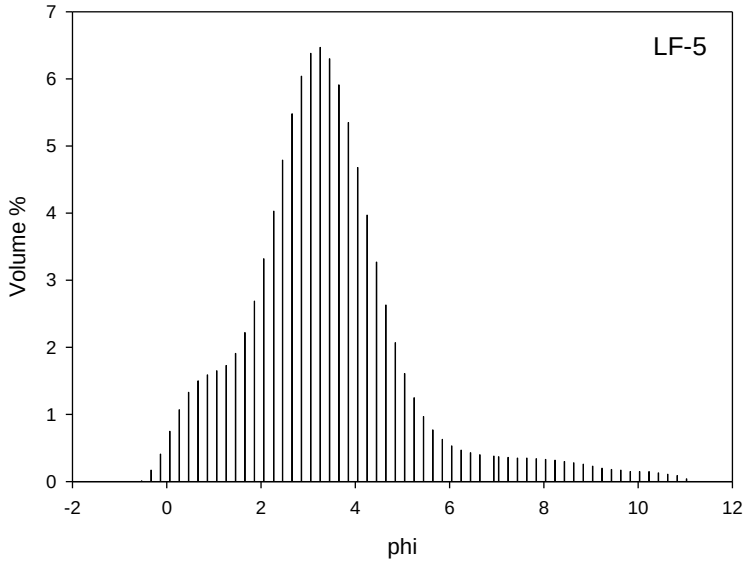

Fig. A1.4 Frequency distribution curve for Wonderkrater surface sample LF-5

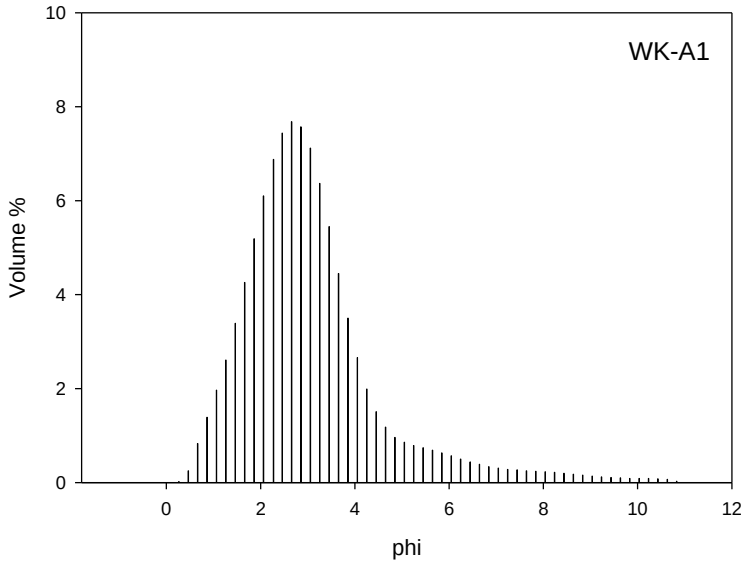

Fig. A1.5 Frequency distribution curve for Wonderkrater surface sample WK-A1

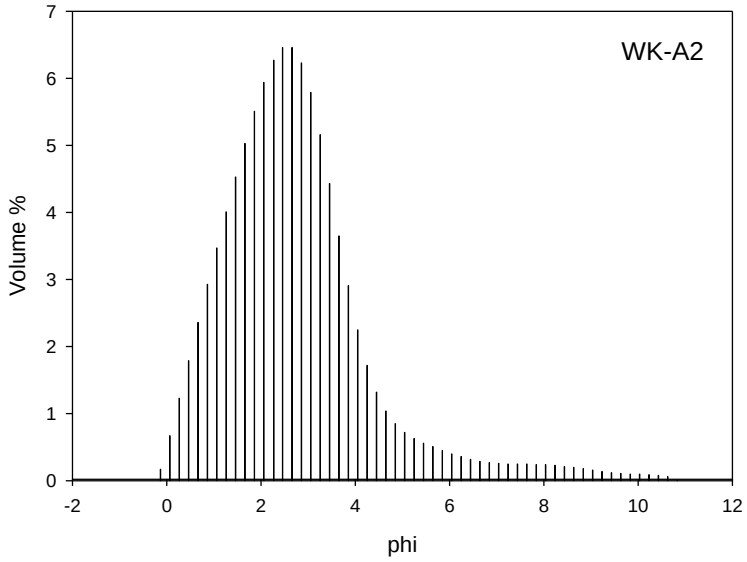

Fig. A1.6 Frequency distribution curve for Wonderkrater surface sample WK-A2

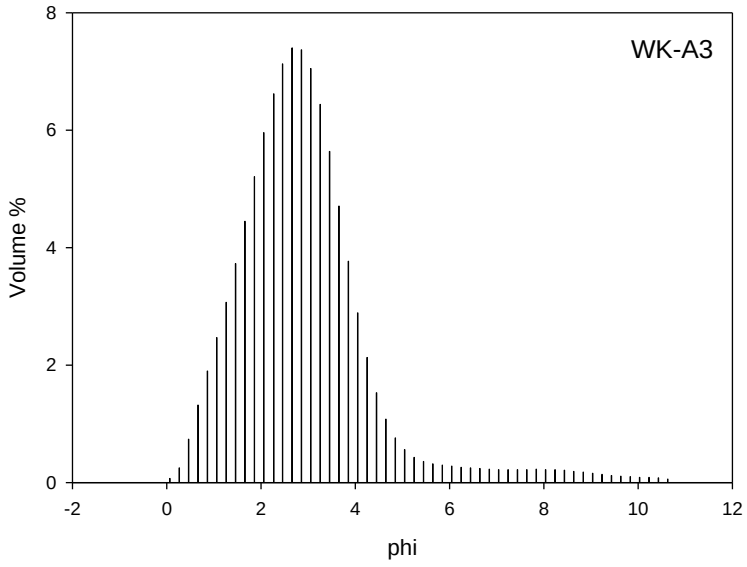

Fig. A1.7 Frequency distribution curve for Wonderkrater surface sample WK-A3

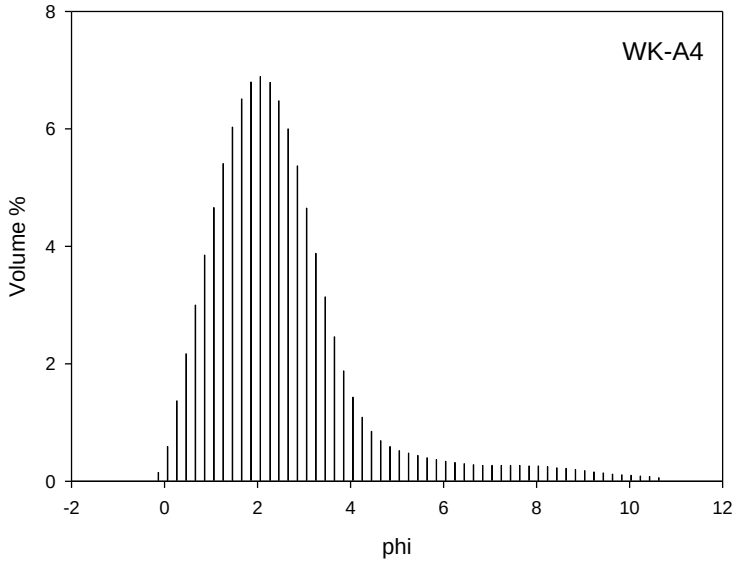

Fig. A1.8 Frequency distribution curve for Driefontein surface sample WK-A4

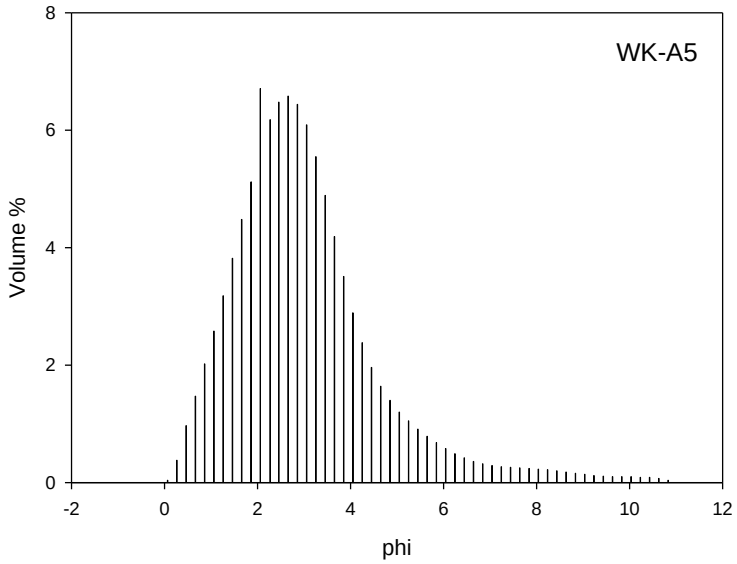

Fig. A1.9 Frequency distribution curve for Driefontein surface sample WK-A5

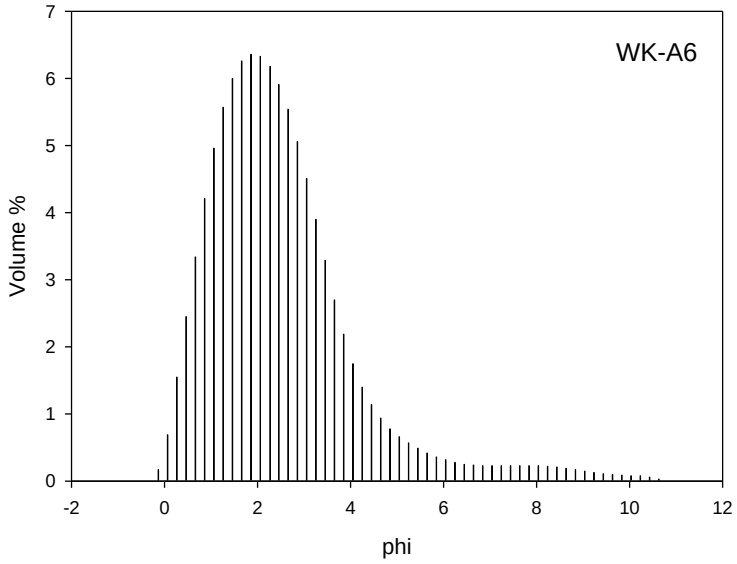

Fig. A1.10 Frequency distribution curve for Driefontein surface sample WK-A6

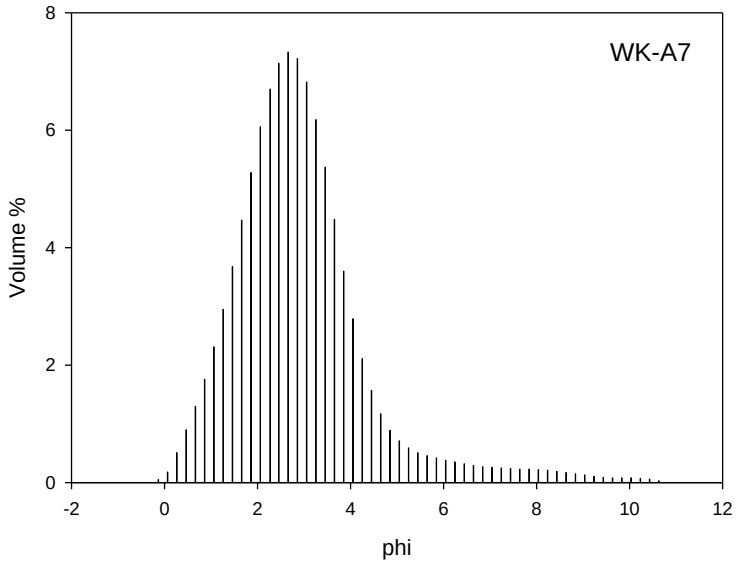

Fig. A1.11 Frequency distribution curve for Driefontein surface sample WK-A7

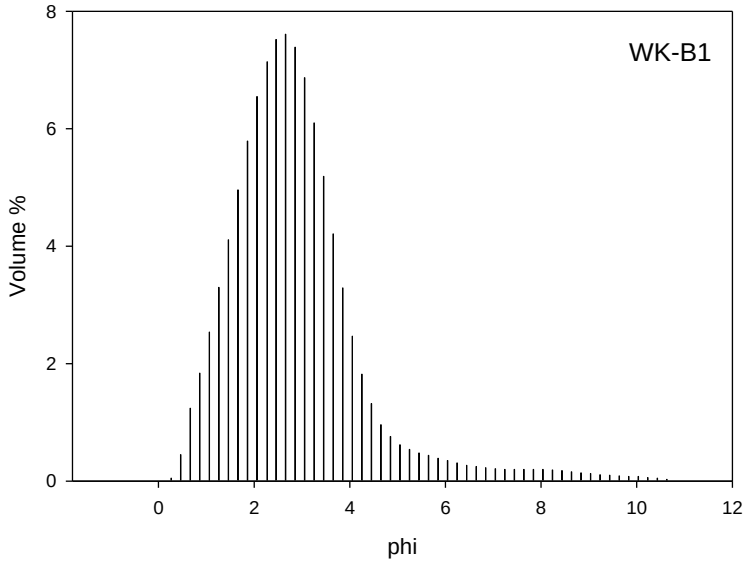

Fig. A1.12 Frequency distribution curve for Driefontein surface sample WK-B1

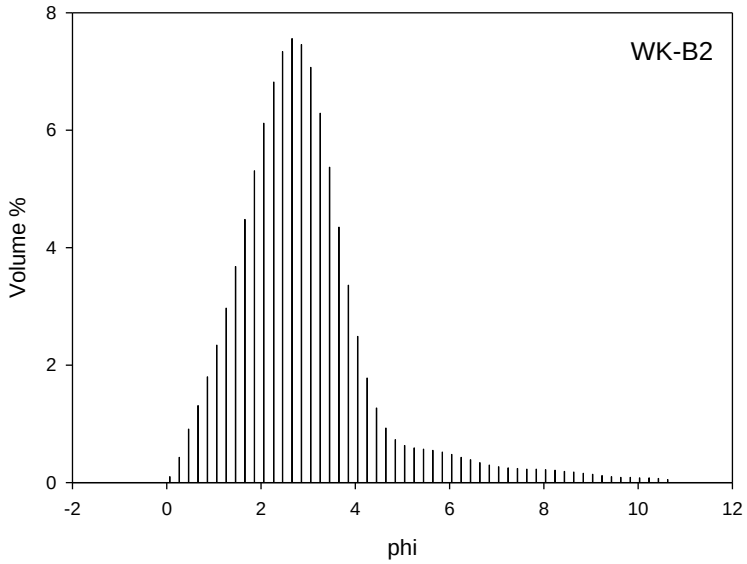

Fig. A1.13 Frequency distribution curve for Driefontein surface sample WK-B2

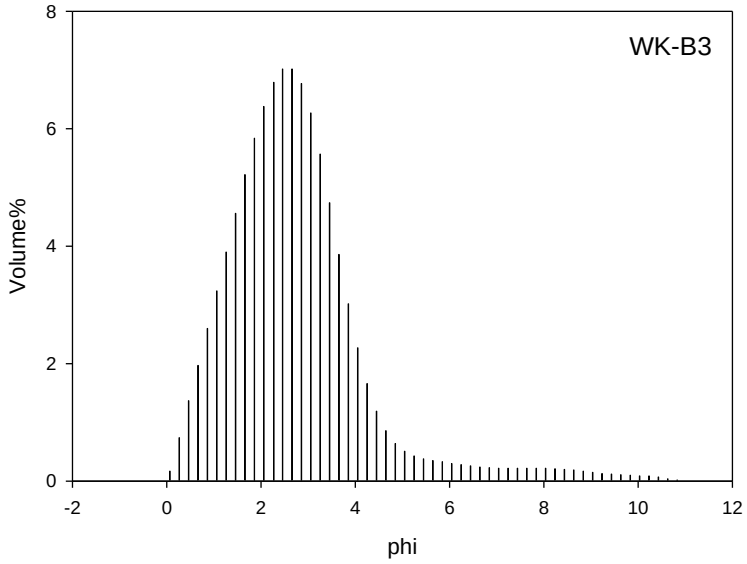

Fig. A1.14 Frequency distribution curve for Driefontein surface sample WK-B3

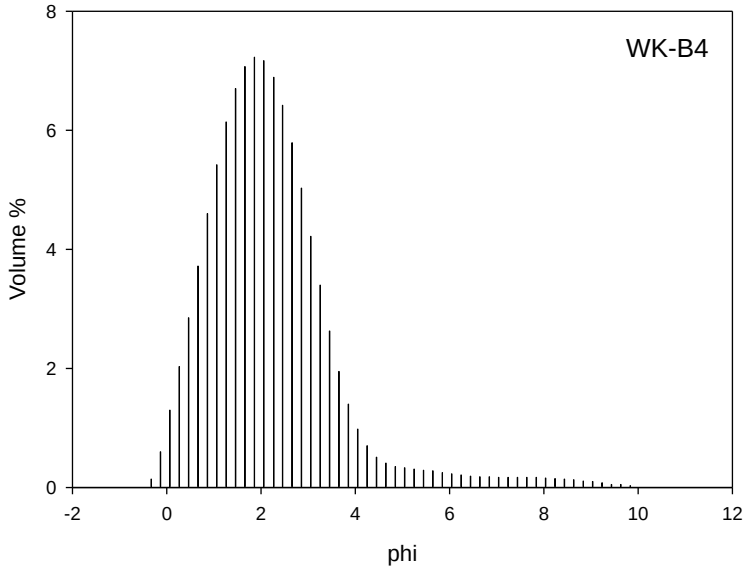

Fig. A1.15 Frequency distribution curve for Driefontein surface sample WK-B4

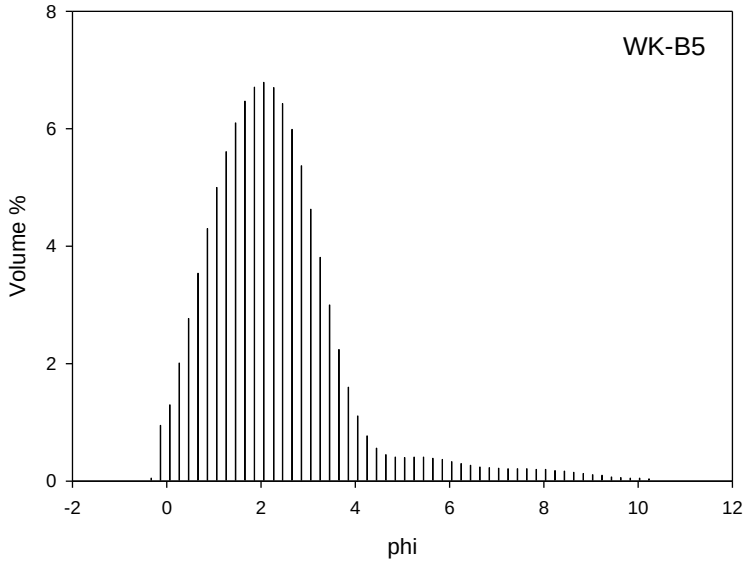

Fig. A1.16 Frequency distribution curve for Driefontein surface sample WK-B5

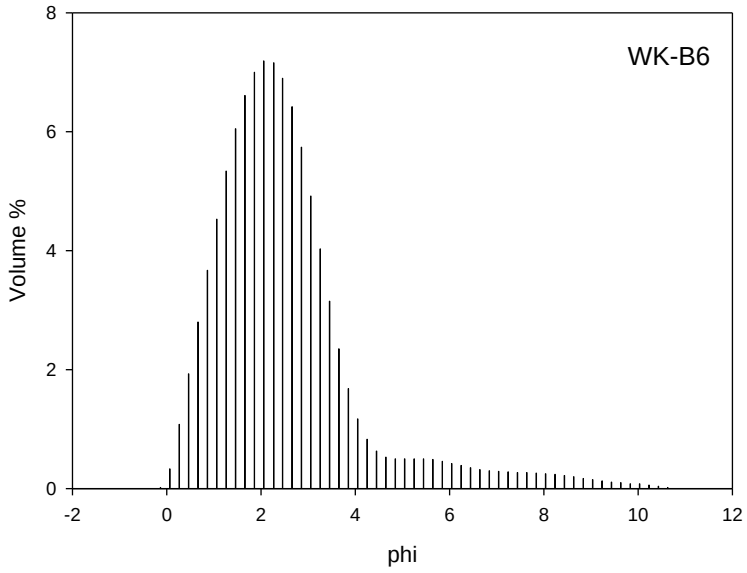

Fig. A1.17 Frequency distribution curve for Driefontein surface sample WK-B6

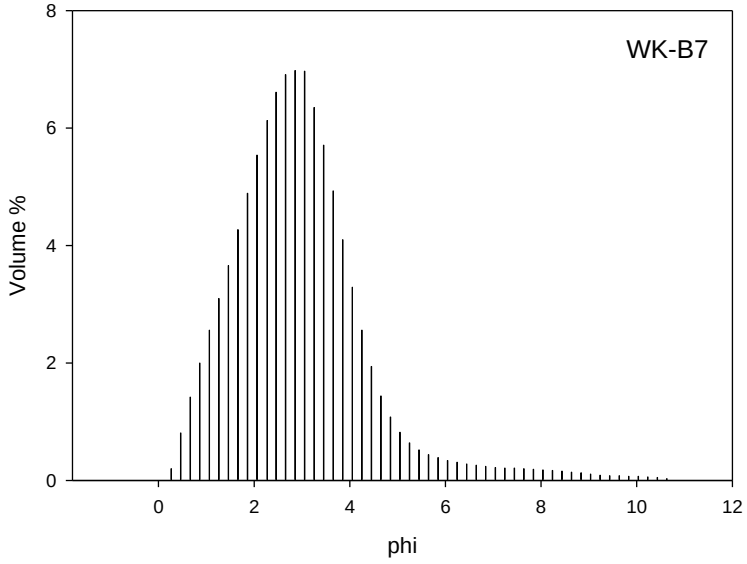

Fig. A1.18 Frequency distribution curve for Driefontein surface sample WK-B7

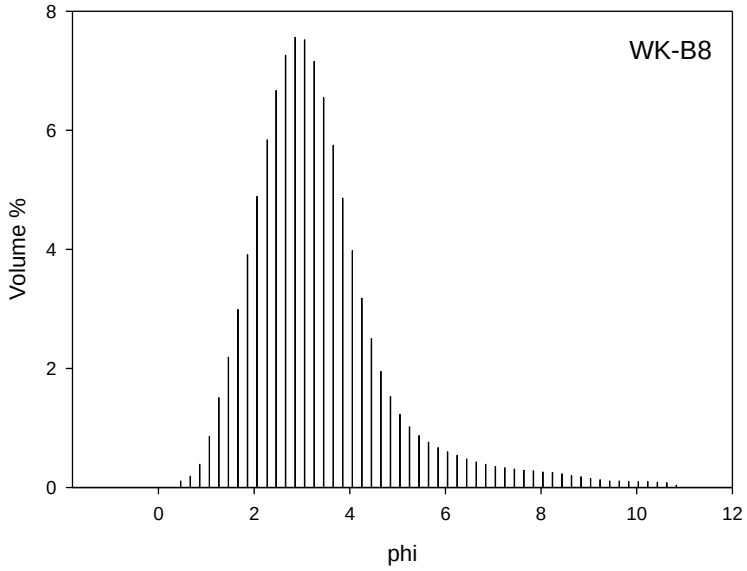

Fig. A1.19 Frequency distribution curve for Driefontein surface sample WK-B8

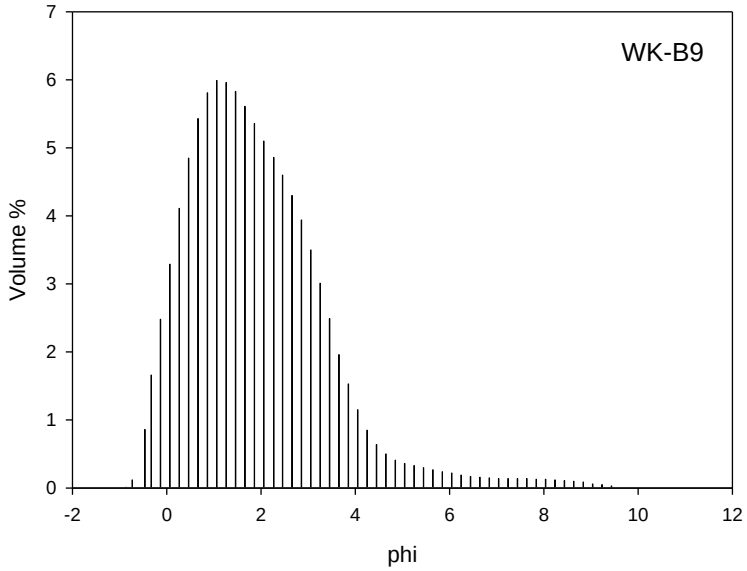

Fig. A1.20 Frequency distribution curve for Driefontein surface sample WK-B9

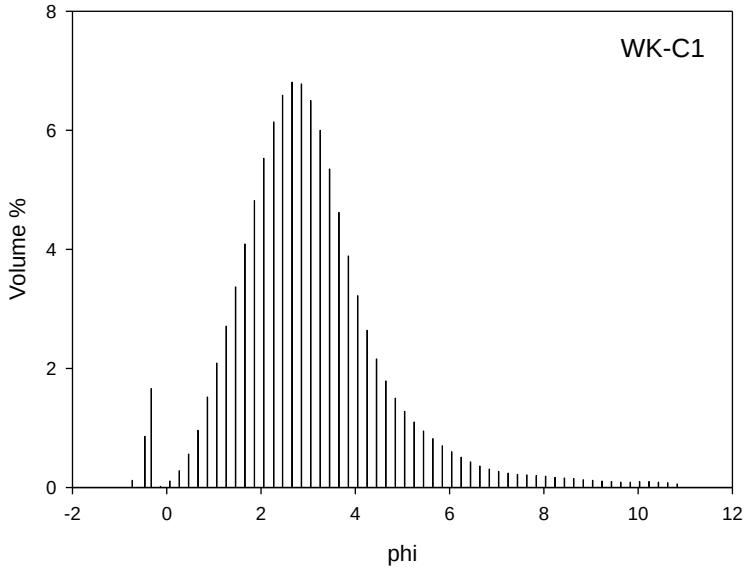

Fig. A1.21 Frequency distribution curve for Driefontein surface sample WK-C1

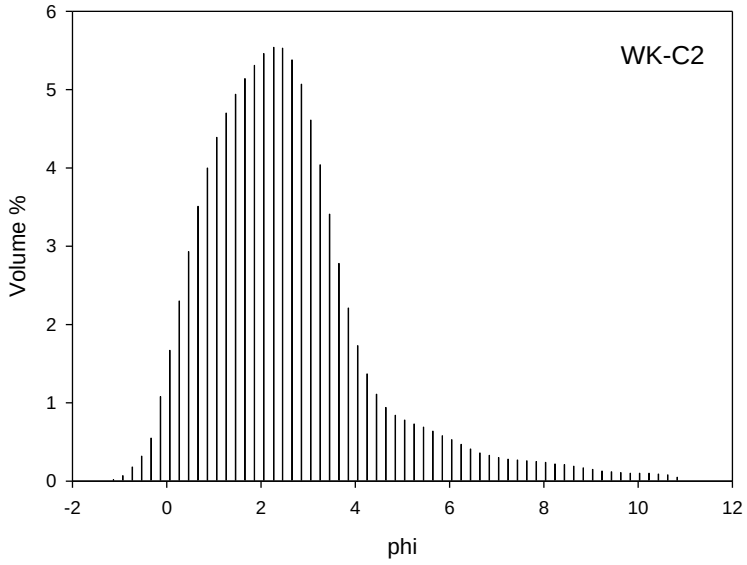

Fig. A1.22 Frequency distribution curve for Driefontein surface sample WK-C2

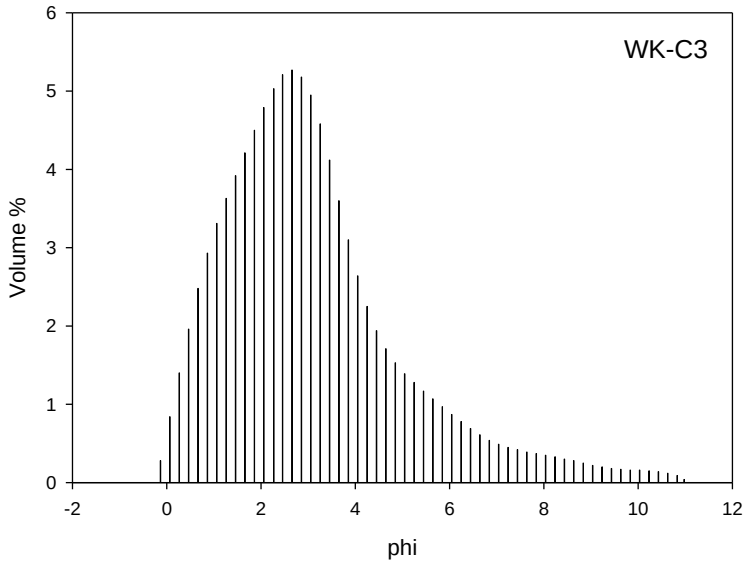

Fig. A1.23 Frequency distribution curve for Driefontein surface sample WK-C3

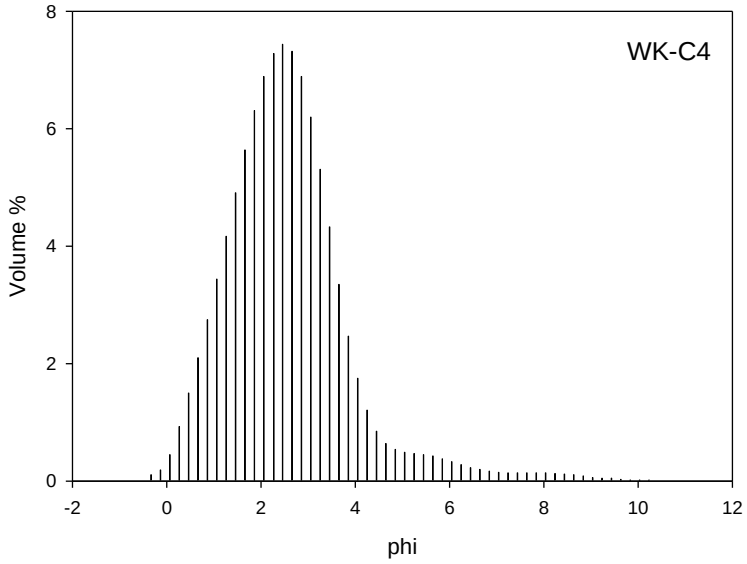

Fig. A1.24 Frequency distribution curve for Driefontein surface sample WK-C4

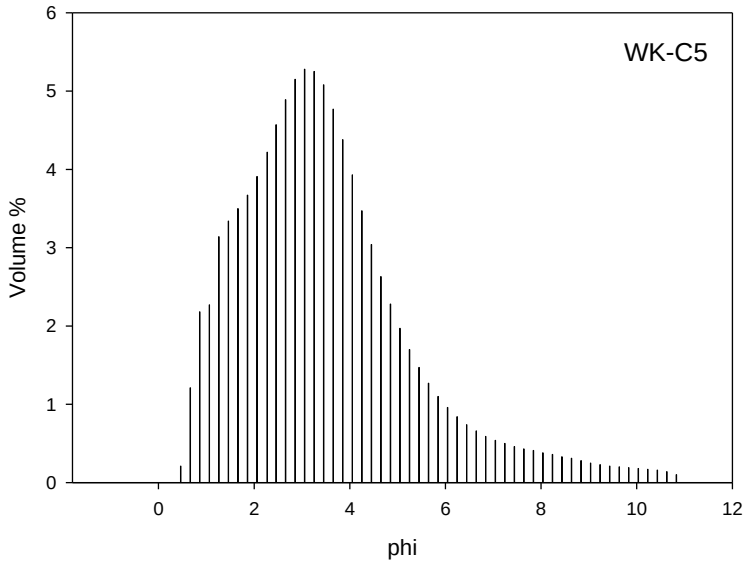

Fig. A1.25 Frequency distribution curve for Driefontein surface sample WK-C5

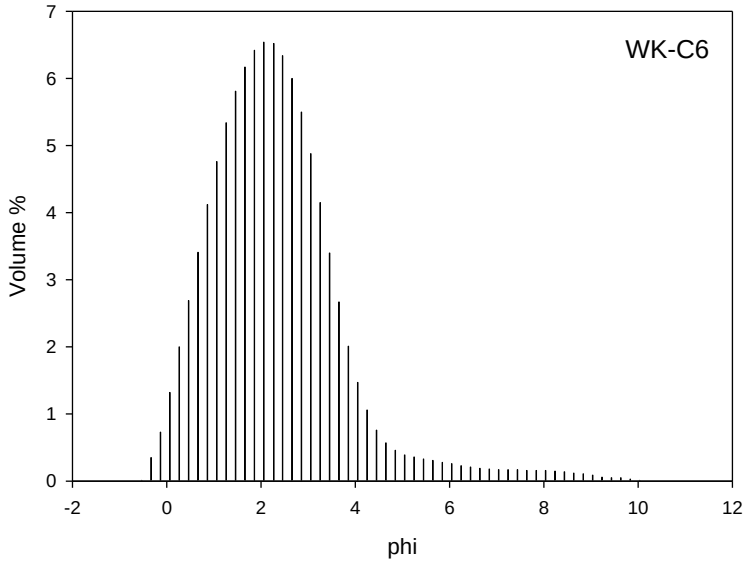

Fig. A1.26 Frequency distribution curve for Driefontein surface sample WK-C6

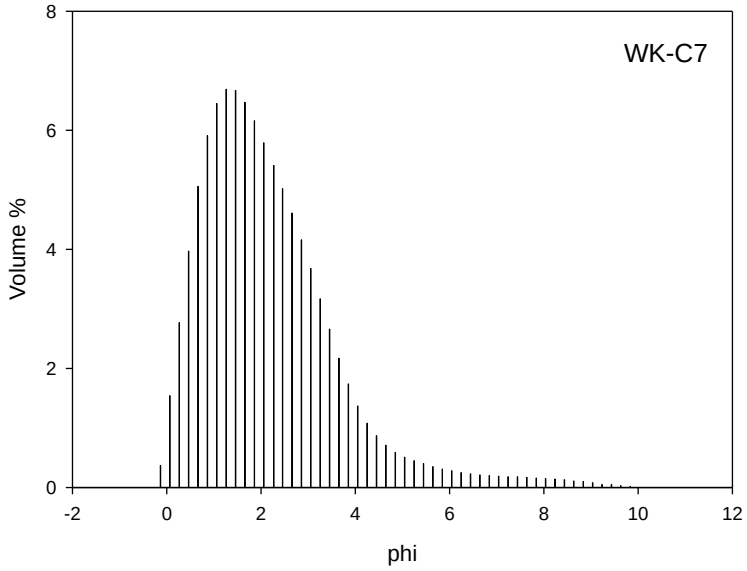

Fig. A1.27 Frequency distribution curve for Driefontein surface sample WK-C7

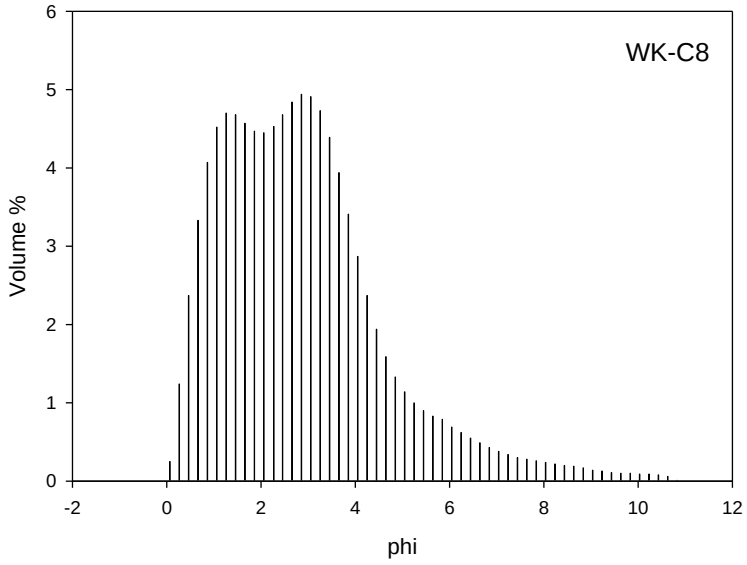

Fig. A1.28 Frequency distribution curve for Driefontein surface sample WK-C8

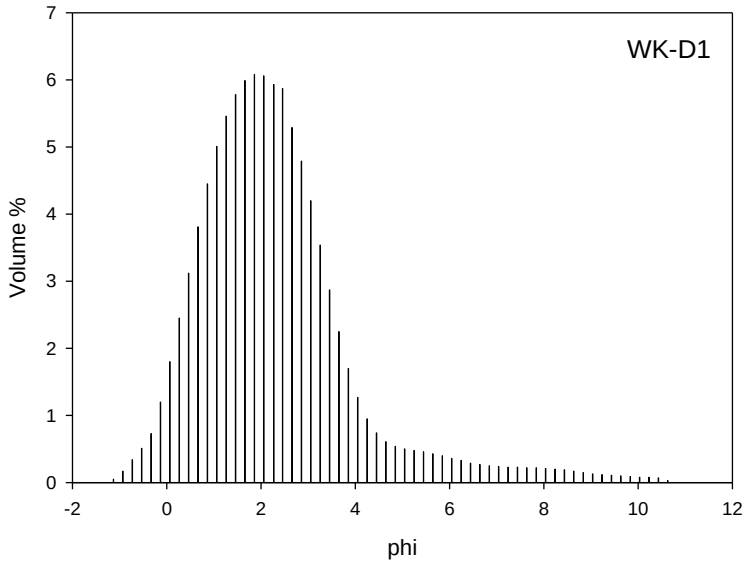

Fig. A1.29 Frequency distribution curve for Driefontein surface sample WK-D1

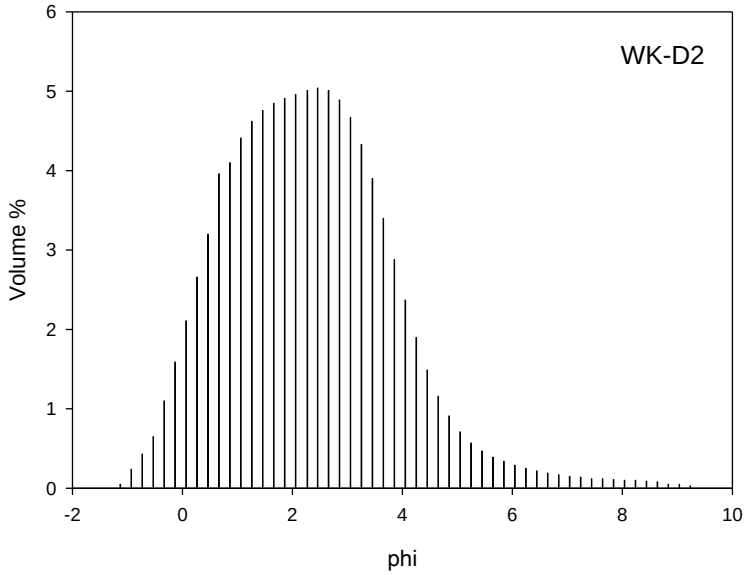

Fig. A1.30 Frequency distribution curve for Driefontein surface sample WK-D2

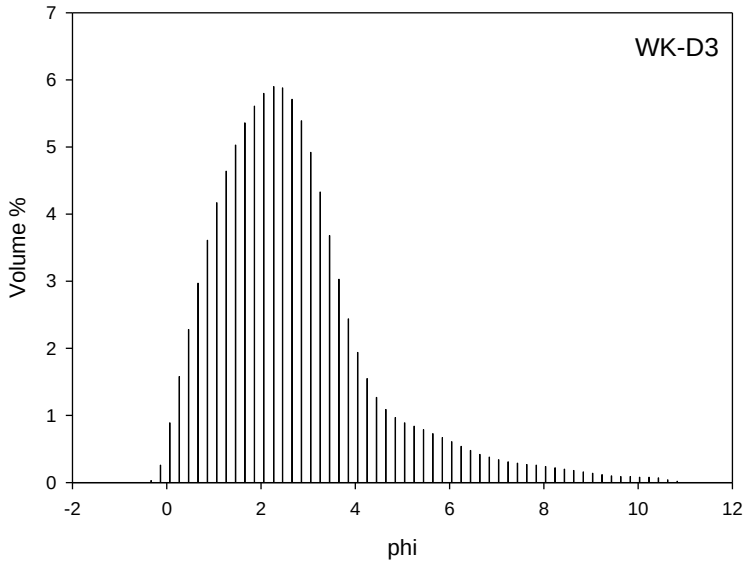

Fig. A1.31 Frequency distribution curve for Driefontein surface sample WK-D3

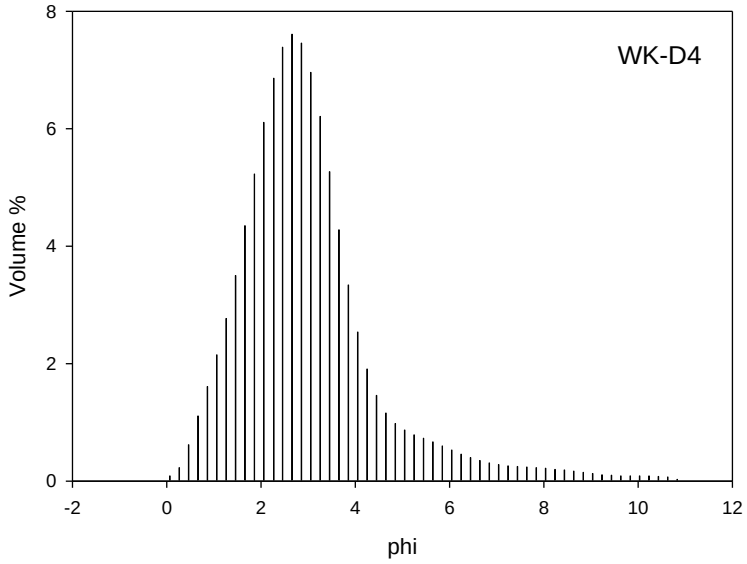

Fig. A1.32 Frequency distribution curve for Driefontein surface sample WK-D4

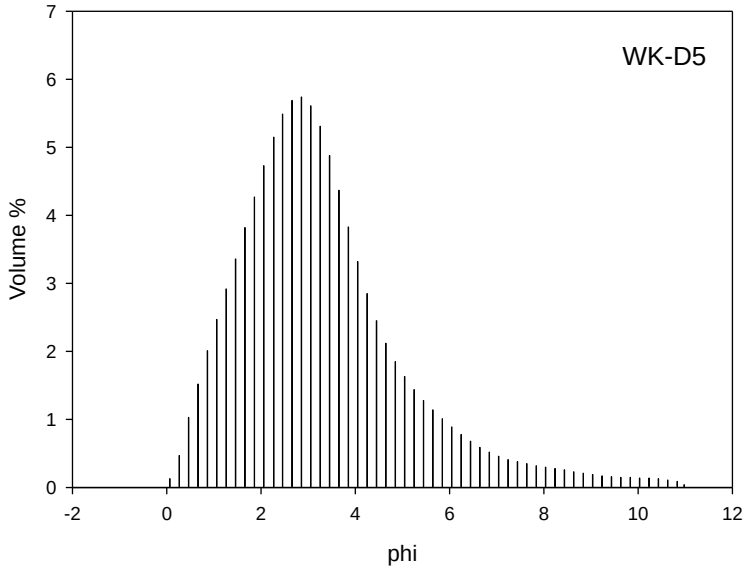

Fig. A1.33 Frequency distribution curve for Driefontein surface sample WK-D5

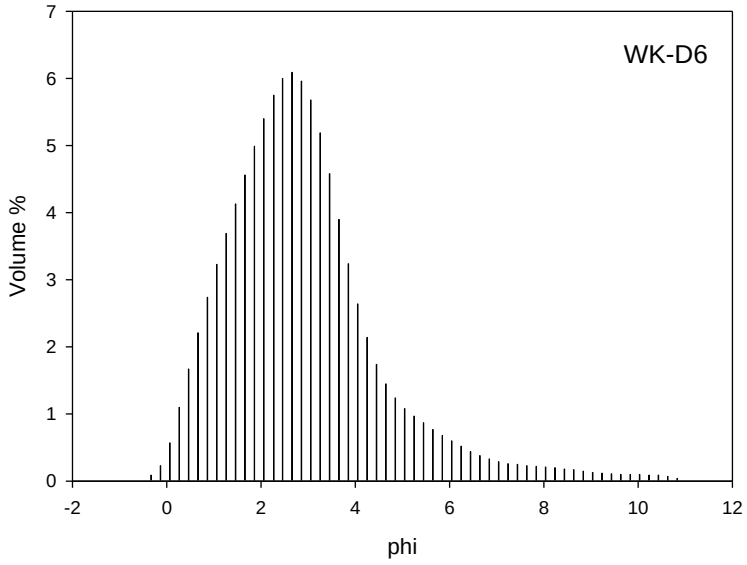

Fig. A1.34 Frequency distribution curve for Driefontein surface sample WK-D6

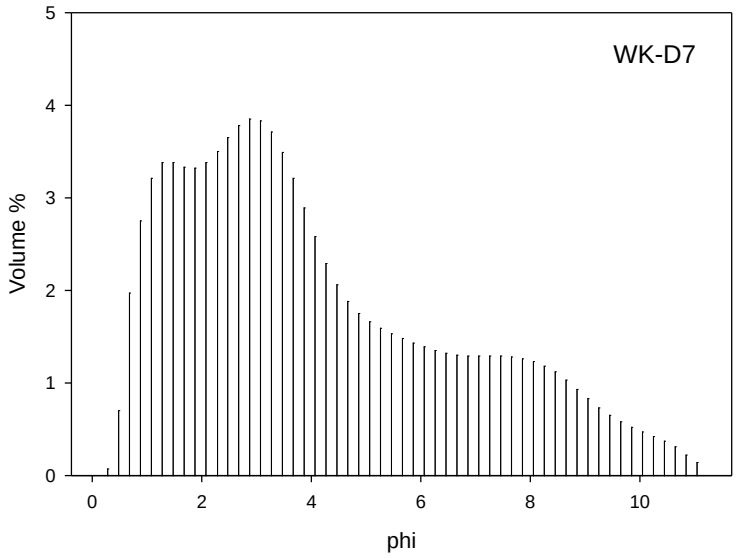

Fig. A1.35 Frequency distribution curve for Driefontein surface sample WK-D7

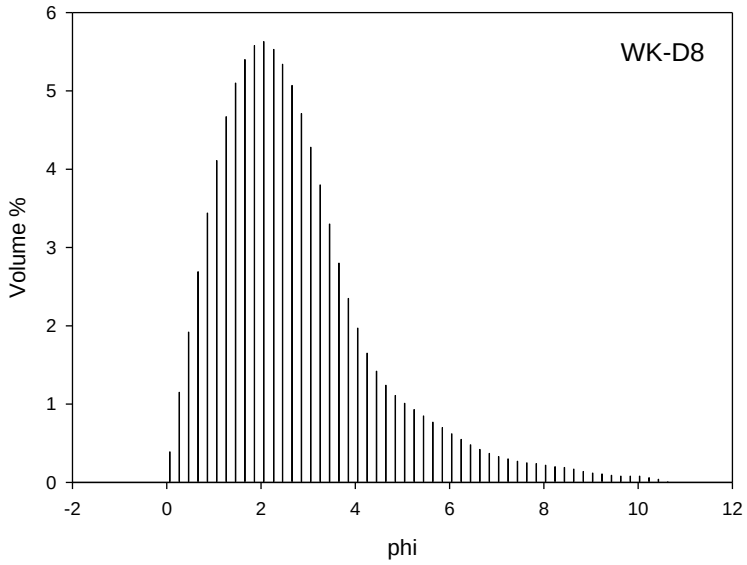

Fig. A1.36 Frequency distribution curve for Driefontein surface sample WK-D8

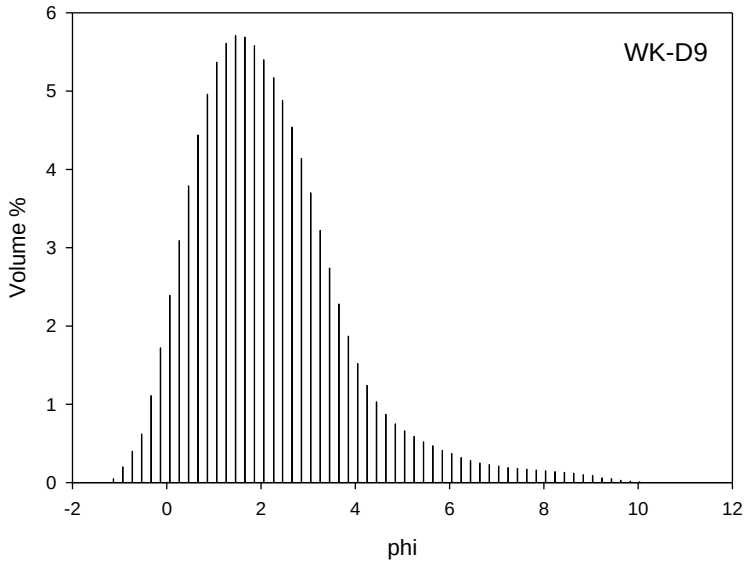

Fig. A1.37 Frequency distribution curve for Driefontein surface sample WK-D9

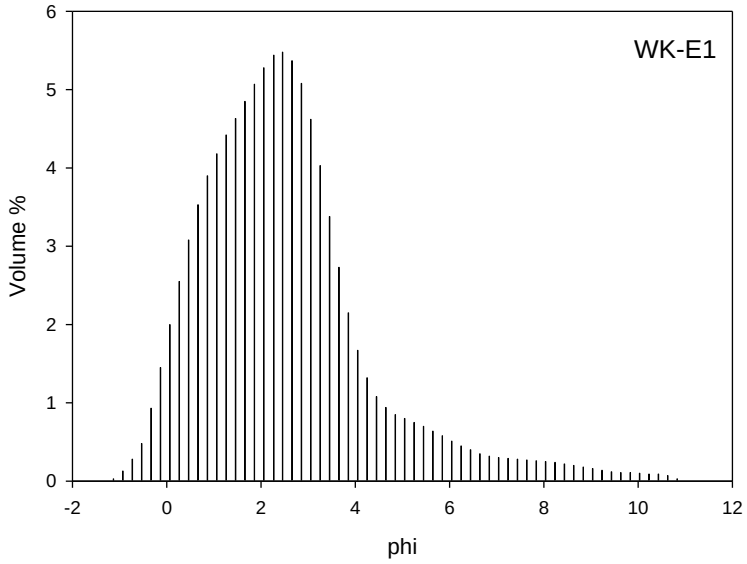

Fig. A1.38 Frequency distribution curve for Driefontein surface sample WK-E1

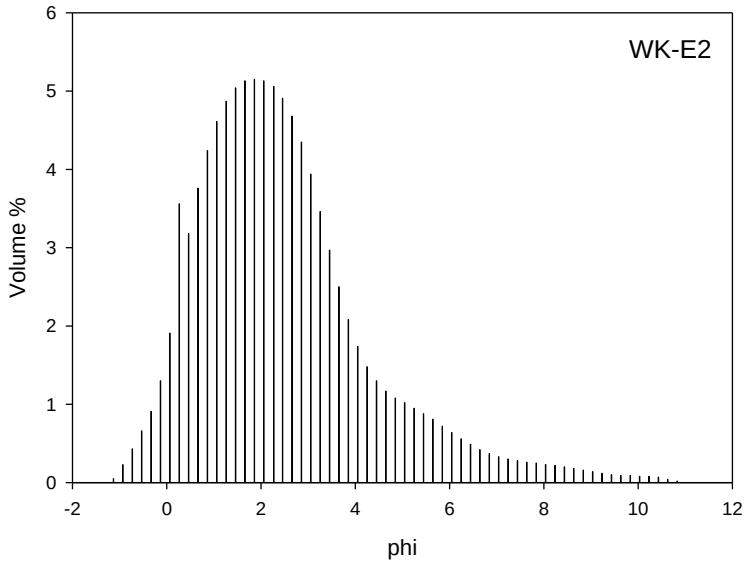

Fig. A1.39 Frequency distribution curve for Driefontein surface sample WK-E2

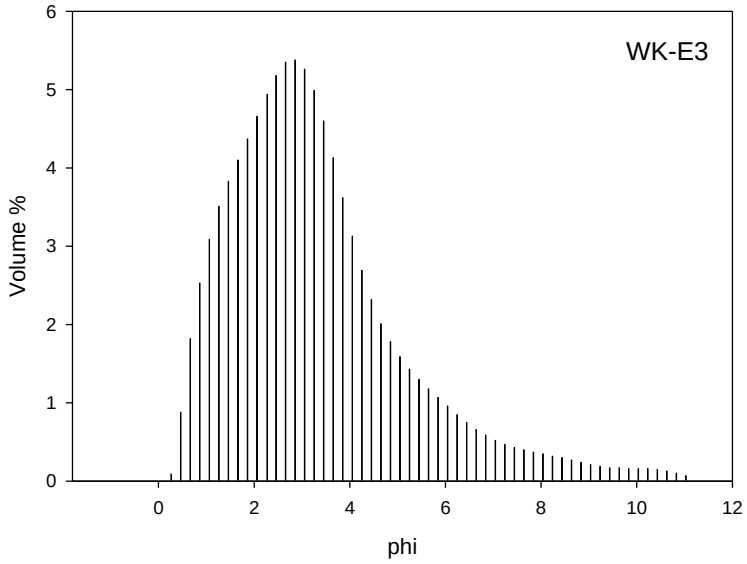

Fig. A1.40 Frequency distribution curve for Driefontein surface sample WK-E3

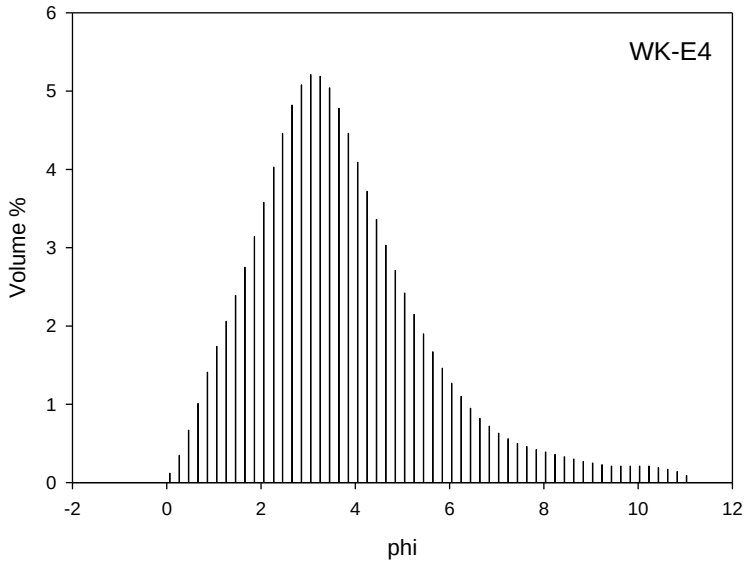

Fig. A1.41 Frequency distribution curve for Driefontein surface sample WK-E4

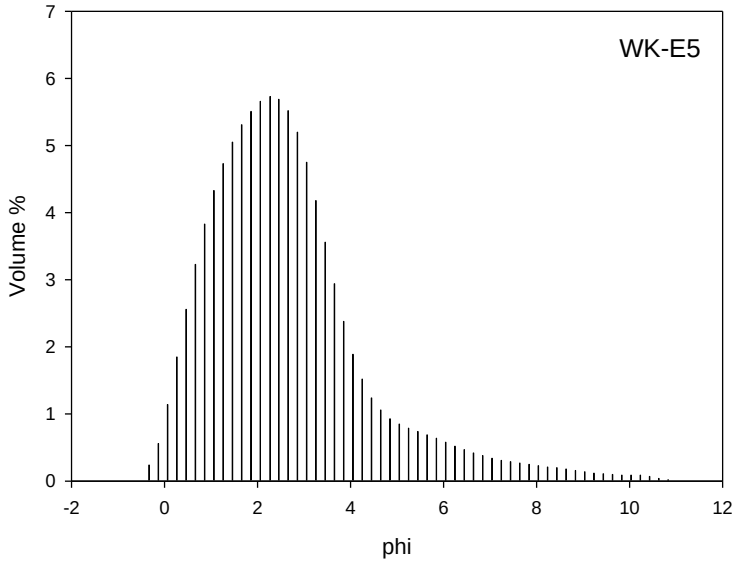

Fig. A1.42 Frequency distribution curve for Driefontein surface sample WK-E5

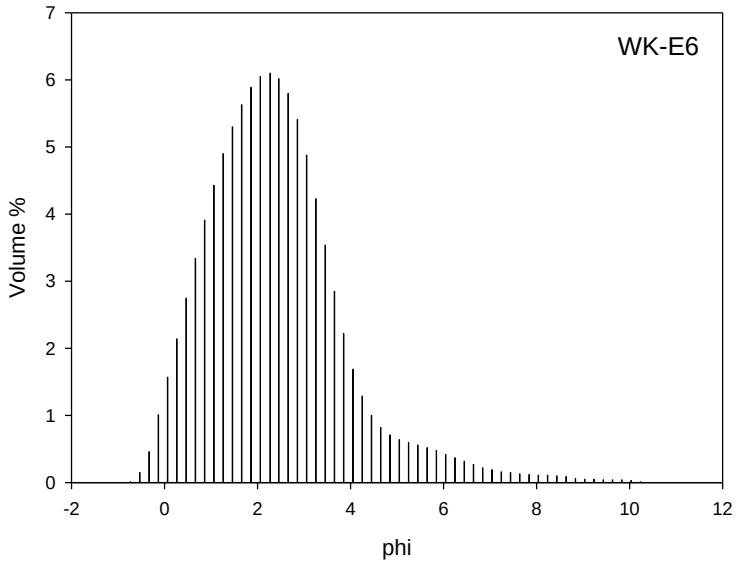

Fig. A1.43 Frequency distribution curve for Driefontein surface sample WK-E6

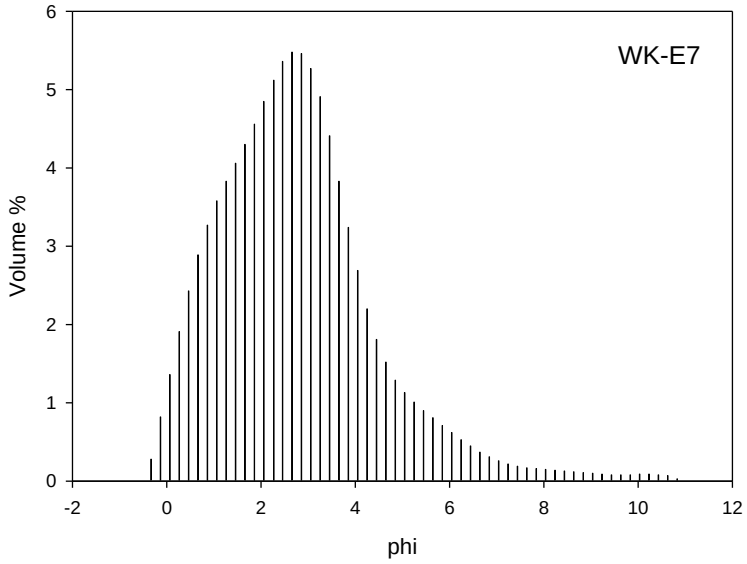

Fig. A1.44 Frequency distribution curve for Driefontein surface sample WK-E7

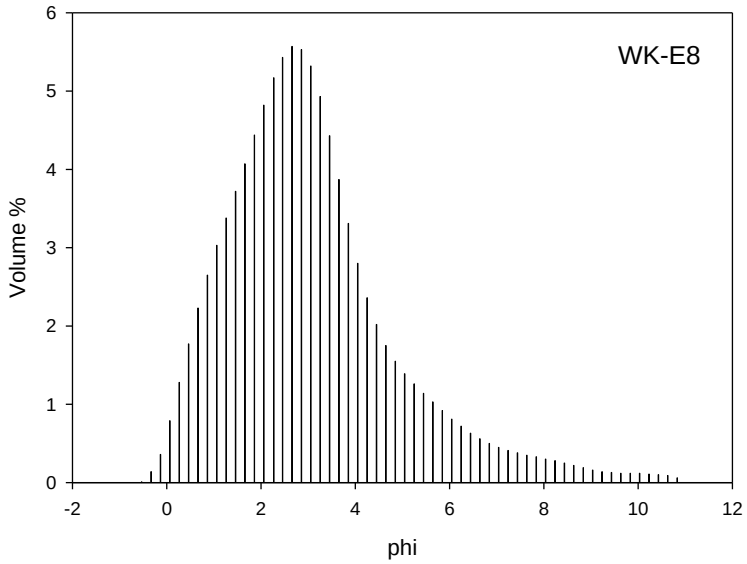

Fig. A1.45 Frequency distribution curve for Driefontein surface sample WK-E8

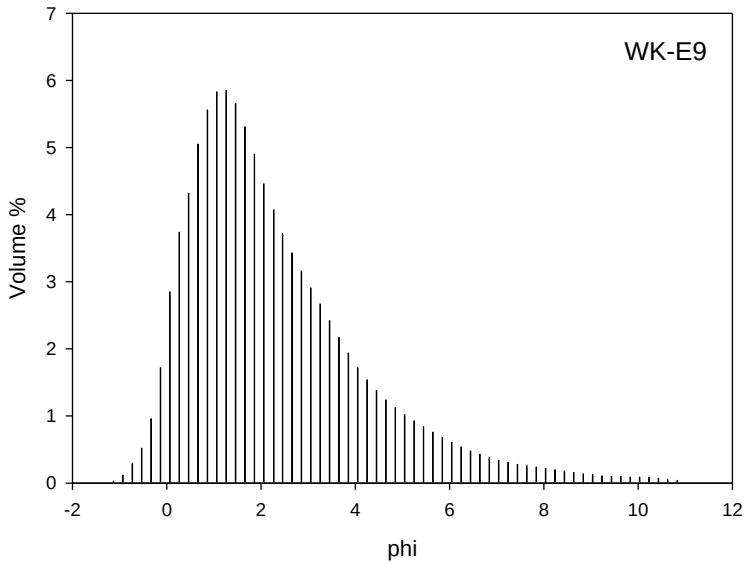

Fig. A1.46 Frequency distribution curve for Driefontein surface sample WK-E9

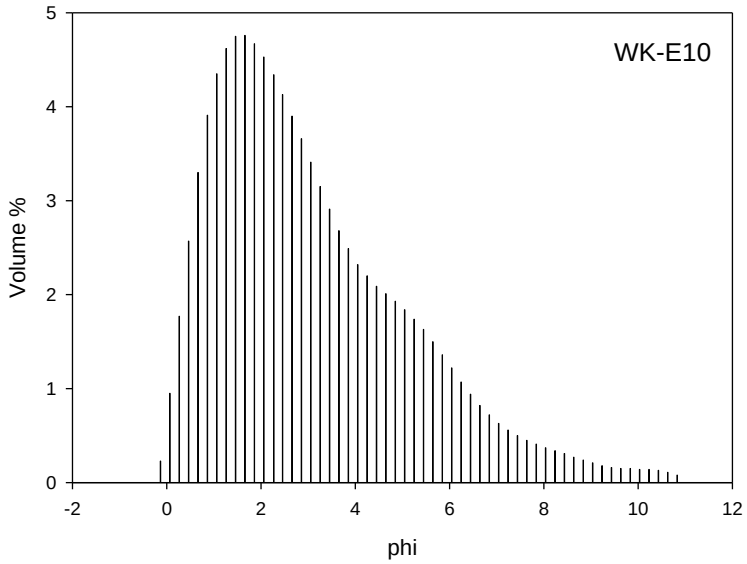

Fig. A1.47 Frequency distribution curve for Driefontein surface sample WK-E10

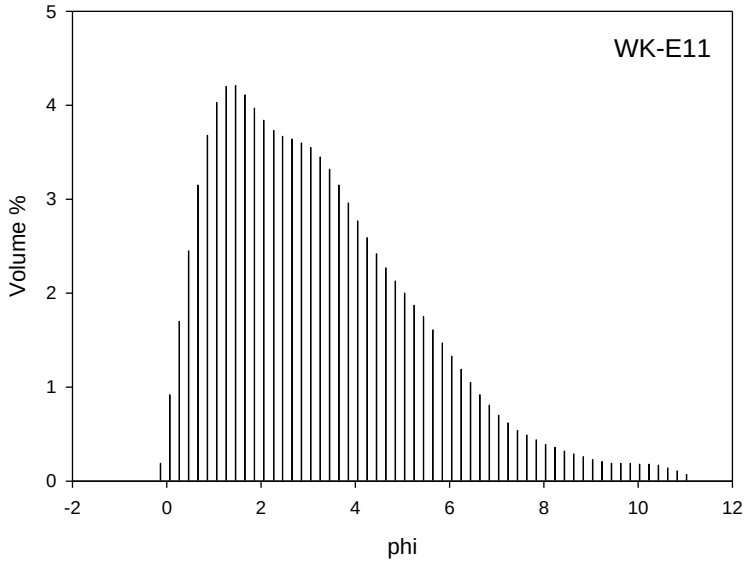

Fig. A1.48 Frequency distribution curve for Driefontein surface sample WK-E11

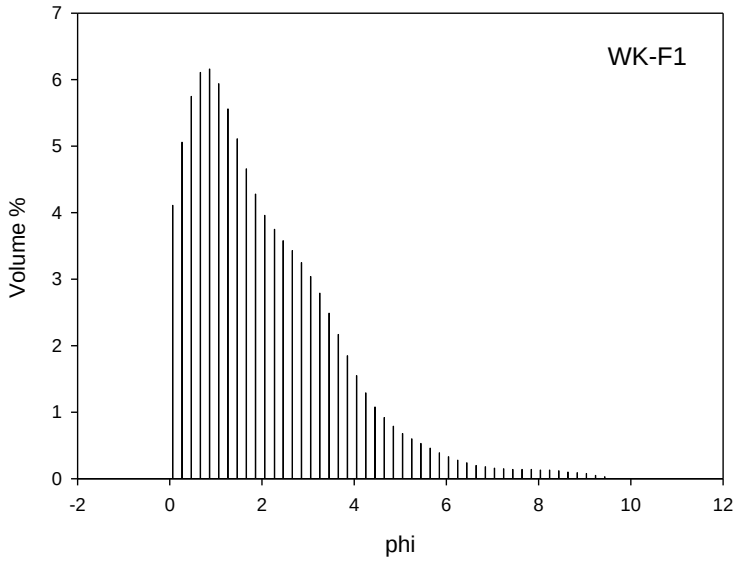

Fig. A1.49 Frequency distribution curve for Driefontein surface sample WK-F1

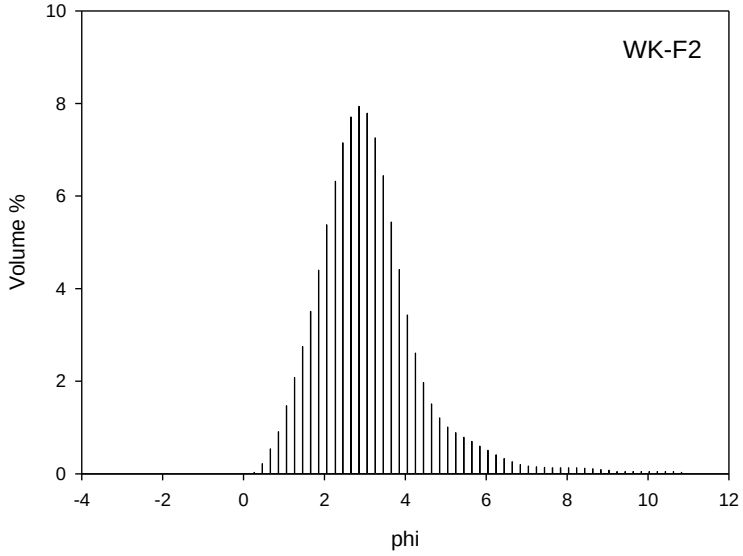

Fig. A1.50 Frequency distribution curve for Driefontein surface sample WK-F2

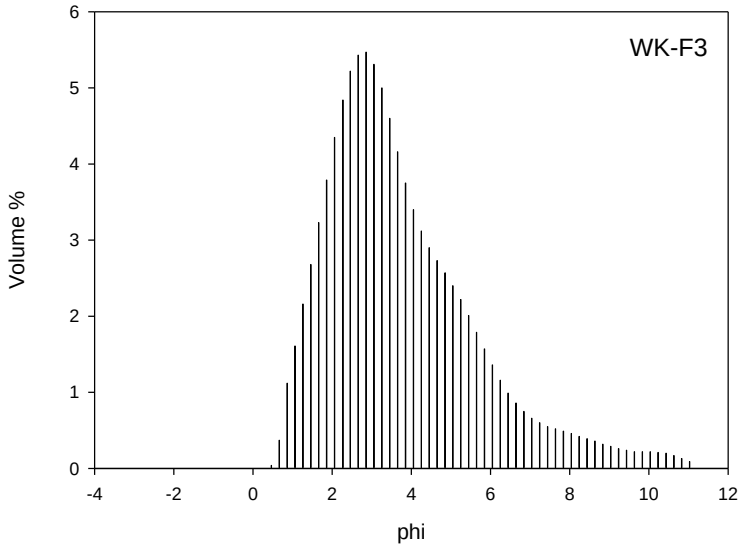

Fig. A1.51 Frequency distribution curve for Driefontein surface sample WK-F3

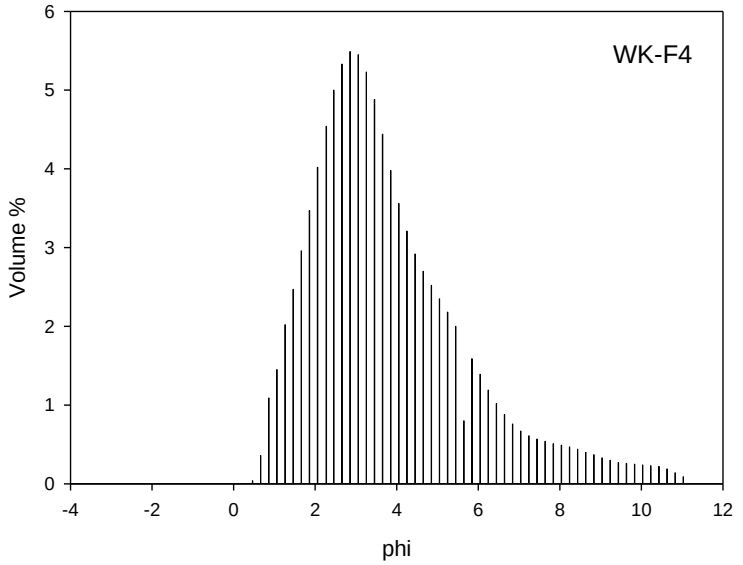

Fig. A1.52 Frequency distribution curve for Driefontein surface sample WK-F4

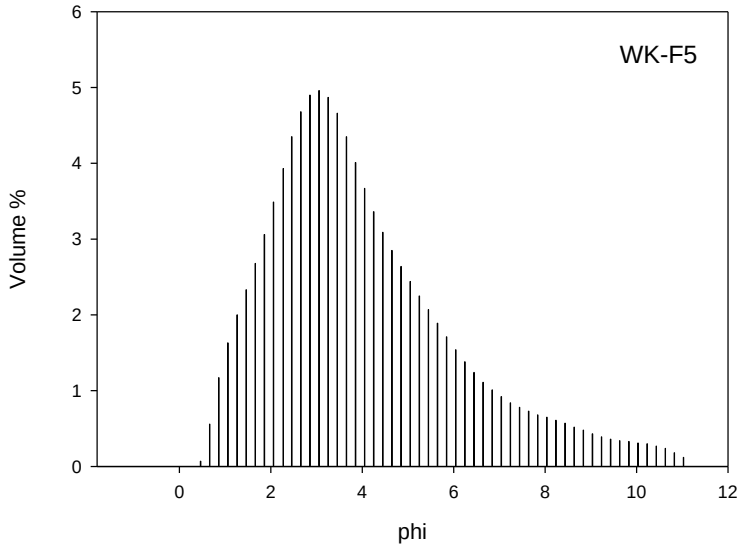

Fig. A1.53 Frequency distribution curve for Driefontein surface sample WK-F5

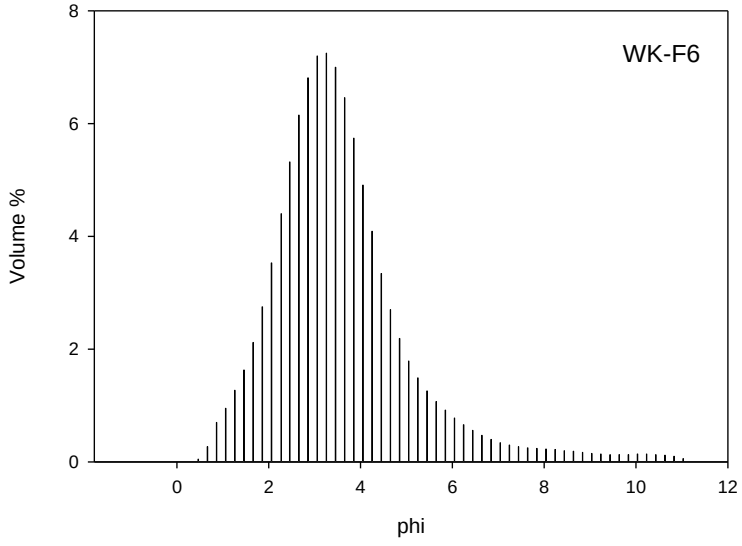

Fig. A1.54 Frequency distribution curve for Driefontein surface sample WK-F6

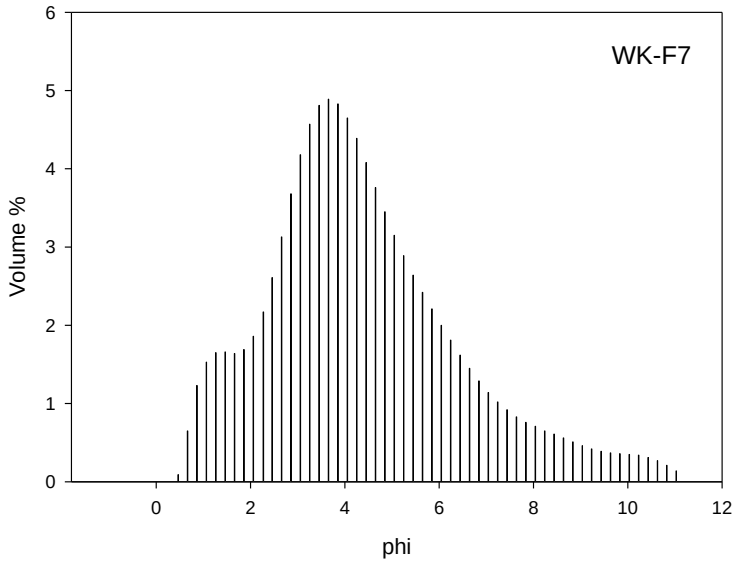

Fig. A1.55 Frequency distribution curve for Driefontein surface sample WK-F7

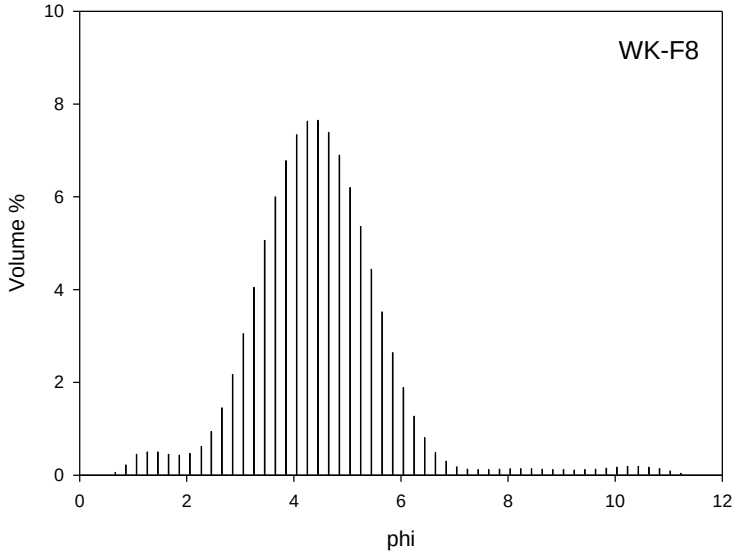

Fig. A1.56 Frequency distribution curve for Driefontein surface sample WK-F8

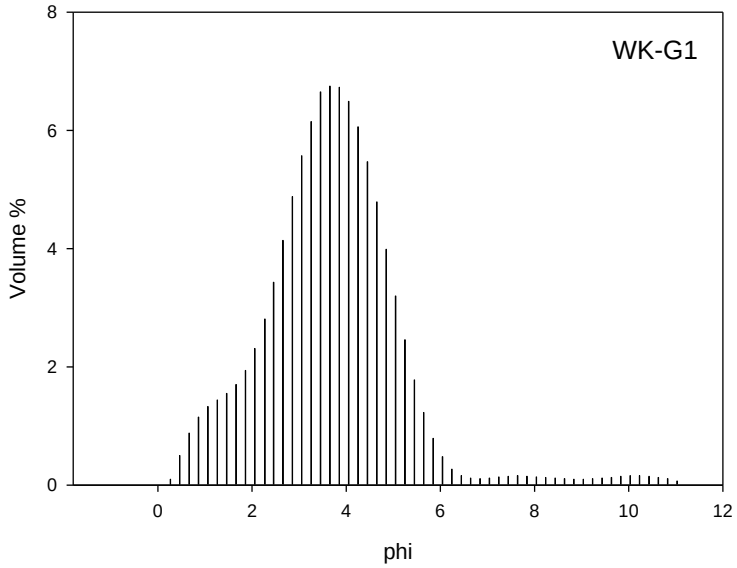

Fig. A1.57 Frequency distribution curve for Driefontein surface sample WK-G1

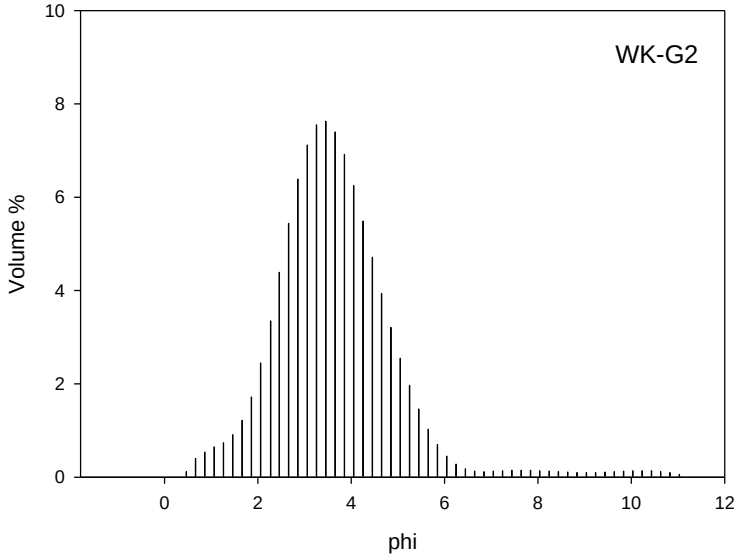

Fig. A1.58 Frequency distribution curve for Driefontein surface sample WK-G2

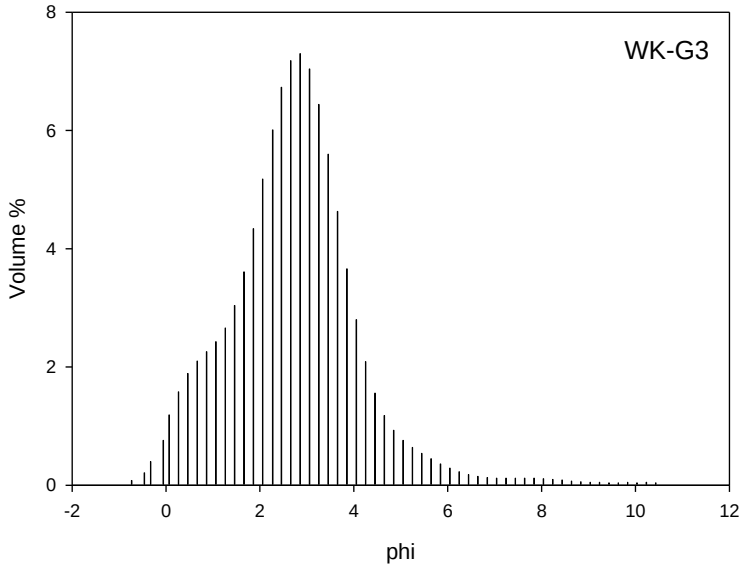

Fig. A1.59 Frequency distribution curve for Driefontein surface sample WK-G3

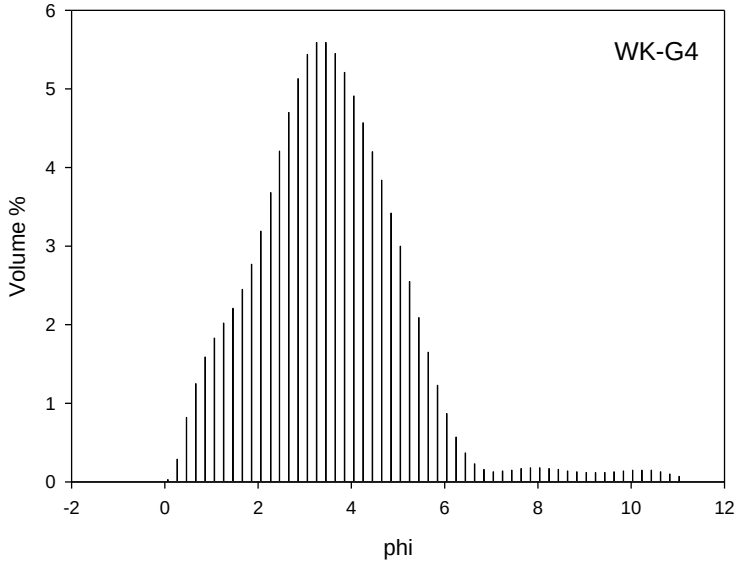

Fig. A1.60 Frequency distribution curve for Driefontein surface sample WK-G4

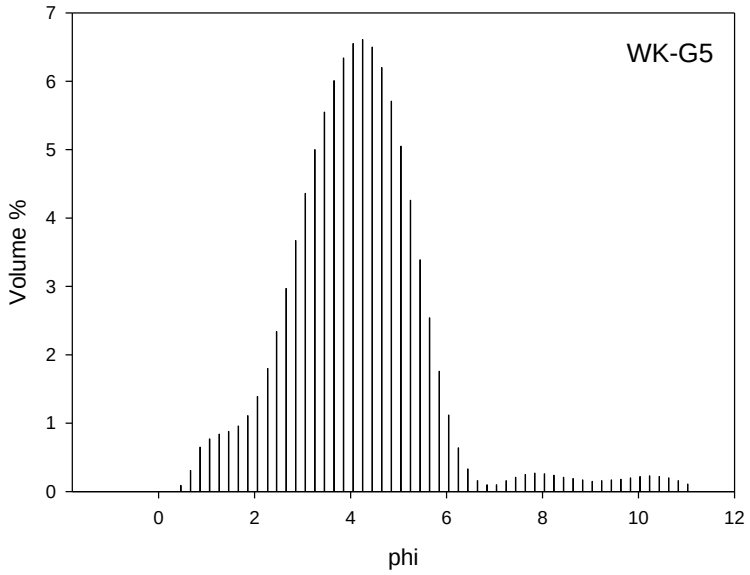

Fig. A1.61 Frequency distribution curve for Driefontein surface sample WK-G5

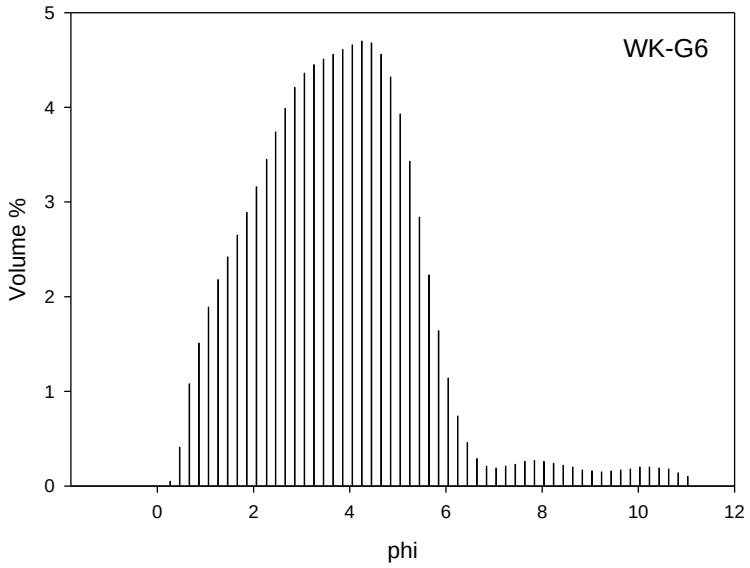

Fig. A1.62 Frequency distribution curve for Driefontein surface sample WK-G6

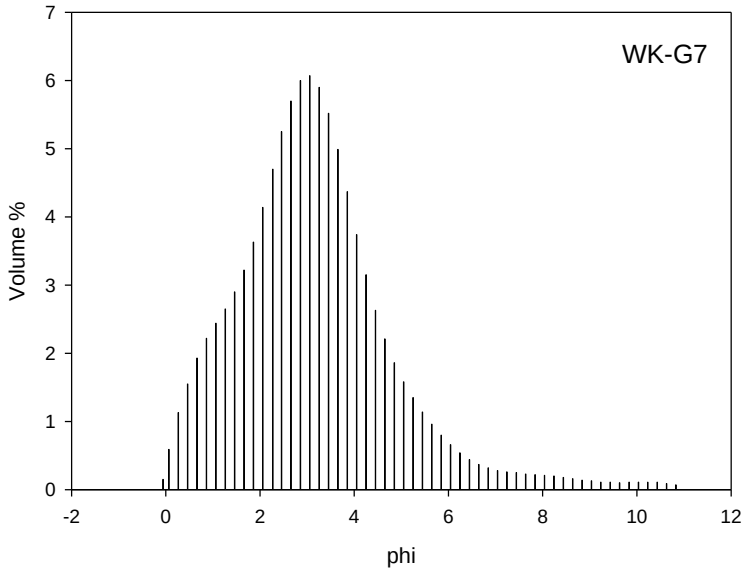

Fig. A1.63 Frequency distribution curve for Driefontein surface sample WK-G7

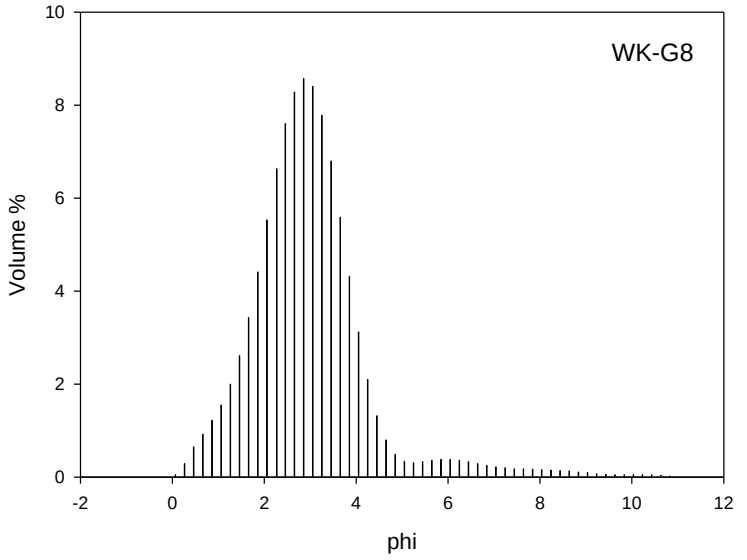

Fig. A1.64 Frequency distribution curve for Driefontein surface sample WK-G8

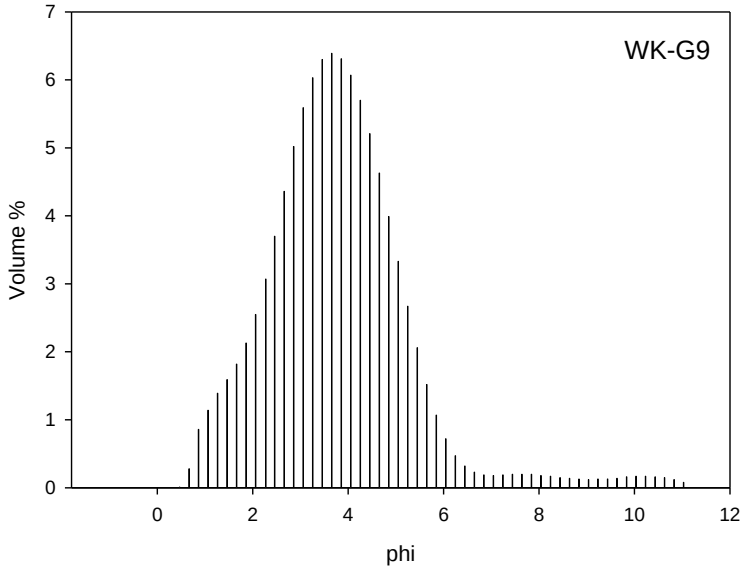

Fig. A1.65 Frequency distribution curve for Driefontein surface sample WK-G9

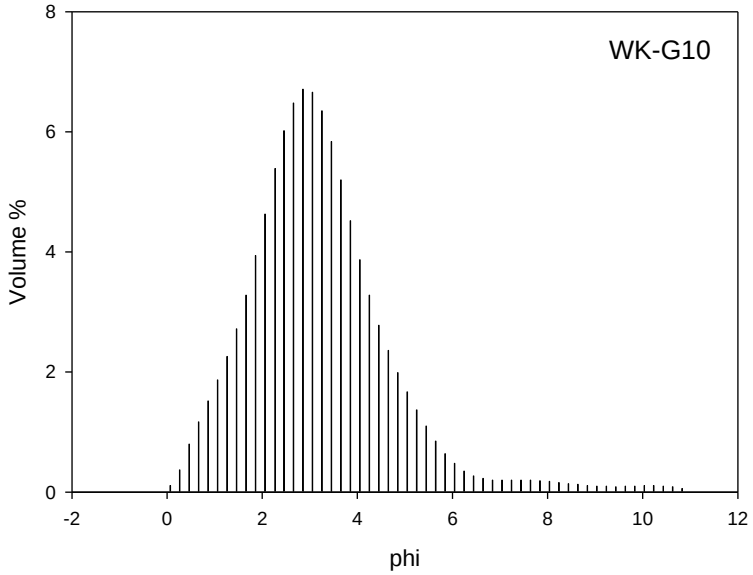

Fig. A1.66 Frequency distribution curve for Driefontein surface sample WK-G10

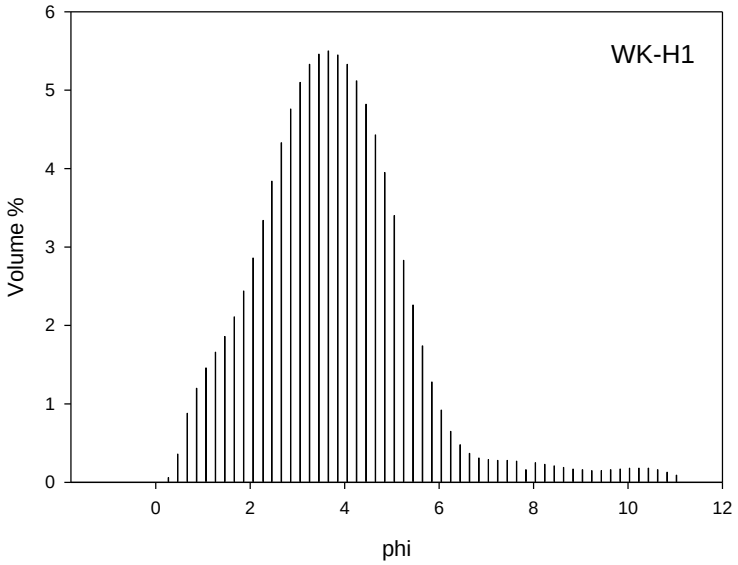

Fig. A1.67 Frequency distribution curve for Driefontein surface sample WK-H1

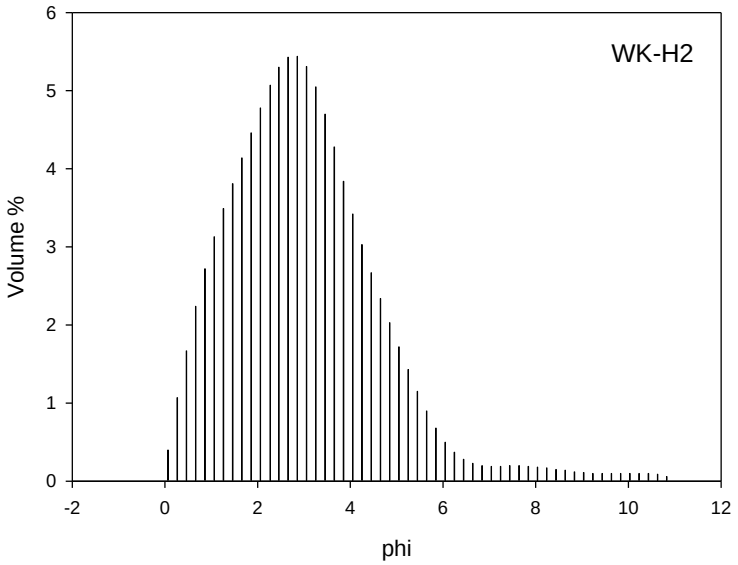

Fig. A1.68 Frequency distribution curve for Driefontein surface sample WK-H2

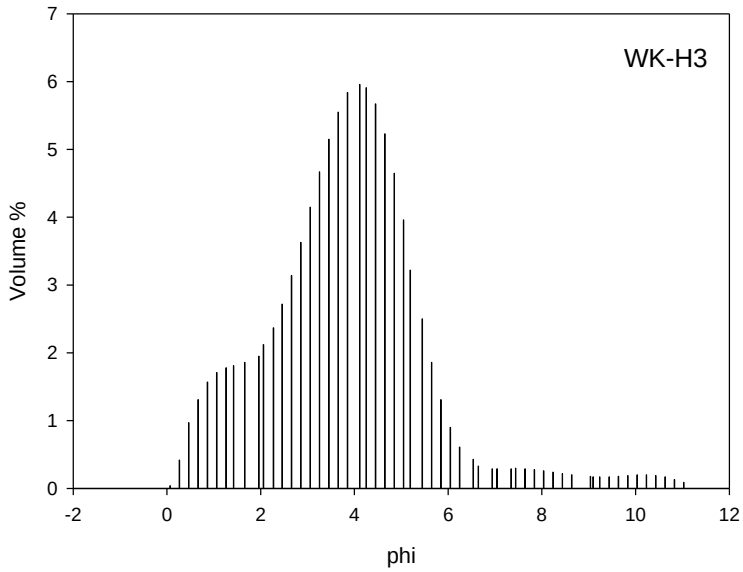

Fig. A1.69 Frequency distribution curve for Driefontein surface sample WK-H3

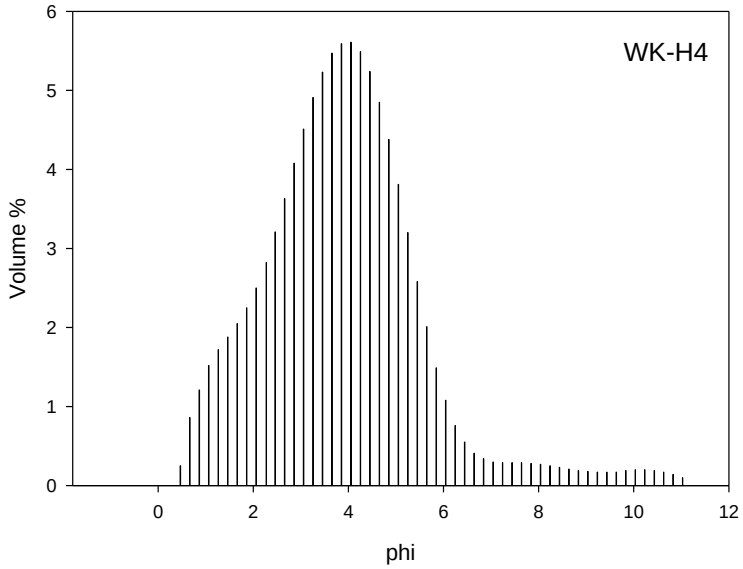

Fig. A1.70 Frequency distribution curve for Driefontein surface sample WK-H4

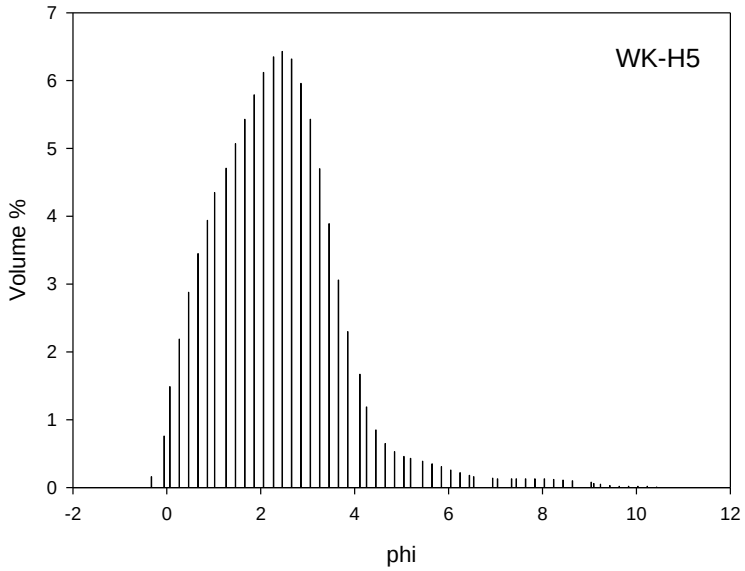

Fig. A1.71 Frequency distribution curve for Driefontein surface sample WK-H5

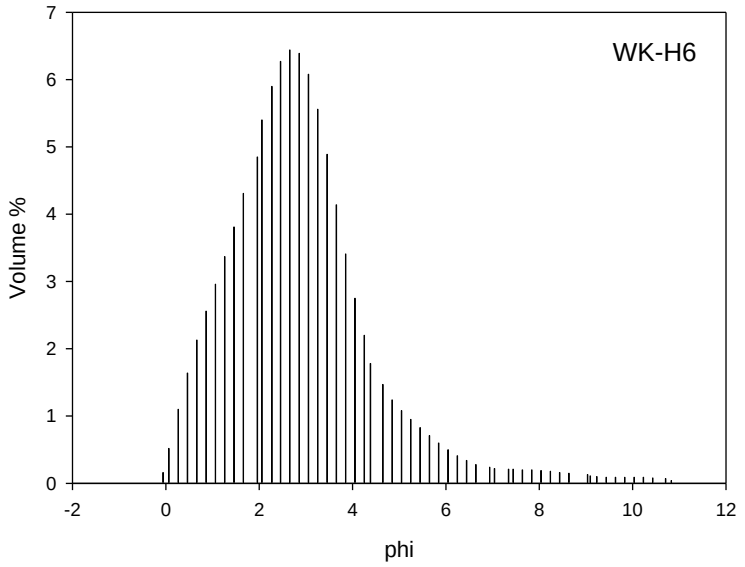

Fig. A1.72 Frequency distribution curve for Driefontein surface sample WK-H6

Grain size distribution of Pit C WK1 samples (OSL samples):

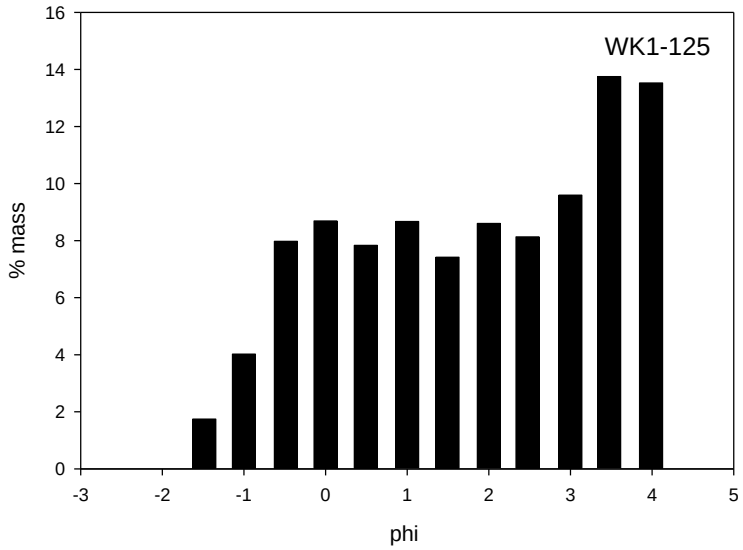

Fig. A1.73 Frequency distribution curve for the Wonderkrater OSL sample WK1-125

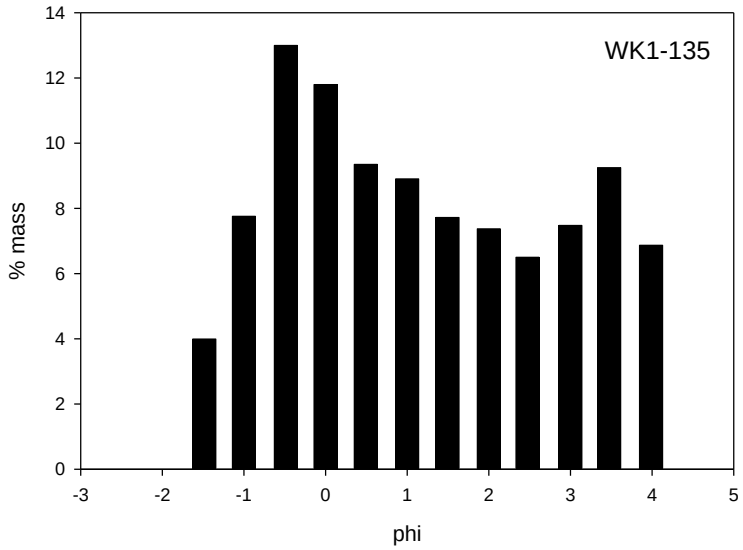

Fig. A1.74 Frequency distribution curve for the Wonderkrater OSL sample WK1-135

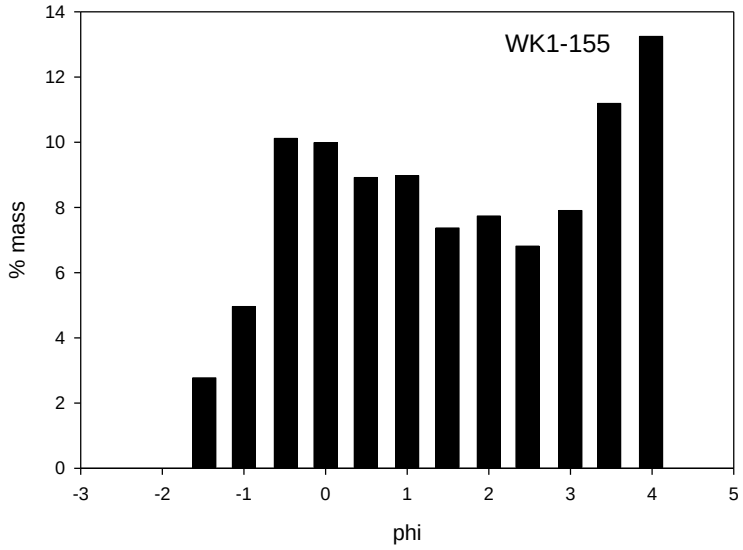

Fig. A1.75 Frequency distribution curve for the Wonderkrater OSL sample WK1-155

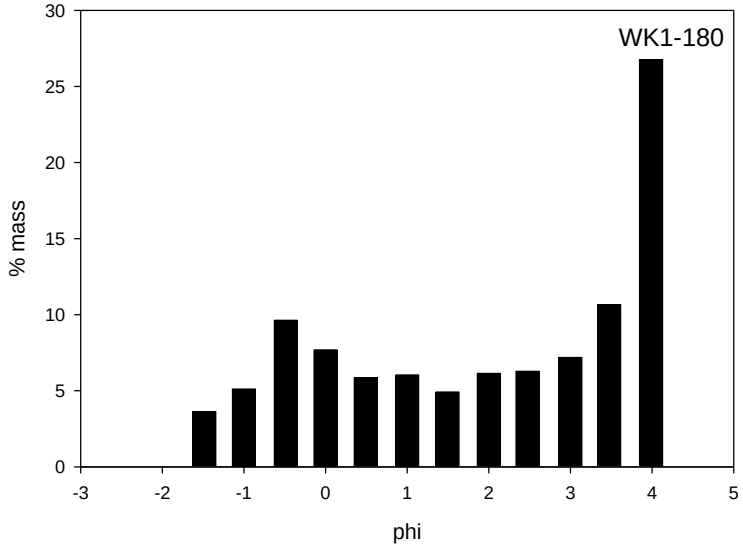

Fig. A1.76 Frequency distribution curve for the Wonderkrater OSL sample WK1-180

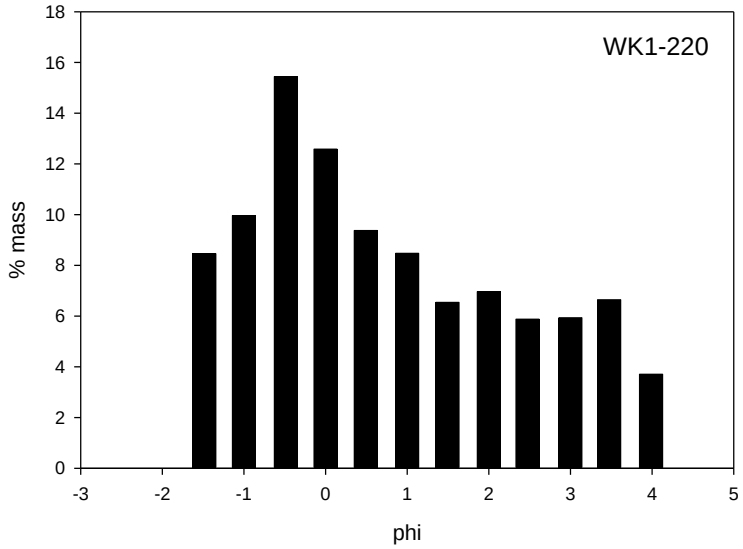

Fig. A1.77 Frequency distribution curve for the Wonderkrater OSL sample WK1-220

Grain size distribution Sub-surface WK2 core samples:

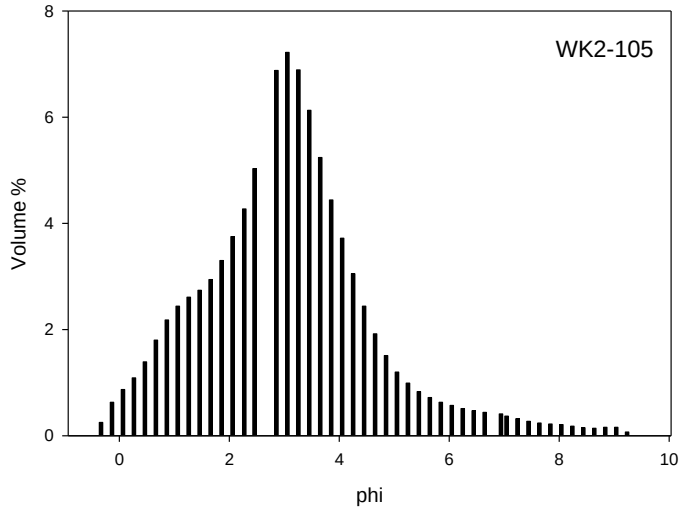

Fig. A1.78 Frequency distribution curve for Wonderkrater WK2 core sample WK2-105

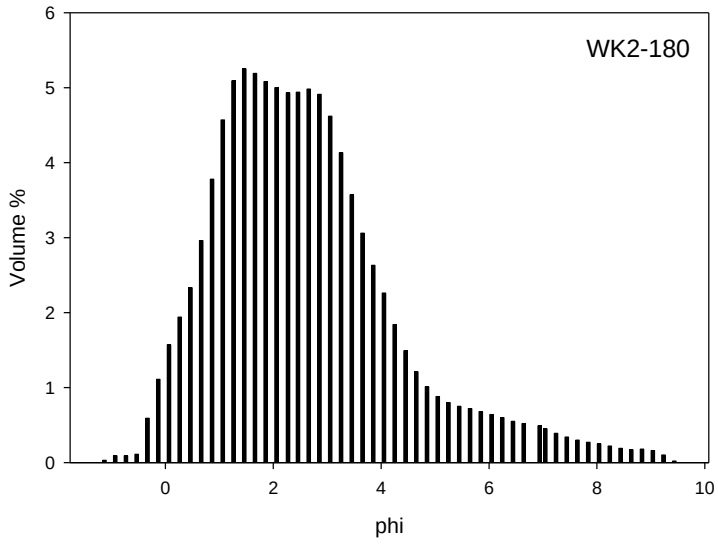

Fig. A1.79 Frequency distribution curve for Wonderkrater WK2 core sample WK2-180

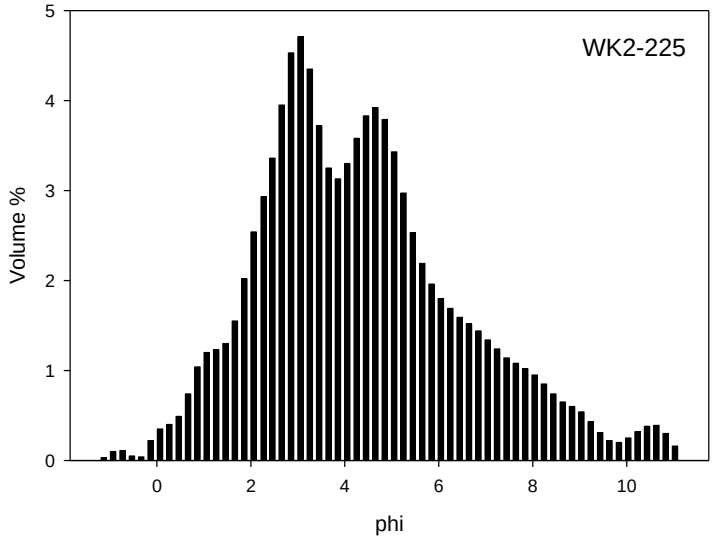

Fig. A1.80 Frequency distribution curve for Wonderkrater WK2 core sample WK2-225

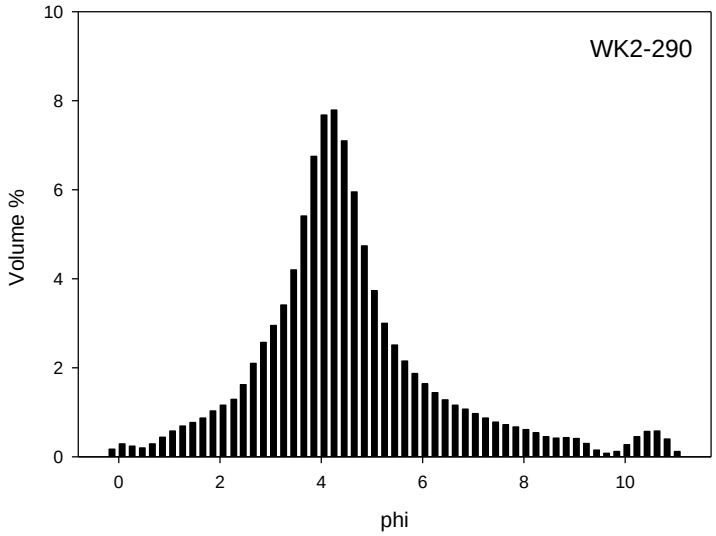

Fig. A1.81 Frequency distribution curve for Wonderkrater WK2 core sample WK2-290

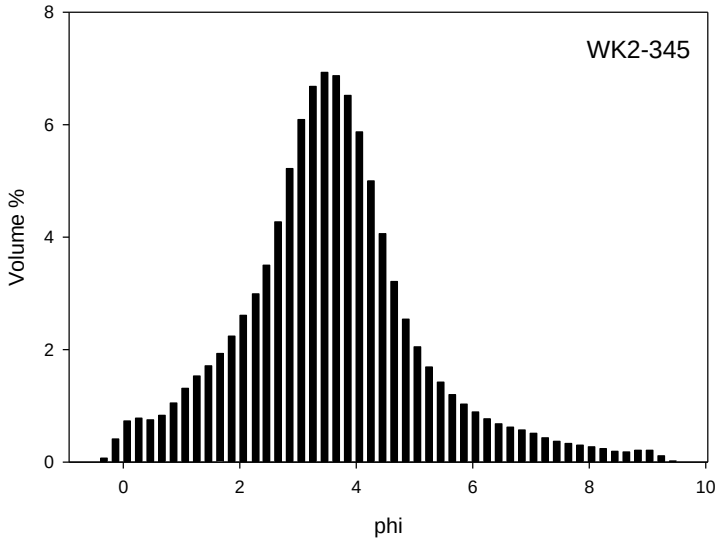

Fig. A1.82 Frequency distribution curve for Wonderkrater WK2 core sample WK2-345

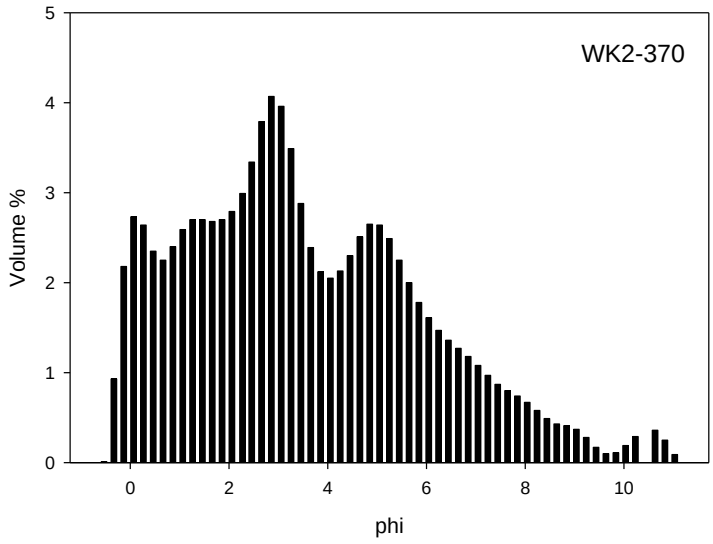

Fig. A1.83 Frequency distribution curve for Wonderkrater WK2 core sample WK2-370

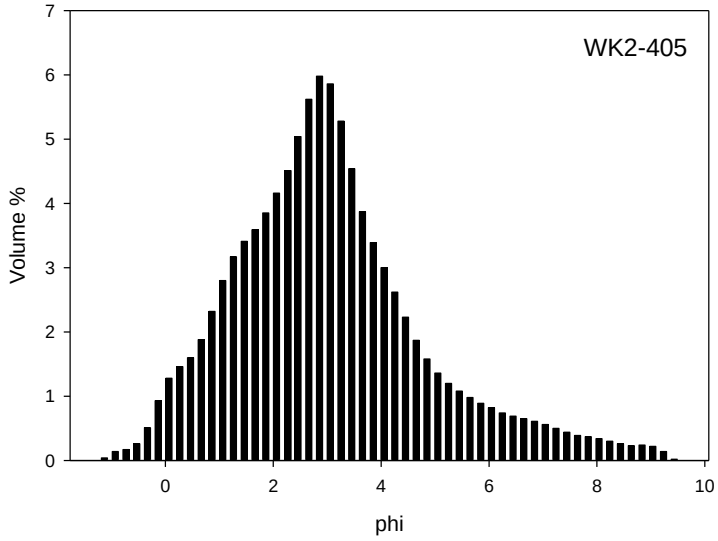

Fig. A1.84 Frequency distribution curve for Wonderkrater WK2 core sample WK2-405

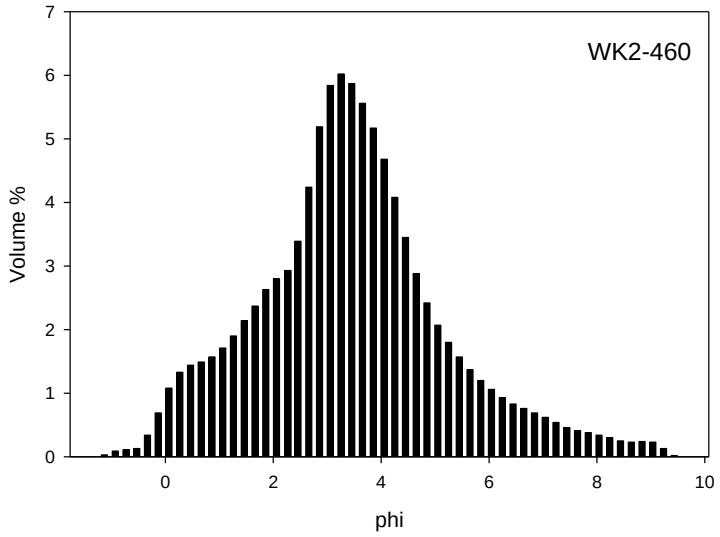

Fig. A1.85 Frequency distribution curve for Wonderkrater WK2 core sample WK2-460

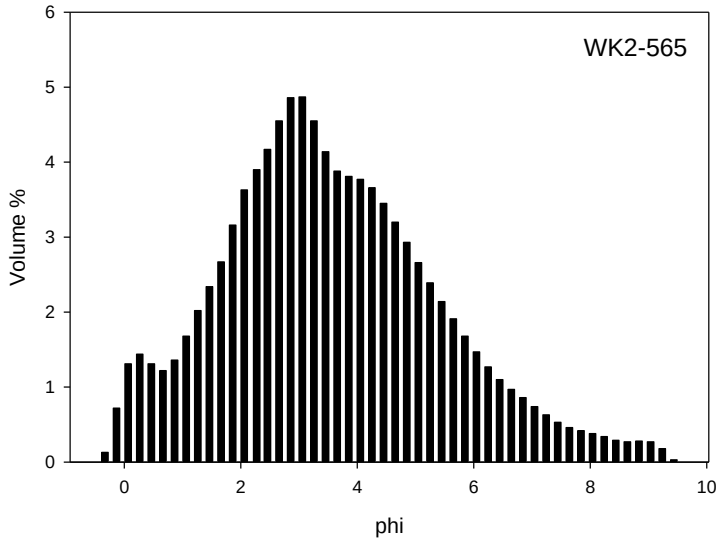

Fig. A1.86 Frequency distribution curve for Wonderkrater WK2 core sample WK2-565

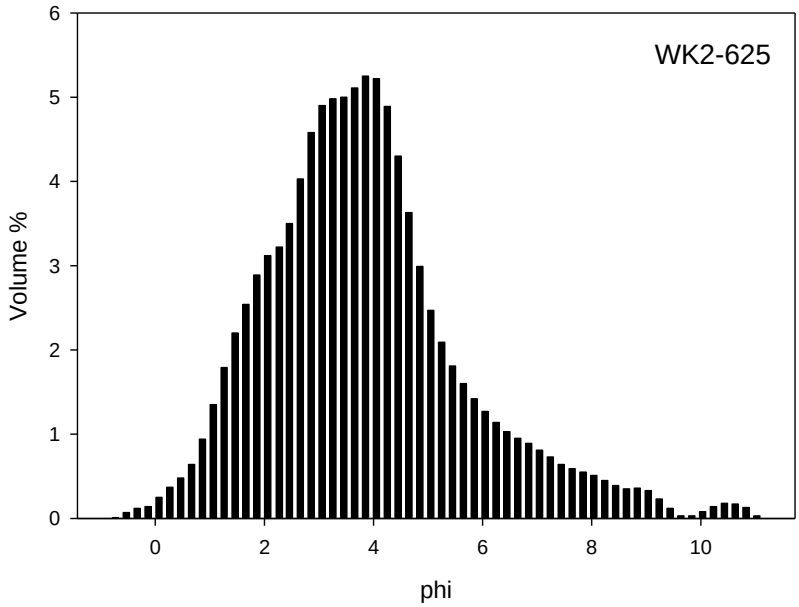

Fig. A1.87 Frequency distribution curve for Wonderkrater WK2 core sample WK2-625

Appendix II

For WK1 OSL samples, recommended SAR protocol for contaminated samples was followed (after Wallinga *et al*., 2002):

1. Give dose, D_i
2. Preheat, 260ºC for 10s
3. Exposed to IR, 175ºC for 100s
4. Simulated with blue, 40s at 110ºC
5. Give test dose, D_t
6. Heat to 180ºC
7. Expose to IR, 175ºC for 100s
8. Stimulated with blue, 40s at 110ºC
9. Repeat steps 1-8 for a range of D_i

Dose recovery test for WK1 samples:

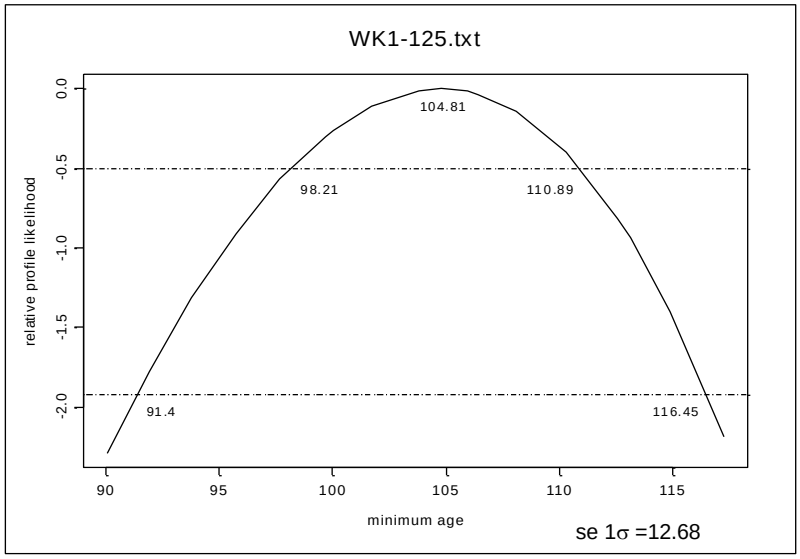

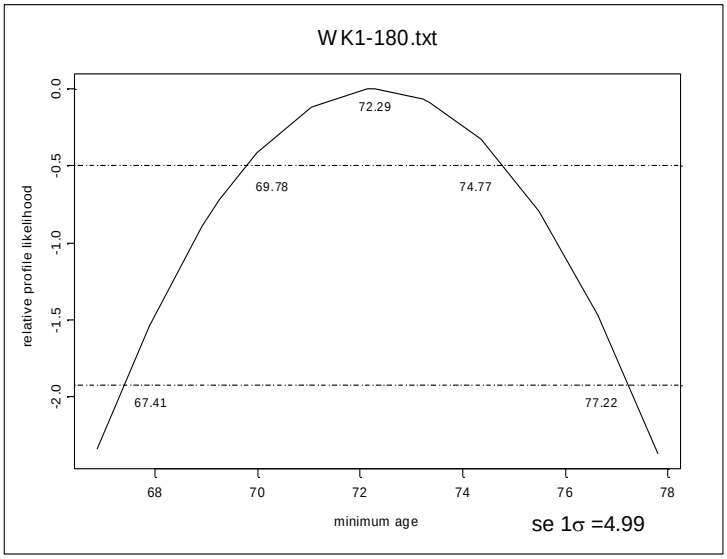

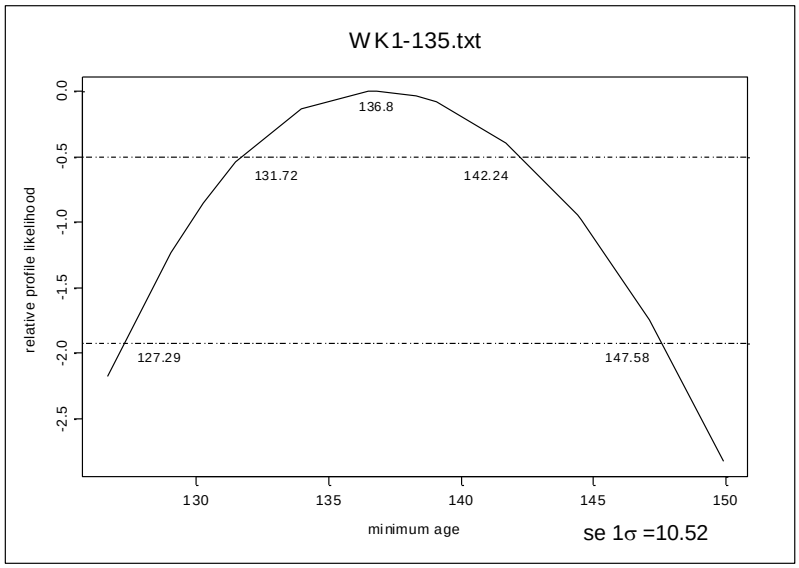

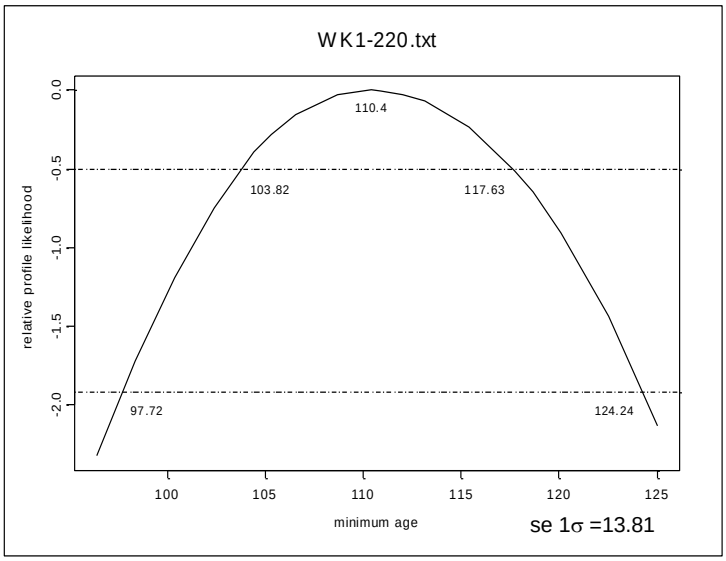

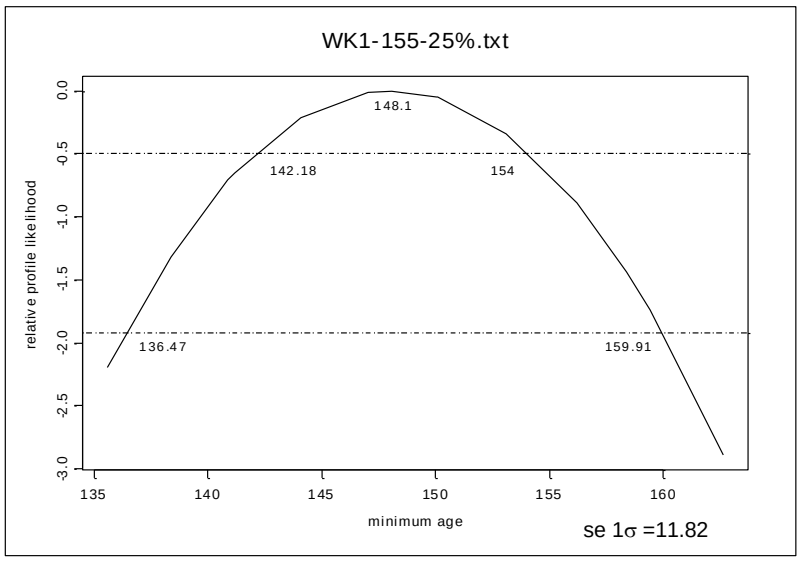

Fig. A2.1 Relative profile likelihood of measured luminescent signal for Single-grain OSL measurements.

Radial plots for OSL results showing equivalent dose rate (D_e) using Monte Carlo methods used for Minimum Age Model:

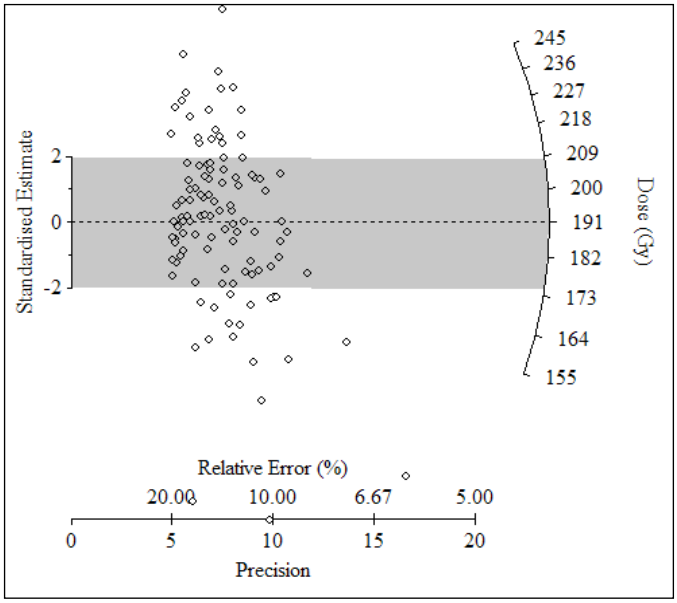

Fig. A2.2 Radial plot of De values for WK1-125, with no more than 20% error on Palaeodose.

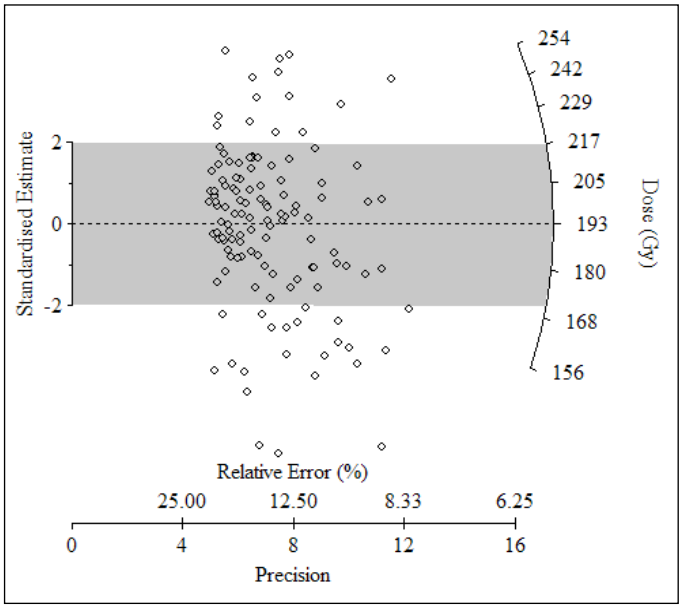

Fig. A2.3 Radial plot of De values for WK1-135, with no more than 20% error on Palaeodose.

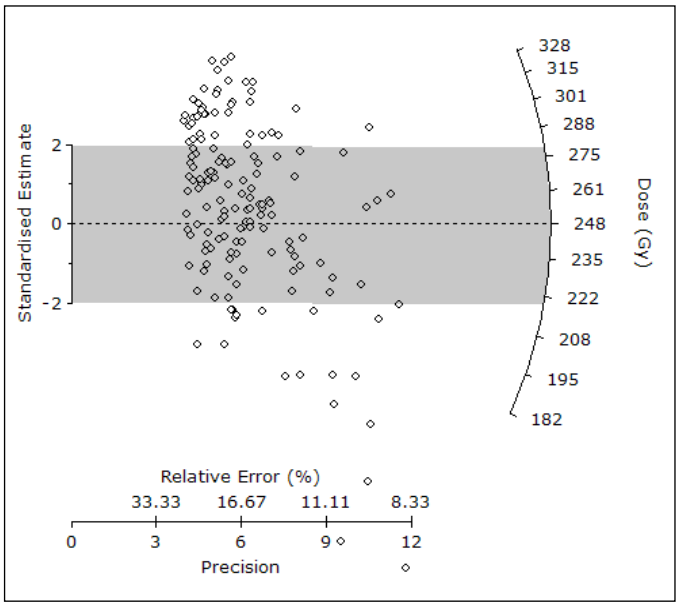

Fig. A2.4 Radial plot of De values for WK1-155, with no more than 20% error on Palaeodose.

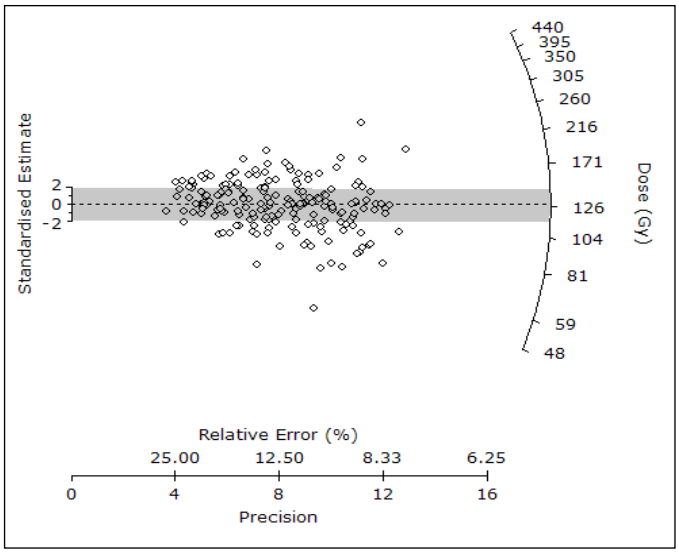

Fig. A2.5 Radial plot of De values for WK1-180, with no more than 20% error on Palaeodose.

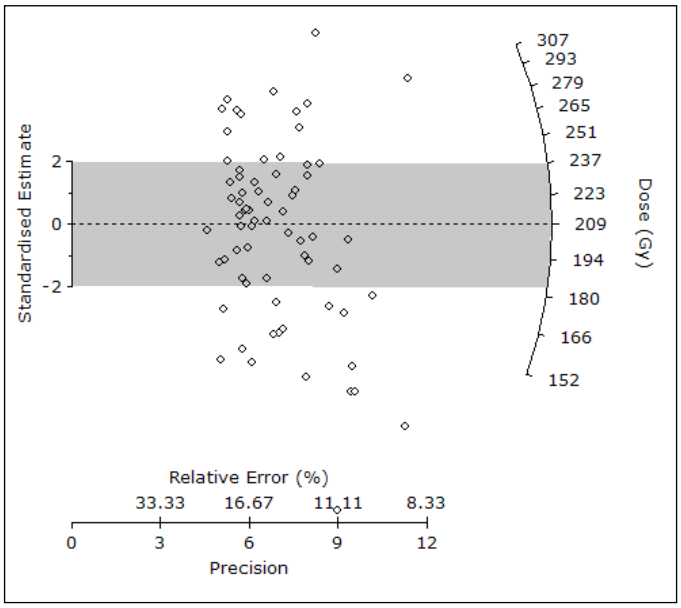

Fig. A2.5 Radial plot of De values for WK1-220, with no more than 20% error on Palaeodose.

Histograms for OSL results:

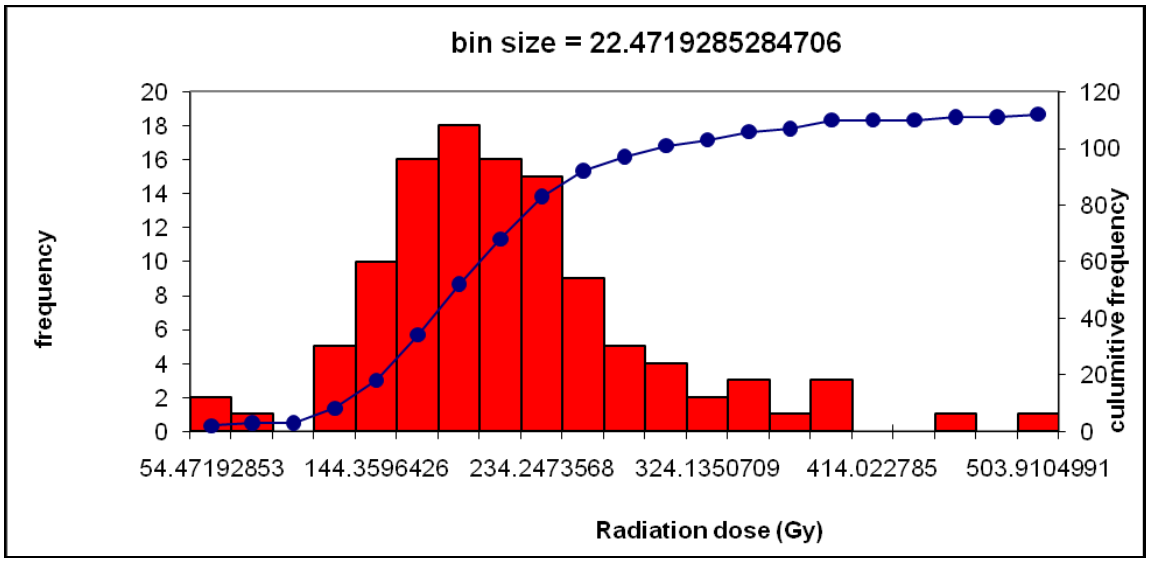

Fig. A2.6 Frequency curves of measured luminescence signal with radiation dose of WK1-125

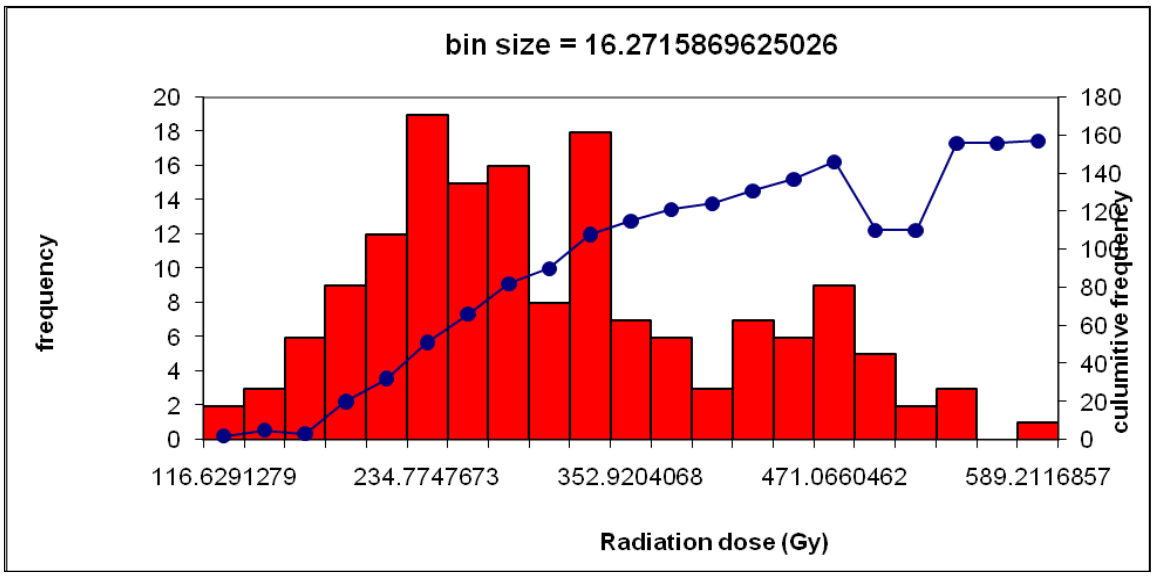

Fig. A2.7 Frequency curves of measured luminescence signal with radiation dose of WK1-135

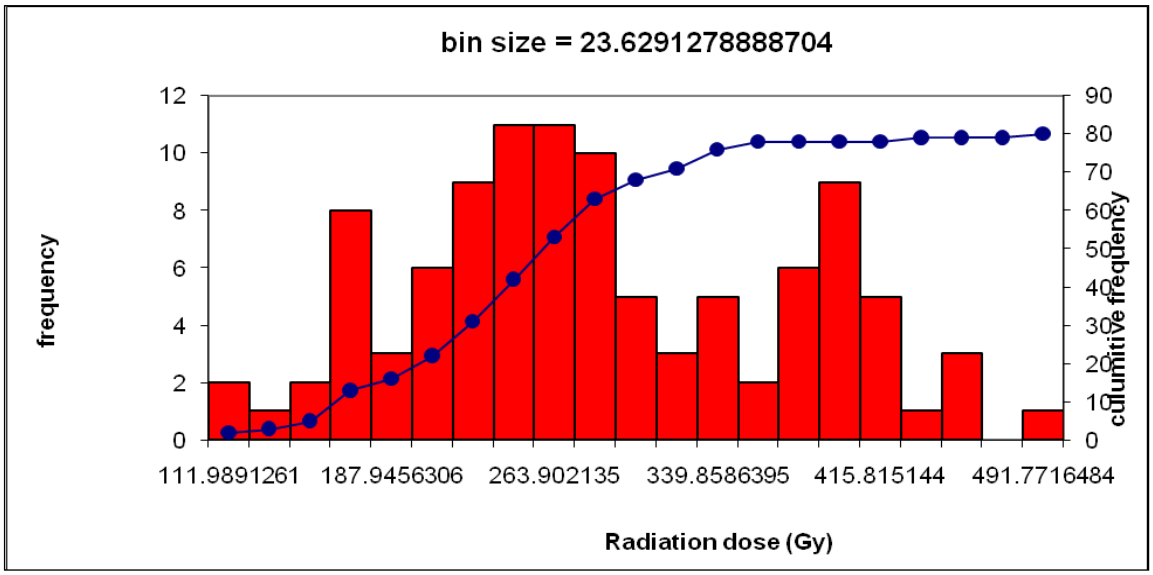

Fig. A2.8 Frequency curves of measured luminescence signal with radiation dose of WK1-135

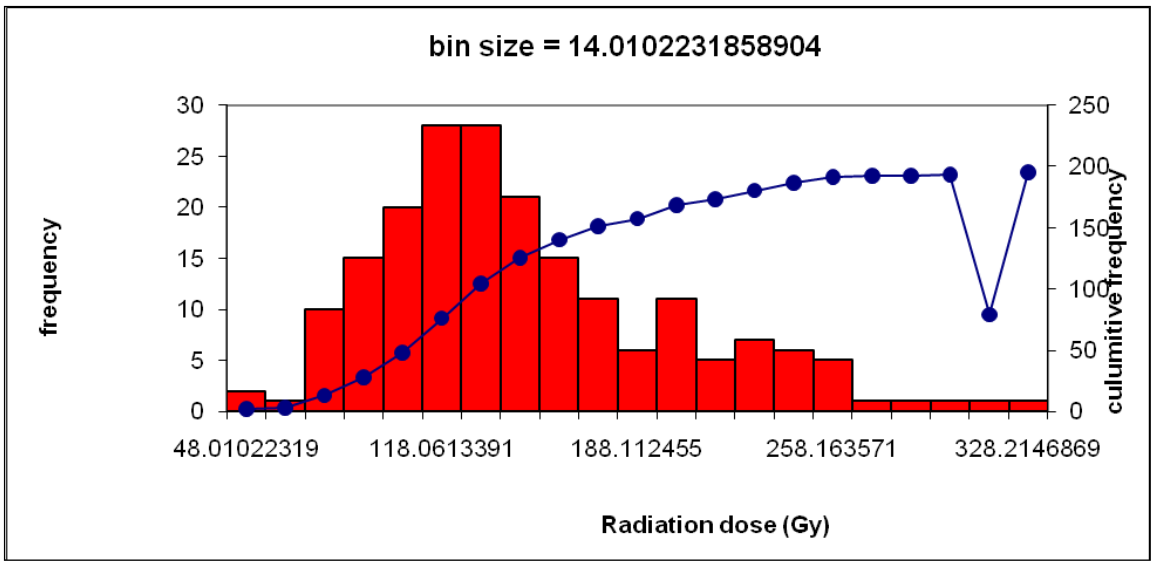

Fig. A2.9 Frequency curves of measured luminescence signal with radiation dose of WK1-180

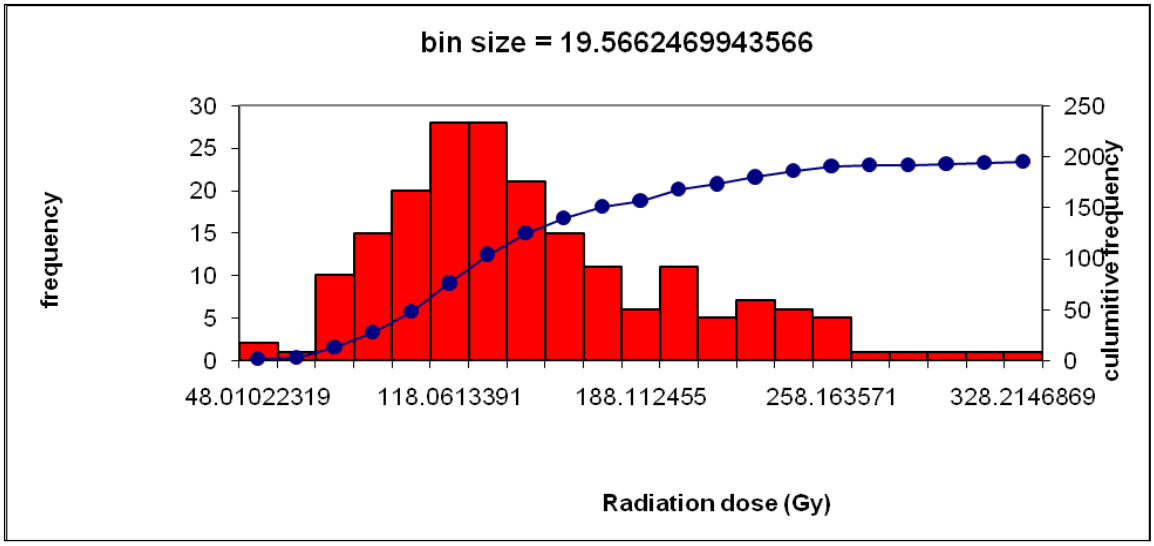

Fig. A2.10 Frequency curves of measured luminescence signal with radiation dose of WK1-220